UNIVERSITY OF
BIRMINGHAM

LOW-VELOCITY IMPACT ANALYSIS OF MONOLITHIC AND LAMINATED GLASS USING FINITE ELEMENT METHOD (FEM)

By

KURUVITA ARACHCHIGE DON

LASITHA PRIYANGA KARUNARATHNA

A thesis submitted to the
University of Birmingham
For the degree of
MASTER OF PHILOSOPHY

School of Civil Engineering
College of Engineering and Physical Science
University of Birmingham
March 2013

ABSTRACT

Low velocity drop ball impact response of monolithic and laminated glasses was studied using analytical and Finite Element (FE) methods. Material linear elastic and damage responses were considered throughout the numerical analysis. The performance of monolithic and laminated plate glasses subjected to the impact loads in normal and oblique angles was thoroughly examined.

In this study, the verification of the analytical and numerical models has been conducted by using one of the previous investigation results. The adopted analytical models include the spring-mass model, energy balance model and wave propagation method for the infinite thick plates, respectively. The results from the wave propagation analytical method found a good agreement with open literature results and it was recommended for future impact predictions. The prediction results obtained include the time histories for impactor-glasses contact force, displacement and velocity during impact under various parameters, such as impact velocity, impact mass and glass plate and PVB interlayer thicknesses. A three-dimensional (3D) finite element method (FEM) is used to model and simulate impact response of both monolithic and laminated glass. The finite element (FE) commercial software package ABAQUS was used in the numerical simulation. The numerical model geometry obtained as a symmetric and full section, which incorporated 8-nodes linear solid (Brick) elements with reduce integration method.

ACKNOLEGMENT

There are many peoples who I would like to acknowledge for the technical and personal supports and encouragement throughout the past three years of my postgraduate study at the University of Birmingham and three years undergraduate study in University of Glamorgan.

Special thanks go for my supervisor, Dr Jian Yang and Prof. Andrew Chan for their invaluable help, constant guidance and wide counselling towards the successful completion of my research work. The positive optimistic attitudes from both supervisors have always given me strength, courage and motivation during the painstaking process of research. I have been enjoying my time working under Dr. Yang.

I would like to thank our research group, Haibo Li, Qiang Liu, Mhomed Wassouff, Jose Manuel Ramirez Leon, Prathan Rungthonkit, Zoe Bao, April Zhao, Tara Morgan, Nastaran Sirigiri for their direct and indirect contributions throughout this process. Also I would like to thank all academic and technical staff in my undergraduate study at the University of Glamorgan.

Finally I would like to thank my mother M.P Perera and father K.A.D Karunarathne and brothers Ajith and Lalith and sisters Manel and Punya for their constant supports, advice and motivation received during this period.

TABLE OF CONTENTS

ABSTRACT ..... **I**

ACKNOLEGMENT ..... **II**

TABLE OF CONTENTS ..... **III**

LIST OF FIGURES ..... **VII**

LIST OF TABLES ..... **XIII**

LIST OF DEFINITIONS ..... **XVI**

CHAPTER 1: INTRODUCTION **1**

1.1 Introduction 1

1.2 Aims and objectives of research 3

1.3 Gaps in knowledge 3

1.4 Methodology 5

1.5 Organization of this thesis 6

CHAPTER 2: LITERATURE REVIEW **8**

2.1 History of glass 8

2.2 Modern glass industry 8

2.3 Basic physical and mechanical properties glass 10

2.4 Type of soda-lime silicate glass and typical strength values 11

2.5 Standard sizes of annealed glass 12

2.6 Laminated safety glass 12

2.6.1 PVB (Polyvinyl Butyral) interlayer 13

2.7 Laminated glass standard size and thickness 14

2.8 Impact 16

2.9 Nature of impact 16

2.10 Impact investigations 25

2.11 Experimental methods and drop-weight test 26

2.12 Experimental implementation of impact events for single layer monolithic glass and multi-layer laminated glass 27

2.13 Numerical implementation of impact events 34

2.14 Numerical implementation of impact events for single layer monolithic glass and multi-layer laminated glass 39

2.15 Summary 41

CHAPTER 3: ANALYTICAL SOLUTIONS FOR LOW-VELOCITY IMPACT ANALYSIS 42

3.1 Analytical model –introduction 42

3.2 The Hertz contact law and contact mechanics 43

3.3 Impact analytical models 45

3.3.1 Spring-mass models 45

3.3.2 Linear spring-mass model 46

3.3.3 Energy – balance model 47
3.3.4 Wave propagation method for infinite thickness plate 49
3.4 Verification of impact dynamic model 52
3.5 Low-velocity impact analysis of monolithic glass plate using wave propagation method 54
3.5.1 Low-velocity impact analysis results of for monolithic glass plate 56
3.6 Low–velocity impact analysis of laminated safe glass plate using wave propagation method 60
3.6.1 Low-velocity impact analysis results of laminated glass plate 64
3.7 Analytical prediction of contact area for monolithic and laminated glass plates subject to impacts 70
3.7.1 Results of contact radius and area for the monolithic glass plate 71
3.7.2 Results of contact radius and area for the laminated glass plate 72
3.8 Summary 74
CHAPTER 4: NUMERICAL MODEL FOR LOW-VELOCITY IMPACT OF MONOLITHIC AND LAMINATED GLASS PLATE 75
4.1 Introduction 75
4.2 Numerical model preparation 75
4.3 Material models in ABAQUS 82
4.3.1 Linear elastic material model 83
4.3.2 Brittle fracture model 83

4.4 Convergence study and verification of FE model.....86

4.5 Low – velocity impact numerical analysis of monolithic glass plate under various parametric conditions and comparison using an analytical method 92

4.6 Low – velocity impact numerical analysis of laminated glass plate under various parametric conditions and comparison using an analytical method 112

4.7 Numerical analysis of contact radius of monolithic and laminated glass plates under various parametric conditions.....127

4.8 Summary.....138

CHAPTER 5: CONCLUTION AND RECOMMENDATION.....141

5.1 Conclusions and recommendation 141

5.2 Future work.....143

APPENDIX A.....145

REFERENCES.....147

LIST OF FIGURES

Figure 2.1 Flat glass manufacturing technique 8

Figure 2.2 Manufacturing of float glass (James, 1913) 9

Figure 2.3: Configuration of laminated glass (Stiles, 2010) 13

Figure 2.4: Target response under low and high velocity impacts (Cremona Rebecca and Hinkley Jeffrey, 2005) 19

Figure 2.5: Projectile or impactor nose shapes for experimental and numerical investigations (Goldsmith, 2001) 22

Figure 2.6: The erosive failure behaviour of ductile and brittle (Wang and Yang, 2008) 24

Figure 2.7: FEA stress distribution of three point bending impact model (Aretxabaleta et al. 2005) 27

Figure 2.8: Single layer glass plate failure patterns (Ball and McKenzie, 1994) 30

Figure 2.9: Monolithic glass plate impact damage patterns – (a) and (b): drop ball test; (c) and (d): Hopkinson pressure bar test (Bouzid et al., 2001) 31

Figure 2.10: Star crack on acrylic plate with different velocities (Liu and Liaw, 2009) 32

Figure 2.11: Contact force time history of acrylic plate under different velocities (Liu and Liaw, 2009) 32

Figure 2.12: Drop ball impact fracture pattern of laminated glass plate (Shutov et al., 2004) 34

Figure 2.13: Finite element (a) 2D plane (b) 2D axisymmetric (c) 3D full model (d) 3D half a symmetric (e) 3D quarter symmetric models 36

Figure 2.14: Mild-steel plate optimum element size and mesh summary (Rusinek et al., 2009) 38

Figure 3.1: Two contact spheres with different radius R_1, R_2 43

Figure 3.2: The contact force for steel plate comparison each analytical models 53

Figure 3.3: Impact results for Case 1 57

Figure 3.4: Impact results for Case 2 58

Figure 3.5: Impact results for Case 3 59

Figure 3.6**:** Sectional view of laminated glass plate 61

Figure 3.7: Impact results for Case 4 65

Figure 3.8: Impact results for Case 5 66

Figure 3.9 Impact results for Case 6 67

Figure 3.10: Impact results for Case 7 68

Figure 4.1: A quarter section of full plate model 76

Figure 4.2: Quarter geometric parts 77

Figure 4.3: Quarter geometric part of steel ball (impactor) 78

Figure 4.4: Mesh of (a) Monolithic glass plate (b) laminated glass plate with PVB inter layer and (c) impactor 79

Figure 4.5: Symmetric boundary condition of monolithic glass plate in X and Z directions 80

Figure 4.6: Symmetric boundary condition of laminated glass plate in X and Z directions .80

Figure 4.7: Fixed support monolithic glass plate (left) and laminated glass plate (right) boundary conditions 81

Figure 4.8: Arrangement of Symmetric boundary condition and pre-define initial impact velocity for impactor 81

Figure 4.9: Post-failure stress displacement curve 84

Figure 4.10: 3D FE quarter model with mesh 87

Figure 4.11: Element preparation of convergence study 87

Figure 4.12: Convergence study - maximum contact force vs. number of elements along plate thickness direction.....89

Figure 4.13: Convergence study – plate central displacement vs. number of elements along plate thickness direction.....89

Figure 4.14: Element size verification 90

Figure 4.15: Comparison of contact force-time history with present FEM, analytical and previous data (Wu and Chang, 1989 - Karas study) 90

Figure 4.16: FE results comparison with previous data (Wu and Chang, 1989) 91

Figure 4.17 : Full plate model of monolithic glass plate (left) and expan view of damage initiate area (right).....93

Figure 4.18: Impact results for Case 1 95

Figure 4.19: Impact results comparison for Case 1 96

Figure 4.20: Contact force-time history damage prediction for Case 1.....97

Figure 4.21: Impact damage response for Case 1 98

Figure 4.22: Impact results for Case 2 101

Figure 4.23: The results comparison for Case 2 102

Figure 4.24: Contact force-time history damage prediction for Case 2 104

Figure 4.25: Impact damage response for Case 2 105

Figure 4.26: Impact results for Case 3 107

Figure 4.26: The results comparison for Case 3 108

Figure 4.28: Contact force history damage response of monolithic glass plate with various impactor masses – Case 3 110

Figure 4.29: Impact damage response for Case 3 111

Figure 4.30: Impact results for Case 4 114

Figure 4.31: The results comparison for Case 4 115

Figure 4.32: Impact results for Case 5 117

Figure 4.33: The results comparison for Case 5 119

Figure 4.34: Impact results for Case 6 121

Figure 4.35: The results comparison for Case 6 122

Figure 4.36: Impact results for Case 7 124

Figure 4.37: The results comparison for Case 7 126

Figure 4.38: Section of a quarter-symmetric square plate for contact area calculation.....128

Figure 4.39: Engaged nodes in monolithic glass plate at peak contact force – Case 1 129

Figure 4.39: Engaged nodes in monolithic glass plate at peak contact force – Case 2 130

Figure 4.40: Engaged nodes in monolithic glass plate at peak contact force – Case 3 131

Figure 4.42: Engaged nodes in monolithic glass plate at peak contact force - Case 4 133

Figure 4.43: Engaged nodes in monolithic glass plate at peak contact force – Case 5 134

Figure 4.44: Engaged nodes in monolithic glass plate at peak contact force – Case 6 135

Figure 4.45: Engaged nodes in monolithic glass plate at peak contact force – Case 7 136

LIST OF TABLES

Table 2.1: Basic physical properties of soda lime and borosilicate glass 10

Table 2.2: Different range of strength properties of brittle glass 11

Table 2.3: Ultimate tensile and compressive stress for all glass types 11

Table 2.4: Typical failure and fragmentation patterns (Stiles, 2010; James, 1913; www.robinson-solutions.blogspot.co.uk) 12

Table 2.5: Mechanical properties of PVB materials 14

Table 2.6: Standard sizes of laminated glass (Norville et al., 1998) 15

Table 2.7: Velocity regimes and representative applications and test methods subject to impacts (Backman and Goldsmith, 1978 and Børvik, 2001) 17

Table 3.1: Maximum contact force and total contact duration comparison 54

Table 3.2: Arrangement of parametric studies for monolithic glass plate 55

Table 3.3: Material properties of glass and steel 55

Table 3.4 Summary of parametric studies using wave propagation method 60

Table 3.5: Material properties of polyvinyl butyral (PVB) 61

Table 3.6: Arrangement of parametric studies for laminated glass plate 63

Table 3.7: Summary of parametric studies using wave propagation method (LG plate) 69

Table 3.8: Summary of peak contact radius and area on monolithic glass plates under various parametric conditions.....72

Table 3.9: Summary of peak contact radius and area on laminated glass plates under various parametric conditions.....73

Table 4.1: Overview of mechanical and physical properties of glass, PVB and steel materials.....79

Table 4.2: Element and node summary of quarter symmetric monolithic glass plate.....92

Table 4.3: Element and node summary of monolithic glass plate full model.....93

Table 4.4: Maximum contact force and displacement results comparison for Case 1 99

Table 4.5: FE elastic and FE damage models maximum contact force comparison for Case 1 99

Table 4.6: Maximum contact force and displacement results comparison for Case 2 103

Table 4.7: FE elastic and FE damage models maximum contact force comparison for Case 2 104

Table 4.8: Maximum contact force and displacement results comparison for Case 3 109

Table 4.9: FE elastic and FE damage models maximum contact force comparison for Case 3 110

Table 4.10: Element and node summary of quarter symmetric laminated glass plate 112

Table 4.11: Maximum contact force and displacement results comparison for Case 4 116

Table 4.12: Maximum contact force and displacement results comparison for Case 5 119

Table 4.13: Maximum contact force and displacement results comparison for Case 6 123

Table 4.14: Maximum contact force and displacement results comparison for Case 7 126

Table 4.15: Numerical and analytical comparison of monolithic glass plate contact area..132

Table 4.16: Numerical and analytical comparison of laminated glass plate contact area ...137

LIST OF DEFINITIONS

ASTM	American Society for Testing and Materials
DEM	Discrete Element Method
DE	Discrete Element
FE	Finite Element
FEA	Finite Element Analysis
FEM	Finite Element Method
LG	Laminated Glass
PVB	Polyvinyl Butyral
PVB	Polyvinyl Chloride
SDOF	Single Degree of Freedom
2D	Two Dimensional
3D	Three Dimensional

CHAPTER 1: INTRODUCTION

1.1 Introduction

Glass is a man-made material that was initially found from Mesopotamia and Egypt in the 35th century BC. Between 1688 and 1691, it was developed into a new form of flat plate of large size in France. However, its physical and mechanical properties and structural behaviours were not well investigated at the same time. The investigations of glass properties were only established in the past few decades. Most recently, glass has been used in a number of self-standing and light weight structures, e.g. making fins, beams, roofs, floors and stair cases in modern buildings as well as windshields in the automotive industry (Ledbetter et al., 2006; IstructE, 1999).

The glass is a brittle but strong material, but it behaves mainly under the elastic range (Ledbetter et al., 2006). However, in brittle nature, glass can fail without any pre-warning signals. Furthermore, the inherent micro-scale surface defects can render low tension strength. In 1921, Griffith first attempted to examine the theoretical fracture behaviour of glass under various loading cases. It is described that the glass surface defects generate cracks that contribute to failure. These surface defects are originally called as glass flaws or Griffith flaws and a failure criterion is called Griffith law.

The glass used in building is mainly soda-lime silicate glass and borosilicate glass. Depending on the processing method, the soda-lime silicate glass is subdivided into annealed, heat-

strengthened, thermally and chemically-strengthened glass for construction purposes. In modern construction, the concept of multilayer glass composite has also been established for structural purpose. The multilayer glass composite is also called laminated glass manufactured by using two or more soda-lime glass panels bonded together with one or more interlayer materials such as PVB or resin. Benefits of applying laminated glass include avoiding large and sharp pieces when shattering and preventing falling glass hitting people (Flocker and Dharani, 1998; IstructE, 1999).

It is well known that understanding the nature and mechanism of breakage of glass when it is subjected to falling objects impact, as well as its influence on safe design and use of glass are challenging tasks in the real world. In general, studies on wind born debris, projectiles and dropped tools induced impacts of glass are limited. This study mainly focuses on the hard-body impact in low to medium velocity range on monolithic and multilayer laminated glass (LG) plates. The study also concerns numerical model developing techniques by using 3D finite element method (FEM) base on the commercial software package ABAQUS. The dynamic explicit method is used to simulate the impact process. Results obtained include the elastic impact response of monolithic and laminated glass panels and the impact damage response of monolithic glass plates under various parameters such as impact velocity, plate thickness, impactor mass and PVB interlayer thickness. Moreover, a wave propagation method based analytical method will be adopted to predict the impact response of the monolithic and laminated glass plate and the obtained results will be compared with numerical predictions.

1.2 Aims and objectives of research

In general, the drop weight is a common scenario occurring in the construction and building maintenance industry. It is a crucial scenario and considered more critical in glass structures when day to day operations and maintenance are required. This study aims to study the steel sphere drop impact response on single layer monolithic and multi-layer laminated glass panels, in which low- to medium- velocity range, i.e. 0 – 50 m/s is considered. Both the numerical simulations and analytical investigations have been carried in order to achieve the project aim and the key objectives of research are listed below:

- Developing a numerical model to analyse the impact response of monolithic and laminated glass under hard-body impact.
- Studying the influence of design parameters, such as impact velocity, impactor mass and geometry, the PVB interlayer and glass ply thicknesses, on the impact response of glass panels.
- Establishing an appropriate analytical model to validate the numerical model.
- Investigating the damage process and crack pattern for monolithic glass subjected to drop weight sphere impacts.

1.3 Gaps in knowledge

The number of glass applications is increasing in modern construction industries. Failure cases due to visible and non-visible damages on glass applications are increasing. However,

the knowledge of impact response of the single layer and multi-layer laminated glass panels are still very limited. This section provides some identified knowledge gaps with regards to the general impact problem, glass subjected impact and numerical and analytical approaches to study impact.

In general, the impact induced by drop weight impact is considered to account for various velocities, geometries and angles (normal or oblique), respectively. The effect of impact object geometry and impact angle has been reported with the typical experimental and numerical investigations.

In the existing experimental studies, the impact damage response of monolithic and laminated plate glasses has been reported concerning various parameters by using various test methods. Information on impact damage patterns of monolithic and laminated glasses can been found from these literatures, but insufficient informations are available for the impact response, impact interaction between contact objects, contact area and the interlayer delamination of the laminated glass.

In most recent numerical studies, the impact and damage responses of laminated plate glasses have been modelled by 2D/3D finite element method (FEM) and discrete element method (DEM) methods. It is well known that glass behaves in a brittle nature and the laminated glass interlayer (PVB and SGP) behaves in a viscoelastic or viscoplastic nature. It is also well known that the majority of FE and DE commercial software packages (ABAQUS, ANSYS, LS-DYNA) adopts different material models for similar material families. For example, ABAQUS uses a brittle cracking model for glass and ceramics and LSDYNA uses Johnson –

Holmquist (JH1 and JH2) for glass and ceramics. However, there is very limited information on how to choose coefficients and parameters required in the material models, which should have been obtained by experimental methods.

1.4 Methodology

The methodology of this research comprises the following steps:

1) Developing an analytical model in order to analyse and predict the dynamic impact response of glass plate and verifying the analytical model by using open literature data.

2) Developing an accurate numerical model of elastic impact which includes:

    - Identifying suitable commercial FE software package for modelling and analysis;
    - Identifying correct material properties and parameters for material models;
    - Implementing the material model in FE software (ABAQUS^{TM});
    - Verifying and validating impact model using open literature results.

3) Implementing the above numerical modelling approach to develop the low-velocity impact of monolithic and laminated glass models.

    - Modelling the PVB interlayer for laminated glass plate

- Identifying and creating the contact between the two glass plies and PVB

4) Predicting the low-velocity impact responses of the monolithic and laminated plate glasses and then comparing these results with the most accurate analytical method.

It is worth noting that in the first part of the numerical study, all material models and impact response are implemented with elastic properties, whilst and in the second part of the study, damage material properties are considered.

1.5 Organization of this thesis

This thesis consists of five chapters as follows:

Chapter 1 includes a general introduction providing the origin and categorization of glass, the research scope, aims and objectives, knowledge gaps, research methodology and thesis outline.

Chapter 2 presents a brief review of literatures carried out in the past years. It begins with a general study about glass, a brief history and the modern uses of glass the industry, followed by the basic physical and mechanical properties of glass, soda-lime silicate glass types and laminated glass. Additional information about standard sizes and thickness of annealed and laminated glasses is provided. The review chapter then extends into the background of

dynamic impacts, impact nature, impact evaluation and experimental and numerical modelling of impacts for the laminated and monolithic glasses.

Chapter 3 presents an analytical solution method in order to predict the impact responses of the glass plate by using spring-mass model, energy-balance model and wave propagation techniques for infinite plate, respectively. This chapter also includes the verification of the analytical model by using the open literature data.

Chapter 4 describes the finite element modelling and analysis for the impact of glass, including the convergence study and numerical verification following the open literature data. Optimum element sizes for the impactor, glass plate and PVB interlayer meshes are established. The chapter also includes the elastic, damage and contact area response analysis and a comparison with the analytical method with various parametric conditions such as impact velocity, impactor mass, plate thickness and PVB interlayer thickness.

Chapter 5 summarises the main findings of the study and includes suggestions for improving the impact performance of both types of glass.

CHAPTER 2: LITERATURE REVIEW

2.1 History of glass

Glass was originally discovered by Phoenician merchants in the region of Syria around 5000-7000 years ago. However, the first man-made glass evidence was found from Egypt and Rome around in 3500 BC. It displayed non-transparent features. In the 11th century, German glass craftsmen and in the 13th century Venetian glass makers manufactured sheet glasses. The flat glass manufacturing technique was widely used across the Eastern Europe from 11th the century. Figure 2.1 shows flat glass types including crown, cylinder and plate glasses manufactured in the 11th century(Schittich et al., 2007; Pankhardt, 2009).

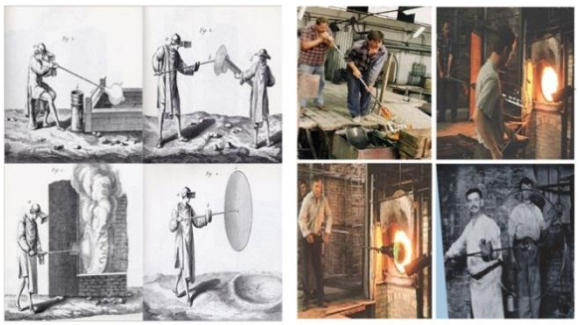

Figure 2.1 Flat glass manufacturing technique
(www.rmears.co.uk/publications; www.tatra-glass.co.uk)

2.2 Modern glass industry

A large scale manufacturing process of sheet glasses was established in the 16th century. In 1608, the historical records have provided details about first glass plant location in

Jamestown, Virginia (United State). Later in 1729, William "Baron" Stiegel, John F. Amelung and Caspar Wister developed sheet glasses (Axinte, 2011) in the industrial scale. Considerable progress was made in glass manufacturing and processing methods such as pressed glass, cast glass and roll glass (Smith, 1997).

In the 20th century, the advanced manufacturing process using machine was introduced in order to maintain a constant large supply. The common form of machine made glass is called flat glass and is used for various applications such as windows and doors. Alistair Pilkington invented the floating process making the best quality flat glass in 1952. In this process, the soda lime silicate glass's raw ingredients of sodium oxide, lime, and silica sand are mixed with broken glass cullet (Haldimann, 2006; Schittich et al., 2007).

The mixed batch is heated up to a specific temperature to melt, and then floated on to a tin bath where the ribbon of float glass is pulled or drawn through the bath (Figure 2.2). The glass ribbon then enters an annealing lehr (oven) for the cooling process and later final finishing (e.g. sizing, cutting, grinding and polishing) to form the glass plate. In the lehr, the rollers rotating speed are defined by the glass plate thicknesses (James, 1913; IstructE, 1999) .

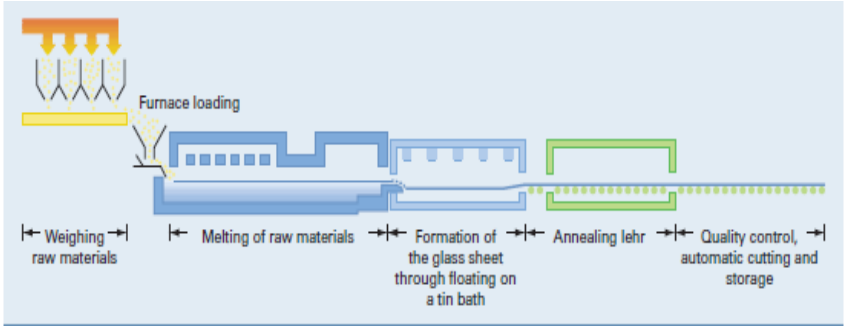

Figure 2.2 Manufacturing of float glass (James, 1913)

2.3 Basic physical and mechanical properties glass

Glass is a homogeneous or isotropic material (James, 1913). The physical and mechanical properties of silicate glass are presented in Table 2.1.

Table 2.1: Basic physical properties of soda lime and borosilicate glass (Haldimann, 2006; Maria, 2011)

Properties	Symbol	Soda-lime silicate glass	Borosilicate glass
Density (Kg/m^3)	ρ	2500	2200-2500
Young's modulus (MPa)	E	70000	60000-70000
Poisson's ratio	μ	0.23	0.2
Shear modulus (MPa)	G	28455	25000-29166
Hardness (Gpa)	HM	6	4.5-6

Glass has micro defects inherently, which are also called surface flaw. The concept of glass flaw was introduced by A.A Griffith in 1921. The same author described the existing surface flaw as significantly influencing the glass strength. Micro defects are originally generated from the glass manufacturing process and they occupy on both surfaces in a random manner. The strength of annealed glass is shown Table 2.2 (Maria, 2011).

Table 2.2: Different range of strength properties of brittle glass

Compressive strength	Tensile strength	Bending strength
880-930 MPa	30-90 MPa	30-100MPa

2.4 Type of soda-lime silicate glass and typical strength values

In the modern glass industry, the annealed glass, heat-strengthened glass, thermally strengthened glass (toughen glass) and chemically strengthened glass are typical glass types. The typical stress values are summarised in Table 2.3 and also, typical failure patterns of these glass types are shown in Table 2.4.

Table 2.3: Ultimate tensile and compressive stress for all glass types

Glass type	Tensile strength (MPa)	Compressive strength (MPa)
	Leitch (2005)	IstructE (1999)
Annealed Glass	45	n/a
Heat-strength glass	70	25 - 40
Tempered glass	120	69
Chemically strengths glass	n/a	n/a

Table 2.4: Typical failure and fragmentation patterns (Stiles, 2010; James, 1913; www.robinson-solutions.blogspot.co.uk)

Glass Type	Annealed	Heat-strength	Toughened	Chemically strengthened
Typical failure pattern			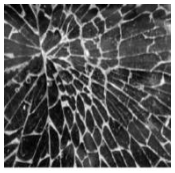	

2.5 Standard sizes of annealed glass

The standard sizes of glass available in the market vary from 400 x 400 mm to 2400 x 2400 mm with typical thicknesses of 3, 4, 5, 6, 8, 10, 12, 15, 19, and 25 mm (James, 1913; IstructE, 1999).

2.6 Laminated safety glass

Modern laminated glass is a type of safety glass, which became popular recently in building and automotive industries, because it provides a safe failure feature. Laminated glass has been manufactured by two or more thin glass plies permanently bonded with Polyvinyl Butyral (PVB), Ethylene Vinyl Acetate (EVA) or other interlayer materials (Figure 2.3) (IstructE, 1999; Weller et al., 2005). The interlayer material can prevent broken glass pieces shattering and falling off from support frame and thus reduce serious a hazard.

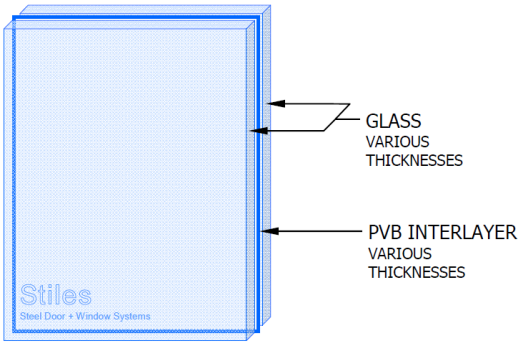

Figure 2.3: Configuration of laminated glass (Stiles, 2010)

2.6.1 PVB (Polyvinyl Butyral) interlayer

PVB is a type of film specially made with sheet form for laminated safety glasses (James, 1913). It has hyperelastic and viscoelastic material behaviours. Also PVB is also a non-corrosive product and includes some additional features such as transparency, insulation, impact resistance, water resistance and tearing resistance (IstructE, 1999 and Weller et al., 2005).

The PVB will alter the response of glass when it is used combination with glass. The key mechanical properties of PVB material are outlined Table 2.5. The elastic modulus (E) and Poisson's ratio (v) are calculated by Equation 2.1 and 2.2 (Zhao et al. 2006) and also used for present study.

$$E = (9KG_0) / (3K+G_0) \quad (2.1)$$

$$v = (3K - 2G_0) / (6K + 2G_0) \quad (2.2)$$

where K and G_0 are the bulk and shear modulus for the PVB material.

Table 2.5: Mechanical properties of PVB materials

Properties	Zhao et al. (2005)	Maria (2011)	Xu et al. (2011)
Bulk modulus (K) (GPa)	20	n/a	20
Young's modulus (E) (MPa)	n/a	6.3	n/a
Poisson's ratio (μ)	n/a	0.4	0.49
Shear modulus (G_0) (GPa)	0.33	n/a	n/a

For commercial purposes, available PVB interlayer thicknesses are specified by the multiples of 0.38 mm, i.e 0.38mm, 0.76mm and 1.52 mm.

2.7 Laminated glass standard size and thickness

The strength of laminated glass depends on the make-up of individual components and their thickness. Ledbetter et al. (2006) pointed out that different types of glasses can be used to produce the laminated glass and yield different strength. According to ASTM-E1300, available top and bottom glass plies and PVB interlayer thicknesses are summarised in Table 2.6. In this study, those highlighted thicknesses in Table 2.6 in addition to be a bespoke thickness (6.0/0.38/6.0) will be considered. All panel sizes are 1 m x 1 m.

Table 2.6: Standard sizes of laminated glass (Norville et al., 1998)

Laminated glass thickness Designation in ASTM E1300 (mm)	Nominal thickness Glass/PVB/Glass (mm)	Minimum thickness Glass/PVB/Glass (mm)
5	2.5/0.38/2.5	2.16/0.38/2.16
5	2.5/0.76/2.5	2.16/0.76/2.16
6	2.7/0.76/2.7	2.59/0.76/2.59
6	3.0/0.76/3.0	2.92/0.76/2.92
6	3.0/1.52/3.0	2.92/1.52/2.92
8	4.0/0.76/4.0	3.78/0.76/3.78
10	5.0/0.76/5.0	4.57/0.76/4.57
11	5.0/1.52/5.0	4.57/1.52/4.57
12	6.0/0.76/6.0	5.56/0.76/5.56
13	6.0/1.52/6.0	5.56/1.52/5.56
16	8.0/0.76/8.0	7.42/0.76/7.42
19	10.0/0.76/10.0	9.02/0.76/9.02

2.8 Impact

Impact is common in the construction, automotive, military, navel, and offshore, aerospace and sport equipment industries. The impact phenomena and impact induced damages are significantly considered, in particular, when brittle materials are involved (Stronge, 2004). This chapter presents a brief review on impact research.

2.9 Nature of impact

It is important to understand the category of impact in terms of the hitting velocity as documented by Backman and Goldsmith (1978), Ball and McKenzie (1994) and Børvik (2001). In summary, the impact velocity regimes are categorised as low velocity, sub-ordnance velocity, ordnance velocity, ultra-ordnance velocity, and hypervelocity and highest velocity. Moreover, each regime has been represented by specific test methods, test apparatus and material test method as is shown in 2.7.

Some researchers have investigated the impact problem by using different impact velocity range with different terms, e.g, that below 250 m/s in low–velocity limit (Zukas (1990), between 500 - 2000 m/s in ordnance velocity limit (Zukas 1990). In this investigation, the low-velocity free fall object impact will select an impact velocity range of 0 – 50 m/s and a steel ball or sphere is the impactor.

In order to classify impact velocity regimes, the importance of characteristic material behaviour of target and impactor was also outlined by Backman and Goldsmith (1978). The-

Table 2.7: Velocity regimes and representative applications and test methods subject to impacts (Backman and Goldsmith, 1978 and Børvik, 2001)

Velocity regime	**Impact test equipment**	**Material test method**	**Typical applications**
Low velocity 0-50 m/s	-drop hammer -pneumatic acceleration	Quasi-static testing machine -hydraulic	- dropped objects - vehicle impact - ship collision
Sub-ordnance 50-500 m/s	-compressed air gun -gas gun	-pneumatic -hydraulic -Taylor impact test -Split Hopkinson Pressure (SHPB)	- free falling bombs And missiles -nuclear industry -fragments due to bomb explosions - fragments due to hurricanes
Ordnance 500-1300 m/s	-compressed gas gun -powder gun	- Taylor impact test -SHPB	- military industry
Ultra- ordnance 1300-3000 m/s	-powder gun -two-stage light gas gun	- Taylor impact test(Plate impact)	- military industry
Hypervelocity > 3000 m/s	-two –stage light gas gun	- Taylor impact test (Plate impact)	- space industry
Highest velocity >12000 m/s	n/a	n/a	n/a

material response was classified as: (1) the elastic response of projectile and target; (2) the plastic deformation in target; (3) the target penetration or propagation in elastic and plastic conditions. In addition, the motion of the projectile, the motion of the target, local deformation and the local damages in the contact area were defined.

As mentioned above, the motion of projectile or impactor is also important in impact event and it is required to satisfy the energy field (kinetic energy) at the beginning of the impact process until the first contact instance occurs. During the impacts, the projectile kinetic energy is transferred into the target under different energy forms, for example fracture energy, thermal energy, kinetic energy, and damage. Similarly, Corran et al. (1983) described the target and impactor material response depending on the impact energy. During the first contact, the target material response is described as follows:

- Elastic vibration in the plate and that dissipate energy at the clamp;
- Plastic deformation in member stretching, bending and shear;
- Local plastic deformation around the projectile

It is also important to understand the difference between projectile and impactor in impact analysis. The main feature of the projectile is to have a striker to generate the initial impact velocity with various angles. The free fall object/tool has been described as impactors. This initial impact velocity is simply written as $v = \sqrt{2gh}$, where v and h are the free falling object hitting velocity and falling height and g is the gravity load equal to 9.81 m/s^2 (Belingardi and Vadori, 2002).

Ryan (1992) reviewed the velocity regime for high and low velocity impacts and the high velocity impact limit was also called the ballistic limit. The target exhibited higher amount of strain rate, sound–wave speed, energy absorption, vibration and stress wave propagation in the high velocity impacts (Backman and Goldsmith, 1978 and Børvik, 2001). However, the target response of low-velocity impact is slightly different when compared with high-velocity impact. The low-velocity impact velocity limit is much lower than the sound-wave propagation speed of the target structure (Ryan, 1992).

Cremona Rebecca and Hinkley Jeffrey (2005) numerically studied the local deformation and energy absorption behaviour of ductile polymer target under low-velocity (2.6 m/s) and high-velocity (260 m/s) impacts. The impact response of the target structure is clearly indicated in Figure 2.4. It can be seen that the localized deformation varies significantly when subjected to high velocity impact, which means that the target with large deformation (plastic deformation) induces damage and some energy storage, energy dissipation and energy absorption during impact. Figure 2.4 also shows the target flexural behaviour, but no damage and energy absorption of the target at the low impact velocity.

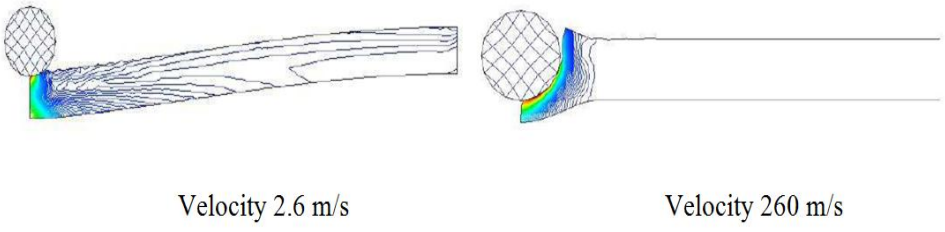

Figure 2.4: Target response under low and high velocity impacts (Cremona Rebecca and Hinkley Jeffrey, 2005)

The low-velocity impact response of target structure has been assumed to be like a quasi-static load response in many impact events. According to this, the low-velocity drop-weight impact test and the quasi-static test are proposed to examine the similarity and distinct behaviours by various researchers, e.g. Swanson, 1992), Nettles and Douglas, 2000) and Li et al., 2012).

Nettles and Douglas (2000) used the low-velocity drop-weight impact test and quasi-static load test to compare the response of laminated composite plates. Both test results indicated similar shape and size damage on plate at the loading level. They also compared the impact load/deflection response of the composite plate under the low-velocity impact and quasi-static conditions and results showed that the deflection exhibited good agreement until the peak level, but a large deviation of deflection during the unloading stage. This suggests that a high similarity prevails during the loading stage between the low-velocity impact and quasi-static analysis. Li et al. (2012) stated that the response between the low-velocity impact and quasi-static indentation show no significant difference and the quasi- static indentation test results were sufficient to produce clear observations of low-velocity impact. Swanson (1992) and Nettles and Douglas (2000) stated that the low-velocity impact results can well resemble a quasi-static test.

Highsmith (1997) pointed out that the impact and quasi-static tests will produce a different response on targeted structure based on the stiffness, loading and damage behaviour of the target structure. Christoforou and Yigit (1998) stated some limitations on the similarity studies between the low-velocity impact and quasi-static loading tests. Moreover, Lagace et

al. (1993) carried out static indentation and low-velocity impact tests to identify the damage propagation and the response of the composite plates. They performed an investigation under two supporting conditions such as clamped support and rigid edge support. During the investigation, they found that the low-velocity impact based composite plate exhibited a higher amount of a damage and more significant impact response.

There are a combination of influencing factors including the geometry and material properties of the impactor and target structure. Zukas (1982) listed a number of different influencing characteristics of projectile including impactor's nose geometry, density, trajectory, impact condition, contact location and final shape after impact. Backman and Goldsmith (1978) listed the following influencing factors:

- Impact angle of the projectile
- Characteristics material behaviour of target
- Characteristics material behaviour of the projectile
- The regime of the initial impact velocity

In real world impact problems, the hitting objects are naturally of various regular and irregular geometric shapes. These geometric shapes are idealized by various researchers in order to analyse impact problems numerically and experimentally. Goldsmith (2001) outlined the most common geometric shapes for the projectile nose as shown in Figure 2.5.

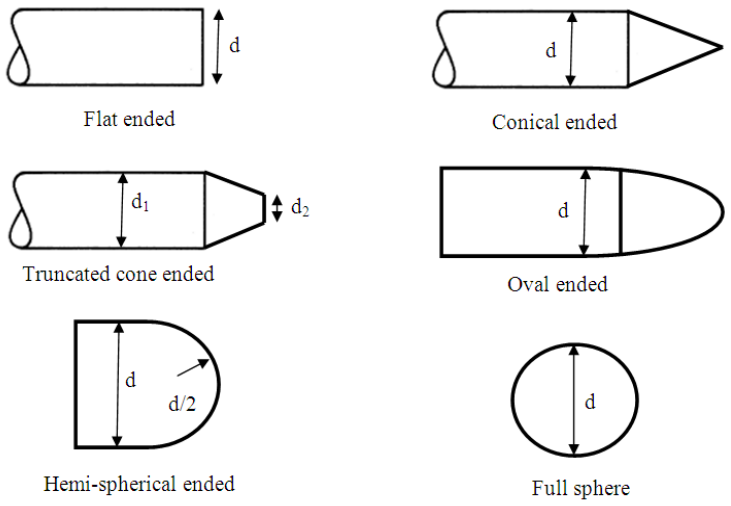

Figure 2.5: Projectile or impactor nose shapes for experimental and numerical investigations (Goldsmith, 2001)

Backman and Goldsmith (1978) also investigated the impact–induced damage patterns of ductile target using various shape steel projectiles. Goldsmith and Finnegan (1986) carried out experimental investigations by using two projectile shapes of cylindro-conical and cylindrical and with two different materials of steel and mild steel impacting on aluminium plate with rotating impact angle of 50^0 from normal. Both investigations found that the target perforation (failure pattern) depends on the interaction between target and projectile as well as other factors such as material properties, projectiles geometry and impact velocity

2D finite element and experimental methods were used to investigate the different projectile shapes impacting ductile targets (Børvik et al., 2002). The blunt, hemispherical and conical shape projectiles were also used identified the various failure patterns and some critical stress fields of target structure. The investigation found that the target energy absorption and failure pattern were directly influenced by projectile nose geometry.

For tool drop impacts, a common geometric shapes (sphere, hemi-spherical, flat or blunt ,cylindrical and conical) of impactor has been study by many researchers, namely, Shutov et al. (2004) , Liu and Liaw (2009) , Zhu and Chai (2010) , Kishi and Bhatti (2010) , Liu (2011) and Dhakal et al. (2012).

The impact angle of projectile or impactor will also have a significant effect on the overall damage response and failure pattern of the target structure. It is also important to make a clear estimation with regards to the proportion of the absorbed, dissipated and stored energies between the target and projectile. Bitter (1963) performed a series of experimental investigations on the local erosion of the ductile and brittle targets using normal and oblique impacts, and it was found that the maximum damage erosion occurred on a ductile target surface with the impact angle between 20^0 and 30^0 and on the brittle target surface with the impact angle at 90^0. Similarly, oblique and normal impact erosions of ductile and ceramic targets were conducted by Alman et al. (1999). They also found that the maximum damage erosion of ductile surface occurs at an oblique angle between 20^0- 40^0 and the brittle surface damage erosion occurs with the impact angle at normal to surface (90^0).

Aquaro and Fontani (2001) investigated the brittle and ductile materials erosion process numerically, analytically and experimentally considering normal and oblique impacts. They established that the peak impact erosion angle for ductile and brittle material surfaces 20^0 and 90^0, respectively. Wang and Yang (2008) studied a similar problem. It was concluded that the erosion behaviour of ductile surface was maximum at the impact angle between 20^0- 30^0 and the material erosion of brittle surface was slightly increased when the impact angle was 90^0 or

normal to the surface. Wang and Yang observed oblique impact erosion and normal impact damage behaviour of the two surfaces shown in Figure 2.6.

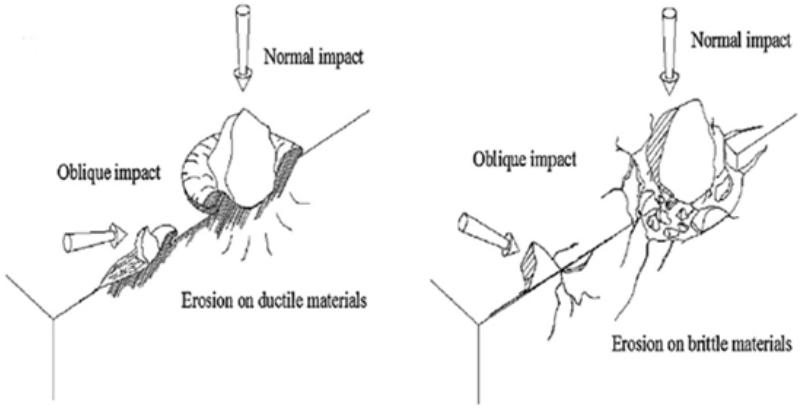

(a) Erosion of ductile materials (b) erosion on brittle materials

Figure 2.6: The erosive failure behaviour of ductile and brittle (Wang and Yang, 2008)

The target geometry is another key influencing parameter on impact dynamics. Various shape targets (e.g. beams and flat plate) have been employed for investigating the impact problems. Schonberg et al. (1987) conducted a low-velocity impact study on isotropic beams and plates under two different support conditions (simply and rigid). They stated that the self-weight or mass of the beam and plate had significant influence of the overall dynamic response. Goldsmith (1964) and Abrate (1998) summarised a series of analytical, numerical and experimental investigations performed by various researchers. It included the classical plate and beam theories used for dynamic impact analysis. They established evaluation solutions for the plate flexural, membrane and shear.

2.10 Impact investigations

For impacts, the number of responses that have been considered for evaluation include impact force, displacement, acceleration, impact energy, energy absorption, impact velocity, damage patterns, contact duration, residual velocity in penetration and the amount of fragmentation.

Goldsmith (1964) performed elastic impact response analysis for the beam and plate structures by using an analytical method with different parameters. They evaluated the impact responses such as the force-time history, contact duration, displacement and velocity. Abrate (1998) used a number of analytical models to predict the impact responses of two different composite structures such as beams and plates. The contact force-time history and total response were studied as well as the parametric effect of target dynamic response, projectile motion and projectile local indentation.

Stronge (2004) performed a numerical method to evaluate the structural response of different materials by using multibody impacts. This study considered the colliding objects' impact velocity –time history and displacement-time history.

Feraboli and Kedward (2004) performed a series of experimental studies to evaluate the low velocity impact response of composite plates. Part of the research was used to discuss the challenges arisen from the large number of parameters in experimental study and their effects on impact evaluation. Two parameters of contact duration and the target coefficient of restitution were studied. More recently, Feraboli and Kedward (2006) also proposed using the Composite Structure Impact Performance Assessment Programme (CSIPAP) to assess and

evaluate the impact performance of composite structures, which concerned multiple parameters namely, critical impact force, dissipated energy, contact duration and coefficient of restitution (COR).

2.11 Experimental methods and drop-weight test

A number of experimental impact test methods are outlined by Backman and Goldsmith (1978) and Børvik (2001). Typically used impact test methods are listed in below:

- Quasi –static test
- Drop –weight test
- Pendulum test
- Gas-gun test
- Split Hokinson pressure bar test

As discussed above, the drop-weight tests are used to simulate the low-velocity impacts. In laboratory, the free fall object impact tests are used with different names, such as drop-dark test, drop-tower test, tool-drop test, drop-weight and ball- drop test.

Many researchers have used the low-velocity drop-weight test to deal with impact behaviour of single and multilayer structural components (Belingardi et al., 2002, Aretxabaleta et al., 2005, Liu and Liaw, 2009 and Zhu and Chai, 2010). However, the concept of free falling object impacts and its effect on structural components is described by Aretxabaleta et al.

(2005).They proposed that the low-velocity regime is the exact velocity, which is produced by large mass impactor during drop-weight impact analysis. They used the 2D finite element model to simulate the stresses distribution in the target structure during the impact. Figure 2.7 shows the distributed compressive and tensile stresses near the target top surface and bottom surface as well as some compressive stress near supports. The transferred impact force between the impactor and the specimen were also evaluated.

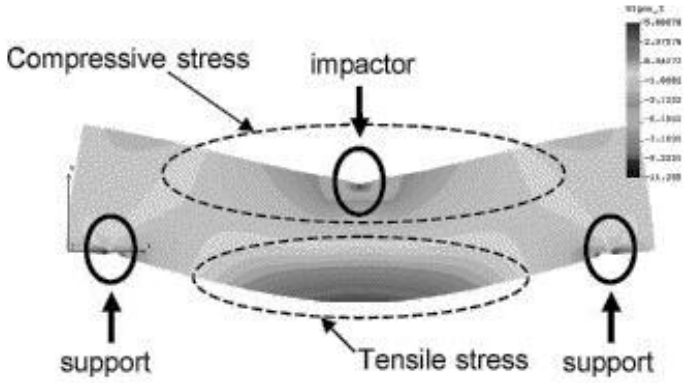

Figure 2.7: FEA stress distribution of three point bending impact model (Aretxabaleta et al. 2005)

2.12 Experimental implementation of impact events for single layer monolithic glass and multi-layer laminated glass

Studies of impact-induced damage on monolithic and laminated glass have been carried out by a limited number of researchers over the past four decades, e.g. Langitan and Lawn (1968), Wiederhorn and Lawn (1977), Kirchner and Gruver (1977), Ball and McKenzie (1994), Ball (1997),Grant et al. (1998) , Grant and Cantwell (1999), Bouzid et al. (2001), and Shutov et al.

(2004). The main features of these investigations are the impactor geometry, drop velocity, material properties and boundary conditions background theories.

As discussed above, the amount of micro defects influences the strength and fracture of the glass. Bouzid et al. (2001) pointed out that the propagation of micro-defects was significantly increased with loading. Furthermore, the brittle glass will exhibit different fracture patterns and follow failure criteria under different load cases such as static and dynamic loads (Langitan and Lawn, 1968).

The impact damage response of single layer glass plate impacted by projectiles of three different materials (glass, steel and nylon) was investigated by using an analytical method and an experimental method for the velocity range below 115 m/s (Kirchner and Gruver, 1977). This study considered a number of responses of the glass plate subject to impact such as contact area, crack length, crack angle, crack patterns, impact velocity and projectile rigidity. The cone, radial and lateral vent cracks and plate crush were identified as the main cracking patterns. They also examined the strength degradation of glass plate under different velocity and projectiles impact and it was found that the increasing velocity of the projectile will penetrate glass plate and the overall strength of the glass plate is reduced by approximately 20% after the impacts. Similarly, the impact study based on the rigidly supported glass plate was performed to investigate the localised damage and kinetic energy loss. The spherical shape impactor made of glass material was used at a velocity of up to 138 m/s. This investigation observed the cone and radial cracks and plate crush during impacts and it was found that no localise damage occurred at velocities up to 29.4 m/s, cone cracks at 30.6 m/s,

radial cracks at 38.8 m/s and the plate crush at 125.8 m/s. There was also a significant amount of kinetic energy losses roughly from 21% - 58% of the glass plate (Kirchner and Gruver (1978).

However, a similar type of impact fracture pattern was identified by Kirchner and Gruver (1977) at an early stage with an impact velocity from 22 m/s to 115m/s. Wiederhorn and Lawn (1977) extended the investigation to a similar target material of brittle glass plate whilst using steel sphere as impactor. The target strength reduction factors were stated, which is dependent on the projectile velocity, density, radius and the target structure toughness, hardness, respectively. The Hertz contact theory proposed to predict the glass plate strength degradation and that was based on steel sphere at velocities from 2 – 300 m/s. The impacted glass plates exhibited two different failure patterns of cone and radial (median) cracks in that velocity range.

Float glass plate with the various thicknesses (3mm – 12mm) was subjected to low-velocity impact and experimentally studied by Ball and McKenzie (1994). The impacts used steel ball as the impactor with a diameter of 3mm and an impact velocity range of 10 – 50 m/s. The authors considered the glass plate front and back (rare) surface damages and the contact surface of the glass plate ring, cone, median, radial and lateral cracks and plate crushed, whilst the rare side of the plate was indicated star shape fractures. They also stated that the factors that influence glass damages include the projectile size and impact velocity and the plate boundary conditions, thickness, surface flaw (micro cracks) and impact stress levels. More

graphical detail of monolithic glass plate impact failure patterns is summarised in Appendix A, Figure A.1 and A.2.

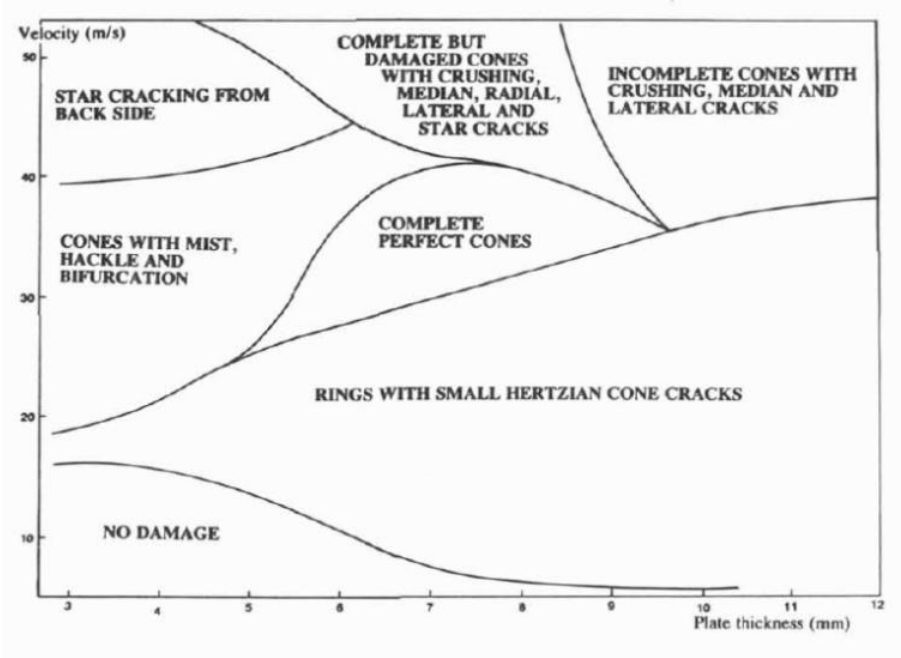

Figure 2.8: Single layer glass plate failure patterns (Ball and McKenzie, 1994)

Experimental drop-weight impact investigation of monolithic plates (ex. glass, ceramics, and acrylic) have been conducted at a relatively limited level by researchers such as Bouzid et al. (2001), Shutov et al. (2004), Liu and Liaw (2009) and Zhu and Chai (2010). The evaluation of damage and fragmentation of monolithic glass plate under impacts was investigated using theoretically (damage volume concept) and experimentally (Hopkinson press bar test and drop ball test) by Bouzid et al. (2001).

From both tests, the impact damage patterns of the glass plate were observed. It was found that the radial (star) cracks are occurred in drop ball impact based glass plate and the surface

crush, perforation, radial and later cracks are occurred from pressure bar test. The generated fracture patterns of each glass plate are summarised in Figure 2.9.

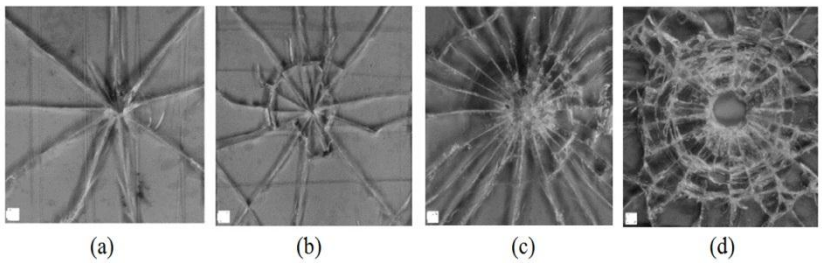

Figure 2.9: Monolithic glass plate impact damage patterns – (a) and (b): drop ball test; (c) and (d): Hopkinson pressure bar test (Bouzid et al., 2001)

A drop-weight impact of acrylic plate under different velocity and temperature was investigated by Liu and Liaw (2009). This approach mainly considered the failure and damage response of the acrylic plate and the radial or star shape crack patterns were found on all acrylic plates. Therefore it was concluded that the crack pattern are of brittle failure pattern at velocity lower range (Figure 2.10).They also concluded that the sudden deviation of contact force occured at peak level and it was a sign of radial crack initiation of the acrylic plate (Figure 2.11). More recently, the low-velocity drop-weight impact damage response of acrylic and polycarbonate was investigated and the brittle and ductile material response of the acrylic and polycarbonate were found, respectively (Zhu and Chai, 2010).

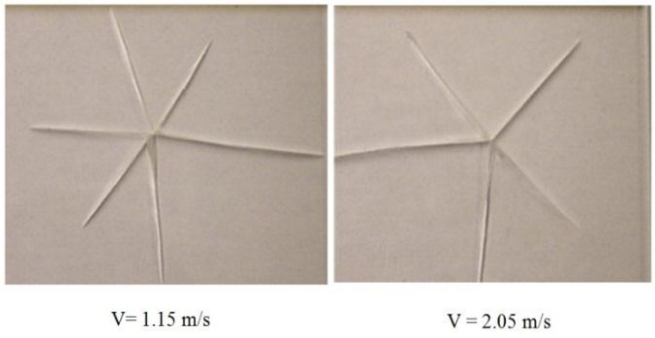

Figure 2.10: Star crack on acrylic plate with different velocities (Liu and Liaw, 2009)

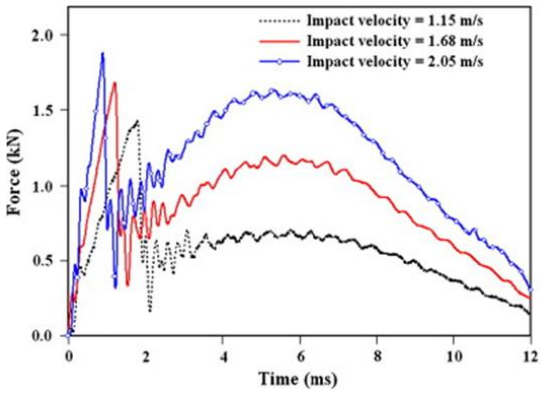

Figure 2.11: Contact force time history of acrylic plate under different velocities (Liu and Liaw, 2009)

Ball (1997) studied the impact stress induced fracture propagation at the front and rare surface of laminated glass-polymer plates experimentally. Plates of various thicknesses (3mm – 12mm) and two different interlayers of PVB and PVC were tested by the steel projectile of diameter 5mm with impact velocity from 10 – 100 m/s. It was found that the laminated glass-polymer plate exhibited the cone and star shape fracture patterns for various velocities and thicknesses.

Grant et al. (1998) carried out an experimental investigation on the overall impact resistance of the automobile laminated glass plates with various inner and outer glass ply thickness and constant PVB interlayer thickness (0.76mm). The projectile impact velocity was in the low-velocity range between 4 – 20 m/s and it was used to observe the damage initiation velocity and damage pattern of the laminated glass plates. They observed mainly four different impact fracture patterns on laminated glass plates such as surface crushing (scratching), star, cone and combine (star, cone, crushing) cracks and it was pointed out that the effect of glass ply thickness is much more significant in damage propagation and impact resistance compared to the other impact parameters, such as impact angle, indenter radius and impact velocity.

In protective glass category, the old type wire glass was used to investigate the ballistic impact damage response with various wire mesh thickness, projectiles (steel, glass, tungsten) and impact energy (0.5 - 40J) (Boccaccini et al., 2007). This test also identified very common impact failure patterns from wired glass plates, which included cone, lateral and radial cracks patterns. The authors found that the amount of damage significantly increases with impact energy and projectile diameter.

Low-velocity, drop weight impact damage of laminated glass plate with dimensions of 500mm x 500 mm were studied using a large mass impactor (4.11kg) with various drop heights (3.5, 6.5 and 9.5 m) by Shutov et al. (2004). They found some impact fracture patterns of laminated glass for various thicknesses, but the name of the exact fracture pattern has not been concluded. However, damage results observed in this investigation seems to be quite

similar to the surface crushing and lateral and radial cracks. The fracture pattern is shown in Figure 2.12.

Figure 2.12: Drop ball impact fracture pattern of laminated glass plate (Shutov et al., 2004)

2.13 Numerical implementation of impact events

There are a number of numerical methods (FEM - Finite Element Method, DEM – Discrete Element Method, BEM - Boundary Element Method, FDM - Finite Difference Method) that have been used for solving different type of engineering problems. Commercial software packages such as ABAQUS, ANSYS, NASTRAN and LS-DYNA are used world-wide. The main features of these commercial software packages are include 2 or 3 dimensional element libraries (e.g. solid, shell, beam, truss, infinite elements) and a material library (e.g. elastic, plastic, hyperplastic, viscoelastic etc.). Furthermore, these packages are regularly used in various engineering problems such as statics, dynamics, and heat transfer etc. Finite element (FE) numerical technique can be used for different types of impact analysis such as normal and oblique impacts. Moreover, the impact induced linear, nonlinear and damage responses can be effectively modelled and analysed by FE technique. In finite element method, the

nonlinear behaviour of structural components depends on applied materials and contact conditions, geometric properties.

Two approaches are normally used in conducting dynamic analysis by using FEA package, i.e. implicit and explicit methods. The explicit method is an appropriate analysis option in order to investigate the transient dynamic problems numerically, such as low and high velocity impacts, blast loads, shock waves, material erosions and seismic analysis (ElTobgy et al., 2005, ABAQUS, 2010a, Khalili et al., 2011 and Poola, 2011).

The main disadvantage of FE 2D option is that the model cannot capture some required fields in structural components with complex geometries, e.g. surface cracks propagation over the surface. But this shortcoming can be overcome by using a 3D finite element method which can capture complex geometries, lateral cracks and damages as well as some parameters in all directions such as accelerations, displacements, principal stresses and strain. The only disadvantage of a 3D FE technique is the large amount of computational time required to simulate the full numerical model. In order to reduce the computational run time, a half or quarter symmetric 3D FE models are used if the model shows symmetric features (ElTobgy et al., 2005, Kishi and Bhatti, 2010, Aryaei et al., 2010 and Khalili et al., 2011). For impacts, a number of researchers have been used 3D finite element models as shown in Figure 2.13 (Nandlall and Chrysler, 1998 and Nandlall and Wong, 1998, Foo et al., 2008 , ElTobgy et al., 2005 and Zhu and Chai, 2010).

As previously discussed, the element types are categorized by the dimensional form, i.e. one-dimensional (1D), two –dimensional (2D) and three- dimensional (3D) elements.

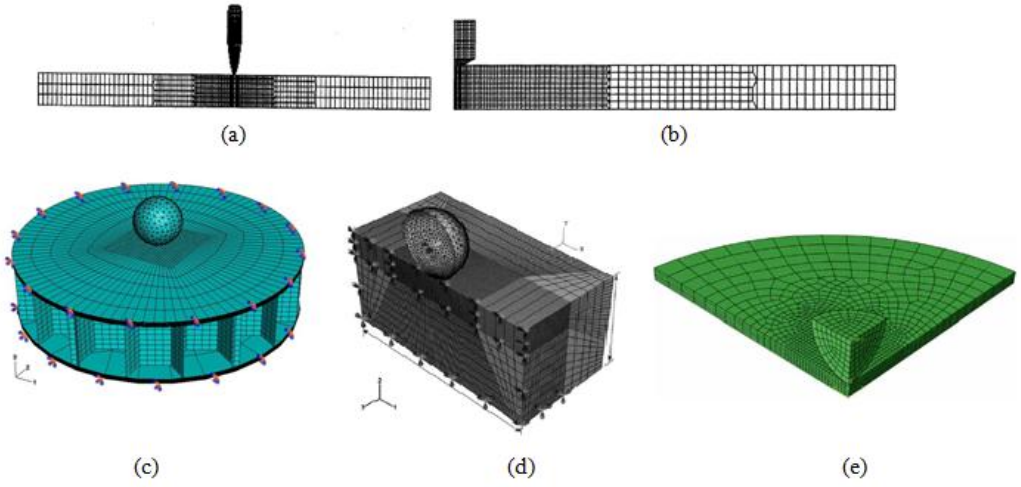

Figure 2.13: Finite element (a) 2D plane (b) 2D axisymmetric (c) 3D full model (d) 3D half a symmetric (e) 3D quarter symmetric models

ElTobgy et al. (2005) used numerical modelling technique to evaluate and observe impact erosion of a titanium (Ti-6AL-4V) specimen. Their model included the Johnson Cook material model, stress/strain rate dependent failure criteria, ABAQUS/Explicit analysis method, half symmetric geometric section, 8-node solid elements and 4-node tetrahedral elements and surface based contact between specimen and impact particles with friction value of $\mu = 0.2$. The fine and coarse mesh patterns were employed in the impact and non – impact zones of the target specimen, respectively. The erosion of target spacemen was observed. Chakraborty (2007) also employed a fine mesh pattern for projectile contact zone of the composite plate. and the contact zone meshed by 8-node layer elements. The impact force-time, plate displacement-time, impactor displacement-time and impact velocity-time histories were evaluated to predict the impact response in the composite plate.

Pashah et al. (2008) predicted the low-velocity impact response of simply supported beam by using the numerical and analytical methods. A full model was used to investigate the elastic and elastic-plastic responses of the beam, numerically. In the model, the following elements were included: the target and projectile exhibiting deformable body response, surface based contact with friction (penalty) and the element types of 4-node linear tetrahedron (C3D4) and 8-nodel solid element (C3D8R), respectively. The investigation examined the influence of contact duration, impact velocity, beam contact stiffness and impact mass.

Liu and Liaw (2009) studied the drop-weight impact response of acrylic plate using the Using 3D finite element method. The acrylic plate was discretized by 8-node solid elements and the similar element type was employed with rigid body material model for the steel ball. The acrylic plate had a tensile stress failure criterion and was assumed to have a linear elastic material response. The damage behaviour of acrylic plate was only identified by the observation of a sudden drop of the force-time curve, but did not show the exact damaging pattern numerically. Similarly, Zhu and Chai (2010) proposed a numerical model used to deal with the low-velocity drop-weight impact response of acrylic and polycarbonate plates and the two plates were assigned with the brittle and ductile damage models, respectively. The contour plots, force-time and force-displacement histories were presented to evaluate the acrylic plate cracks initiation and the polycarbonate plate deformation, respectively.

Rusinek et al. (2009) modelled mild steel plate by using 3D finite element method and ABAQUS/Explicit solution technique for high-velocity projectile impacts. The suggested the optimum element size being approximately 0.1mm x 0.15 mm x 0.15 mm (see Figure 2.14).

Kishi and Bhatti (2010) modelled the reinforced concrete beam for drop weight impacts by using tensile fracture energy model. The beam element with uniform mesh pattern and a surface base contact with frictionless effect were included in the model. The impactor drop-weight velocity is 14 m/s and the total contact duration was set up to be 400ms (millisecond) and the model analysis time increment was around 0.8 μs. Khalili et al. (2011) proposed the numerical model to analyse the low-velocity elastic impact response of the composite plates and cylindrical shells. The 8-node continuum shell (SC8R) elements and 4-node conventional shell elements (S4R) were used to create the mesh in composite plate and cylindrical shell, respectively. In analysis, the element verification, convergence and parametric studies were conducted. They stated that the accuracy of impact models depends on the type of elements, mesh arrangement, solution method and impactor rigidity, contact behaviour between impactor and target. They also recommended that the explicit algorithm is a useful technique to solve transient dynamic events.

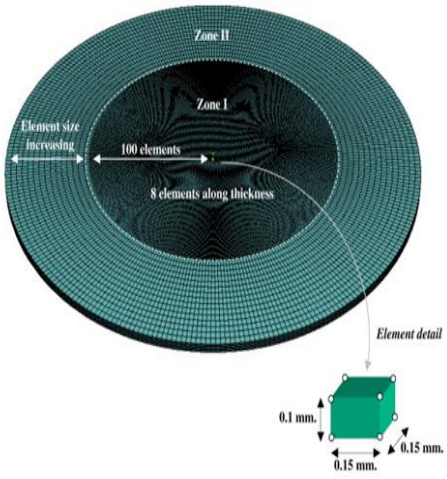

Element Type	C3D8R
Number of elements	229792
Number of Nodes	259875

Figure 2.14: Mild-steel plate optimum element size and mesh summary (Rusinek et al., 2009)

2.14 Numerical implementation of impact events for single layer monolithic glass and multi-layer laminated glass

Flocker and Dharani (1997a) studied the impact failure response of laminated architectural glass plate by using a hard missile projectile at a low-velocity of 35.8 m/s. A cone shape failure pattern has already been found which was characterised by the cone angle, cracking depth and the rate of cone crack propagation.

Similarly, Flocker and Dharani (1997b) numerically investigated the impact induced damage response of laminated glass plate subjected to missile projectile impact at low-velocity of 10m/s. The laminated glass model was constructed by 2D axisymmetric elements with 4642 nodes for projectile and 17058 nodes for PVB and glass layers. The impact induced stresses of laminated glass plate were analysed and it was found that an increase panel size and interlayer thickness significantly reduced maximum principal stress in the non-impact side of the glass plate and also found higher principle stress in the laminated glass plate when increasing projectile mass and velocity. However, this investigation did not discover any failure, penetration and damage pattern of laminated glass plate.

Flocker and Dharani (1998) subsequently modified their previous experiments by increasing the number of layers and layer thickness for low-velocity small missile impact. They concluded that three layer laminated composite sections had a higher impact resistance than the five and seven layer composite sections. Ji et al. (1998) studied the probability of damage in laminated glass under a low velocity missile impact. They identified cone failure patter on

the impact side of the glass ply, but no significant effect from PVB interlayer for this failure pattern. They also concluded that damage probability at the impact side glass ply depended on impact velocity and the strength of glass ply and the thickness. The results of this investigation include the surface crack initiation, the cracks propagation in thickness direction and the ultimate impact failure response. Dharani et al. (2005) addressed the importance of numerical investigation for damage evaluation of the laminated architectural glasses. They pointed out that under impacts, the viscoelastic nature of laminated glass and its behaviour could be conveniently analysed by the 3D model as well as a nonlinear finite element method.

Zang et al. (2007) used three dimensional finite element (3D FEM) and discrete element methods (3D DEM) to analyse the impact response of the monolithic and laminated glass plates, which included elastic and damage analysis, respectively. A uniform mesh was used to discretize the glass plates, impactor and PVB interlayer of the numerical model. They considered a solid element with a size of 0.38 mm for DEM models and 0.76mm for FEM models. This investigation found that the FEM elastic analysis results closely agreed with DEM results but disagreement arose in the damage analysis. It is also noted that very limited research has been conducted for impact on a single layer monolithic glass.

Timmel et al. (2007) proposed a model for the laminated glass impact response, which included the impact damage propagation of laminated glass plate and the load resistance of PVB interlayer. The shell and membrane elements were used to discretise the glass plies and PVB interlayer of the laminated glass plate, respectively. The constitutive relation based on the brittle cracking model was used to model the response of each of the glass plies and the

PVB interlayer with hyperelastic models of Blatz-Ko and Mooney – Rivlin material models. Wu et al. (2010) proposed a laminated glass impact model by using the Jonson – Holmquist model for glass and linear isotropic plasticity model inter layer, respectively. They used uniform mesh for laminated glass plate and solid (cube) elements for steel ball and the optimum element size of 1.5 mm x 1.5 mm x 1.5 mm. Various parametric effects of laminated glass plate were studied such as velocity, impactor size and adhesion strength. This study also provides a velocity limit for the laminated glass plate impact damage as 100 m/s.

2.15 Summary

From the literature review, it can be found that various studies have conducted for the impact analysis of structural members, some of which are of brittle nature like glass. However, the damage analysis for monolithic and laminated glass that is used for structural purpose and experiencing low velocity impact caused by large projectile is still limited. The initiation of the impact damage and the crack propagation of glass will be crucial to the failure mechanism of glass under hard-body impact. The obtained information will also inform the characterisation of failure pattern and the development of prediction model for impact resistance of such type of glass for engineering purpose.

CHAPTER 3: ANALYTICAL SOLUTIONS FOR LOW-VELOCITY IMPACT ANALYSIS

3.1 Analytical model –introduction

Four different type of analytical models have been discussed by Abrate (1998), Abrate (2001) and Olsson (2000), which are:

1. Spring – mass models
2. Complete models
3. Energy - balance models
4. Wave propagation method for infinite thickness plate

These models will all lead to the overall impact response prediction for given structure components under various parametric conditions. Each analytical model has to make necessary simplification assumptions in order to obtain a solution. These assumptions may be the ignorance of damping and friction effects or assuming the impactor to be rigid.

The purpose of this chapter is to develop an accurate analytical model for low-velocity impact response analysis of monolithic and laminated glass plates.

3.2 The Hertz contact law and contact mechanics

Two or more object surfaces touch with each other is call contact. It can be generated as a hard and soft contact, which depends on material rigidity. The surface geometry, surface friction and damping effects are also considered as other factors in the contact process. However, the majority of surface based contacts are included in various contact theories such as Hertz, JKR, Bradley and DMT (Johnson, 1987). For these theories, the material elasticity, rigidity and some assumptions are considered specifically.

The first theory on surface based contact is introduced by Heinrich Hertz in 1882. It is called Hertz contact theory and the majority of surface based contact is vitally used. Under elastic response, two spherical shape geometries have been used to expressive the Hertzian contact theory (see Figure 3.1).

The theory is mainly described a contact force and the local indentation due to transverse load and the relationship between contact force (F) and local indentation (α) can be expressed as follows (Johnson, 1987):

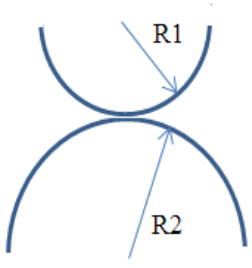

Figure 3.1: Two contact spheres with different radius R_1, R_2

$$F=k_c\alpha^{3/2} \tag{3.1}$$

The elastic contact stiffness k_c can be expressed as:

$$k_c=(4/3)\ ER^{1/2} \tag{3.2}$$

where R and E contact parameters given by:

$$1/R = 1/R_1 + 1/R_2 \tag{3.3}$$

$$1/E = (1-\nu_1^2)/E_1 + (1-\nu_2^2)/E_2 \tag{3.4}$$

where R_i, ν_i and E_i are the radius, Poisson's ratios and Young's modulus of two contact objects, respectively. Indicates i = 1, 2 two contact bodies. For the spherical objects, the deviation Eq.3.2 can be expressed following Eq.3.3 and 3.4. Therefore, The Hertz contact stiffness, k_c given by:

$$k_c = \frac{4}{3}\frac{\left(\frac{R_1R_2}{R_1+R_2}\right)^{\frac{1}{2}}}{\left(\frac{1-\nu_1^2}{E_1}+\frac{1-\nu_2^2}{E_2}\right)} \tag{3.5}$$

The contact can also occur between two flat surfaces or flat and spherical or cylindrical surfaces. Therefore, it is important to understand some modifications with regards to contact objects of different shapes. The modified parameters of contact stiffness have been described Goldsmith (1964) and Johnson (1987).

The current study will focuses on contact between spherical (radius - R) and flat surfaces. The modified contact stiffness has been proposed by various researchers, e.g., Mittal (1987), Cantwell (2007) Schmidt and Cheng (2009),Setoodeh et al. (2009).

The modified Hertizian contact stiffness, k_c for isotropic plate given by:

$$k_c = \frac{4}{3}\frac{(R)^{\frac{1}{2}}}{\left(\frac{1-\nu_1^2}{E_1}+\frac{1-\nu_2^2}{E_2}\right)} \tag{3.6}$$

where *k*c is the modified Hertizian contact stiffness for composite plate expressed by

$$k_c = \frac{4}{3}\frac{(R)^{\frac{1}{2}}}{\left(\frac{1-\nu_1^2}{E_1}+\frac{1}{E_2}\right)} \tag{3.7}$$

3.3 Impact analytical models

3.3.1 Spring-mass models

Spring-mass model is a kind of simple and accurate analytical method for small size plate specimens. Abrate (1998 and 2001) have presented the spring-mass technique for predicting the impact dynamic response of structural plates as well as considering linear and non-linear responses, respectively. They described models to be generally categorised as a single and two degrees of freedom spring-mass models and can also be subdivided into linear two-

degree-of-freedom model (TDOF), linear single-degree-of-freedom (SDOF), spring-mass model and finally nonlinear single-degree-of-freedom (SDOF) spring-mass model. For this study, the chosen analytical models are described in the following section.

3.3.2 Linear spring-mass model

A simplified version of two-degree-of-freedom spring-mass model is based on number of assumptions. Assumptions are considered: (1) linear elastic response; (2) neglecting indentation of contact zone; (3) neglecting effective mass of impactor and structure; (4) the impactor and structure move together at contact moment. In approximation, the impact force-time history function has been derived by Abrate (1998).

$$F(t) = V(K_{bs}M_1)^{1/2} \sin \omega t \ \ (\omega t < \pi) \tag{3.8}$$

$$t = T_c = \pi / \omega \tag{3.9}$$

$$T_c = \pi(M_1 / K_{bs})^{1/2} \tag{3.10}$$

where,

- $F(t)$ is the impact force
- V is the initial impact velocity
- K_{bs} is the bending and shear stiffness (Xu et al., 2009 – Equation 20)
- M_1 is the mass of impactor or projectile
- T_c is the total contact duration

- ω is the natural frequency of structure

Without considering damages and energy loses, the single degree of freedom spring-mass model provides elastic impact response of the plate structure. Furthermore, it has a frequency function to define the total duration of contact.

3.3.3 Energy – balance model

The kinetic energy of the projectile or impactor is playing a significant role in the impact process at initial stage until reaching the contact moment and it is dissipated into the whole system with various energy forms after the first contact. The mechanism of impact energy dissipation into the system is used to express the energy-balance relationship and it is also called as an energy-balance model in literatures (Abrate, 1998 and Schmidt and Cheng, 2009). In this model, the dynamic response of the target structure is assumed to be quasi-static behaviour for low-velocity impacts. The total deformation of the target depends on the initial kinetic energy of the impactor or projectile. The system equation of energy-balance model can be expressed by Abrate (1998).

$$\frac{1}{2}MV^2 = E_b + E_s + E_m + E_c \tag{3.11}$$

where M is mass of the impactor and V is the velocity at impact movement. The E term indicates dissipated energy into system in various forms namely bending (E_b), shear (E_s), membrane stretching (E_m) and the local deformation due to the contact (E_c).

The energy-balance model simplified form written as:

$$MV^2 = K_{bs}\omega^2 + \frac{K_m\omega^4}{2} + \frac{4}{5}\left[\frac{\left(K_{bs}\omega + K_m\omega^3\right)^5}{n^2}\right]^{1/3} \tag{3.12}$$

where ω is the maximum deflection of the plate and is given by $\omega = F_{\max} / K_{bs}$, where $F_{\max}$ is the maximum impact force and n is the contact stiffness parameter equal to the K_c. In order to K_b, K_m, K_s and K_{bs} describes bending, membrane, shear and combine bending/shear stiffness and its relations given by Eq.3.13 (Shivakumar et al., 1985 and Abrate, 1998).

$$\begin{aligned}
K_b &= \frac{\left(4\pi E_r h^3\right)}{\left(3\left(1-\nu_r^2\right)a^2\right)} \\
K_m &= \frac{\left(\left(353-191\right)\nu_r\right)\pi E_r h}{\left(648\left(1-\nu_r\right)a^2\right)} \\
K_s &= \frac{\left(4\pi G_{zr} h\right)}{3}\left(\frac{E_r}{E_r - 4\nu_{rz}G_{zr}}\right)\left(\frac{1}{4/3+\log(a/a_c)}\right) \\
K_{bs} &= \frac{K_b K_s}{K_b + K_s}
\end{aligned} \tag{3.13}$$

where E_r, G_r, ν_r, h, a, a_c are the young's modulus, shear modulus, Poisson's ration, thickness, radius and contact radius of the plate. They used that the radius (a) directly for the circular plate and the assumed half value of the square plate length or width (a= l/2 or b/2) is approximately equal to radius (a), where l and b is the length and width of the square plate. Also, the half a thickness (h/2) of the plate equal to the contact radius (a_c) and it was a_c=h/2.

Abarate (1998) re-wrote this energy-balance equation by substituting maximum deflection $\omega = F_{\max} / K_{bs}$ into Eq.3.13 and assumed that the thickness higher specimens membrane stiffness is equal to zero (that is K_m=0).

$$\frac{1}{2}MV^2 = \frac{1}{2}\frac{F_{\max}^2}{k_{bs}} + \frac{2}{5}\frac{F_{\max}^{\frac{5}{3}}}{k_c^{\frac{2}{3}}} \tag{3.14}$$

For a thick specimen, it is assumed that the deformation of the structure is negligible compared to the local indentation and then the maximum contact force can be written as:

$$F_{\max} = V\left(K_{bs}M\right)^{1/2} \tag{3.15}$$

This expression provides a linear relationship between maximum the contact force and impact velocity, and the maximum contact force is independent from the total time duration of contact.

3.3.4 Wave propagation method for infinite thickness plate

There are a number of analytical implementations of using impact wave propagation as proposed by Abrate (1998),Olsson (2000) and Schmidt and Cheng (2009). The impact waves can be generated in a short duration, which a moving object impact with a rigidly supported target and the overall dynamic response is predicted by wave propagation theory. This theory is another type of closed-form, dimensionless and non-linear analytical solution technique and it has been originally developed by using flexural waves and Hertz contact law. Moreover, this theory is compatible with any kind of material properties (homogenise and non-homogenise) assumed an infinite thickness of the structural components (Tillett, 1954).

Following Newton's second law, the dynamic equation of motion for impactor is given by

$$M_1 \ddot{w} + F = 0 \tag{3.16}$$

where F is the impact force and M_1 is mass of the impactor. After double integration, the displacement of the impactor w_2 is given by

$$w_2 = Vt - \frac{1}{M}\int_0^t \int_0^t F\left(\tau^{'}\right) d\tau^{'} d\tau \tag{3.17}$$

where V and t is the initial velocity of an impactor and total time duration of the impact and τ is the time variable. The displacement of the plate (w_1) and the indentation (δ) equation are given by

$$w_1 = \frac{1}{8(I_1 D)^{1/2}} \int_0^t F(\tau^{'}) d\tau \tag{3.18}$$

$$\delta + w_1 - w_2 = 0 \tag{3.19}$$

Differentiate twice with time and incorporating Eq.3.17 and Eq.3.18 and the Hertz contact law $F=K_c\,\delta^{3/2}$, then non-linear differential equation is given by

$$\frac{d^2\delta}{dt^2} + \frac{1}{8(I_1 D)^{1/2}} \frac{3}{2} K_c \delta^{1/2} \frac{d\delta}{dt} + \frac{K_c}{M}\delta = 0 \tag{3.20}$$

To simplify the solution process, the indentation and impact time are converted to under non-dimensional variables, this is, $\bar{\delta} = \frac{\delta}{TV}$ and $\bar{t} = \frac{t}{T}$, where T is the time constant. Therefore the

non-dimensional ordinary differential equation can be expressed as;

$$\frac{d^2\bar{\delta}}{dt^2} + \lambda \frac{3}{2} \delta^{1/2} \frac{d\bar{\delta}}{d\bar{t}} + \bar{\delta}^{3/2} = 0 \tag{3.21}$$

The non-dimensional parameter of plate mobility factor (λ) is the only parameter that can change the nonlinear ordinary differential equation and the deformation of the plate. This variable described by Yang (1971) .

The initial conditions in Eq.3.21 are $\bar{\delta}(0) = 0$ and $\frac{d\bar{\delta}}{d\bar{t}}(0) = 1$ the plate mobility factor λ is given by

$$\lambda = \left(\frac{4E_g}{3} \right)^{2/5} \frac{\left(r_s^{1/5} V^{1/5} M \right)}{\left(8\sqrt{I_1 D} \right)} \tag{3.22}$$

where M, V and r_s are the mass, impact velocity, radius of the impactor, and I_1, D are the total mass and flexural rigidity ($D = \frac{E_g h^3}{12(1-v_g^2)}$, h= plate thickness) of the plate. In order to solve Eq. 3.21, we directly developed algorithm using one of the commercial software package of MAPLE.

The total contact duration can be expressed by

$$T = \left[\frac{M}{K_c V^{1/2}} \right]^{1/2} \tag{3.23}$$

Finally the peak impact force is expressed by

$$F = \left[K_c^2 M^3 V^6 \right]^{1/5} \delta^{3/2} \tag{3.24}$$

3.4 Verification of impact dynamic model

To verify the impact analytical model, the linear spring-mass and energy –balance models and wave propagation analytical method have been implemented. To validate this analytical model, the impact problem described by Wu and Chang (1989) was revisited. The steel plate has a dimension of 0.2 m x 0.2 m x 0.008 m with all four edges rigidly supported. The spherical impactor mass, diameter and initial velocity are 0.0329 kg, 20 mm and 1m/s, respectively. The steel material properties are: Young's modulus E_s=200 GPa, Poisson's ratio v_s= 0.3 and density ρ_s = 7800 kg/m^3.

The contact force response is considered to comparing the results of proposed analytical models and the comparison shown in Figure 3.2. It is indicates that the loading and unloading cycles coincident with wave propagation method and literature result (Wu and Cheng 1989). The estimated peak contact force by wave propagation method was slightly lower than the value provided from the literature. It can also be seen that the energy balance model and spring-mass model are significantly under – predicts the peak contact force and over –predicts the contact duration in the spring-mass model. The energy balance model can only predict the peak contact force.

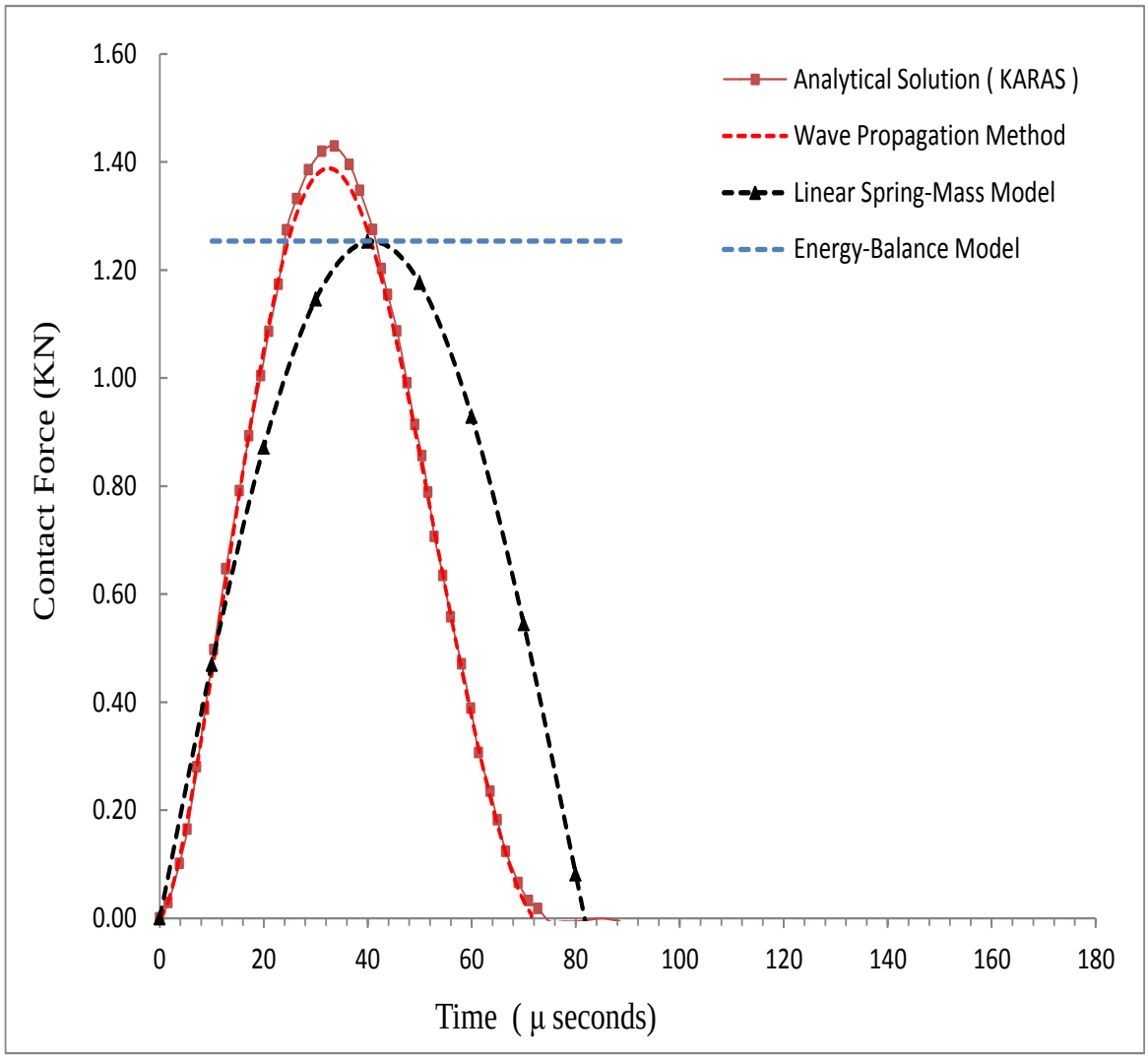

Figure 3.2: The contact force for steel plate comparison each analytical models

Table 3.1 provides a summary of the peak contact force and total contact time collected from literatures by using the spring-mass and energy balance models. The wave propagation method provided close results for impact response. Therefore, the wave propagation method is recommended for further low-velocity impact response predictions of the monolithic and laminated plate glasses.

Table 3.1: Maximum contact force and total contact duration comparison

Dynamic Impact model	Max Contact force (kN)	Contact Duration (μs)
Karas (Analytical model) Wu and Chang (1989)	1.42	72.77
Linear spring-mass model Abrate (1998)	1.25	81.70
Energy-Balance model Abrate (1998, Cantwell (2007)	1.25	n/a
Wave propagation method Abrate (1998)	1.38	70.27

3.5 Low-velocity impact analysis of monolithic glass plate using wave propagation method

Considering monolithic glass plate length and width are 1m, and thicknesses (t_g) are 12 mm, 15 mm and 18 mm and the steel impactor masses (M_i) are 0.5, 1.0, 2.0 kg and the initial impact velocities (V_i) are 5 m/s, 20 m/s and 40 m/s. The arrangement of parametric studies is shown in Table 3.2, which includes mainly effects of impact velocity (Case 1), impactor mass (Case 2) and plate thickness (Case 3). The contact force-time and displacement-time histories are considered to predict the impact response of the monolithic glass plate. The analytical solutions are performed under elastic manner for the glass, steel and PVB materials and these material properties are presented in Table 3.3.

Table 3.2: Arrangement of parametric studies for monolithic glass plate

Case 1	Glass plate size : 1 mx 1 m x 0.012 m; M_i = 1kg **Studied parameter** : The impact velocity (V_i) , i = 1,2,3 V_1 = 5 m/s , V_2= 20 m/s , V_3= 40 m/s
Case 2	Glass plate size :1 m x 1 m; M_i = 1kg ; Impact velocity : 20 m/s **Studied parameter** : The glass plate thickness (t_{glass}) , glass = 1,2,3 (l_a/ t_{glass} /l_b) 1 m x 0.012 m x 1 m ; t_1= 12 mm 1 m x 0.015 m x 1 m ; t_2 = 15 mm 1 m x 0.018 m x 1 m ; t_3 = 18 mm
Case 3	Plate size : 1 mx1 mx 0.012 m, Impact velocity : 20 m/s **Studied parameter** : The impactor mass (M_i) , i = 1,2,3 M_1 = 0.5 kg , M_2 = 1 kg , M_3 = 2 kg

Table 3.3: Material properties of glass and steel

Material Type	Young's modulus (GPa)	Poisson's ratio	Density (kg/m^3)
Glass	74.40	0.24	2500
Steel	210	0.3	7800

3.5.1 Low-velocity impact analysis results of for monolithic glass plate

According to Table 3.2, the predicted low-velocity impact responses on monolithic glass plate concerning the impact velocity, plate thickness and impactor mass will be described. Figures 3.3(a), 3.4(a), and 3.5(a) shows the contact force vs. time history curves under differing values of impact velocity, impact mass and plate thickness.

All three cases, the force – time history responses of monolithic glass plate has an un-symmetric curves which are approximately linear variation loading section until the contact force peaks and shows nonlinear variation after the peak level. It can be seen that the maximum contact force of the monolithic glass plate increase with impact velocity, plate thickness and impact mass.

The total contact duration is also found to be less effected by the impact velocity. The effect of plate thickness is more evident for the force-time result as expected. The displacement – time histories are shown in Figures 3.3(b), 3.4(b) and 3.5(b) for Case 1, 2 and 3 respectively. The displacement-time history curves show a similar shape as the contact-time history curves. It can be seen that the plate central displacement increases when increasing impact velocity and impact mass and decreasing plate thicknesses. It can be seen that the mass of impactor has more significant effect on the contact duration than the impact velocity and plate thickness (Figure 3.5b). For monolithic glass plates, the predicted peak contact force and peak displacement results are summarised in Table 3.4 with various parametric designs.

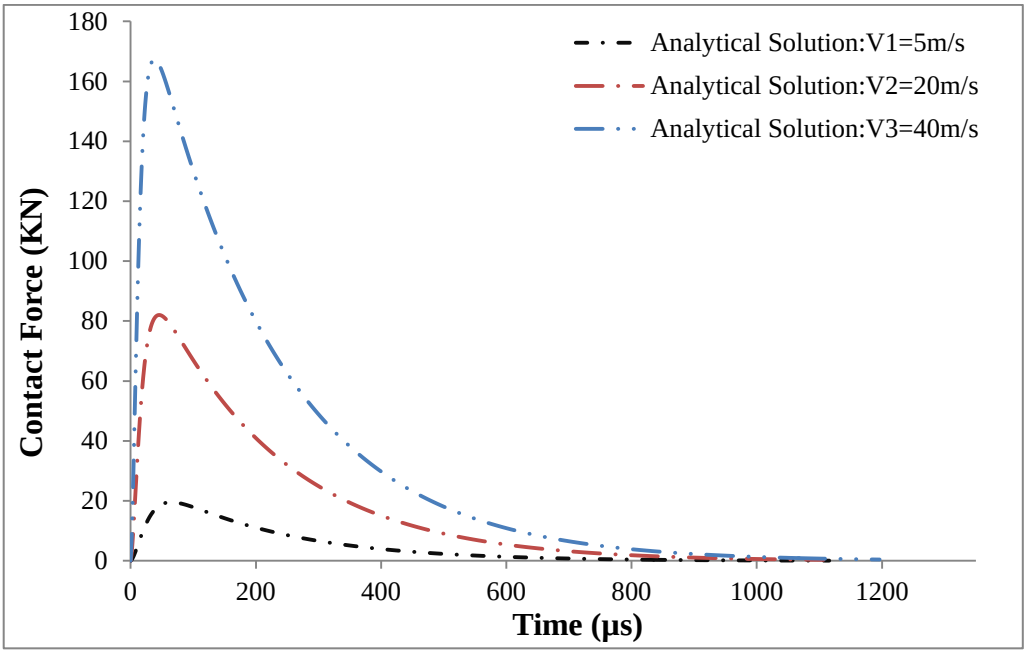

(a) Contact force-time history

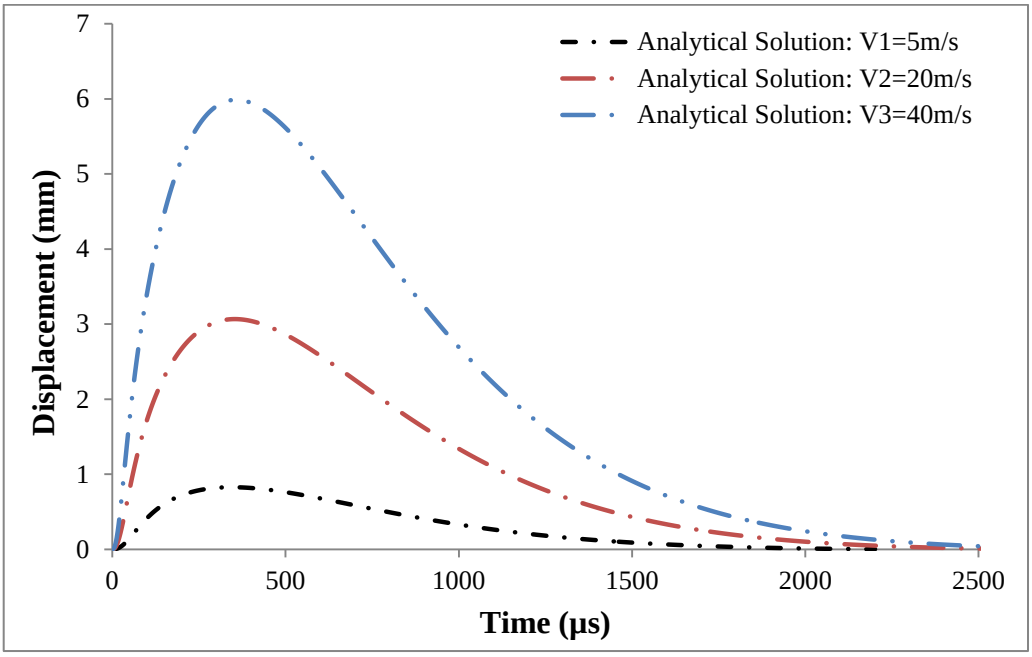

(b) Displacement-time history

Figure 3.3: Impact results for Case 1

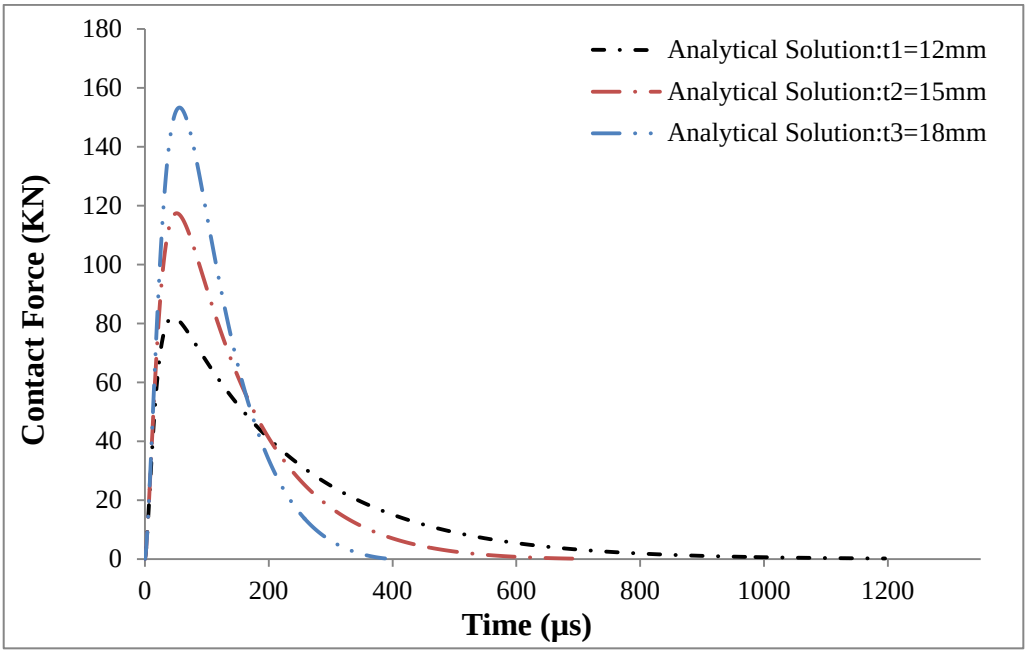

(a) Contact force-time history

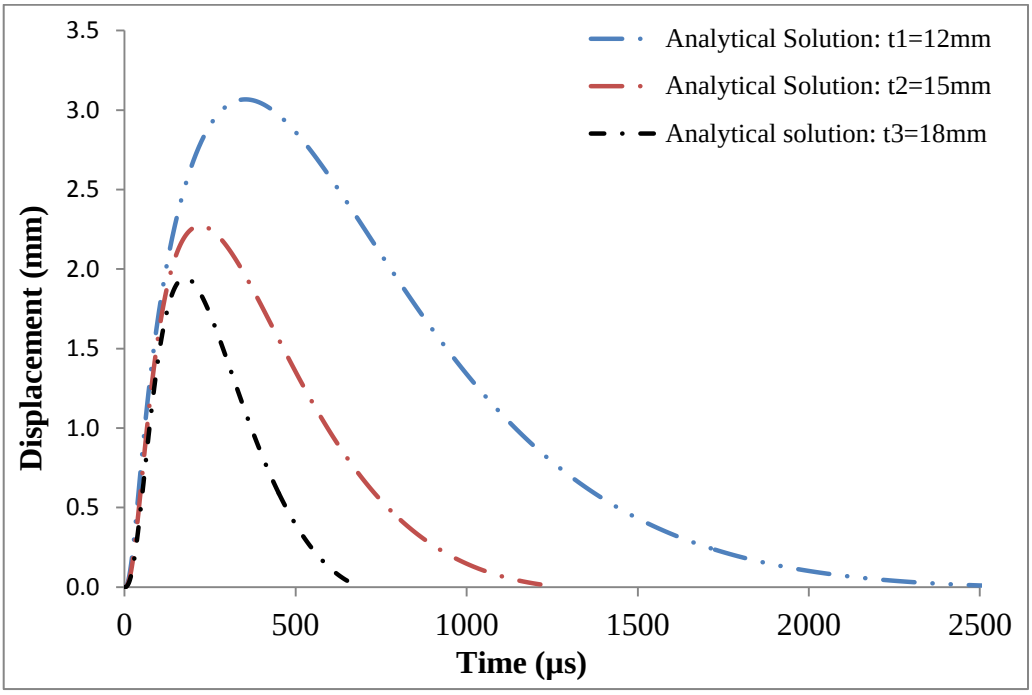

(b) Displacement-time history

Figure 3.4: Impact results for Case 2

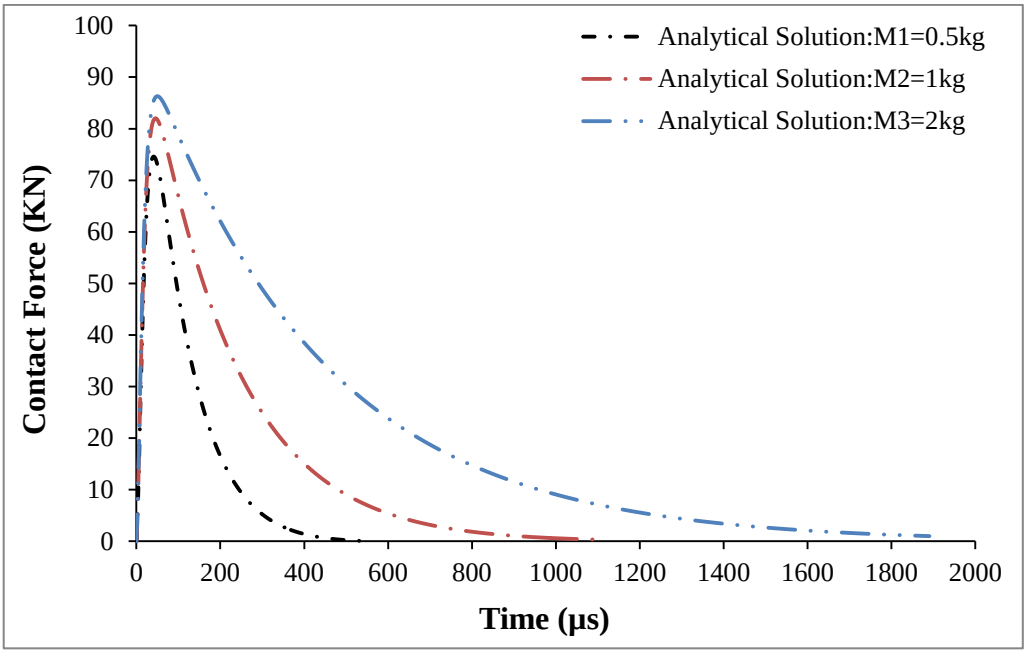

(a) Contact force-time history

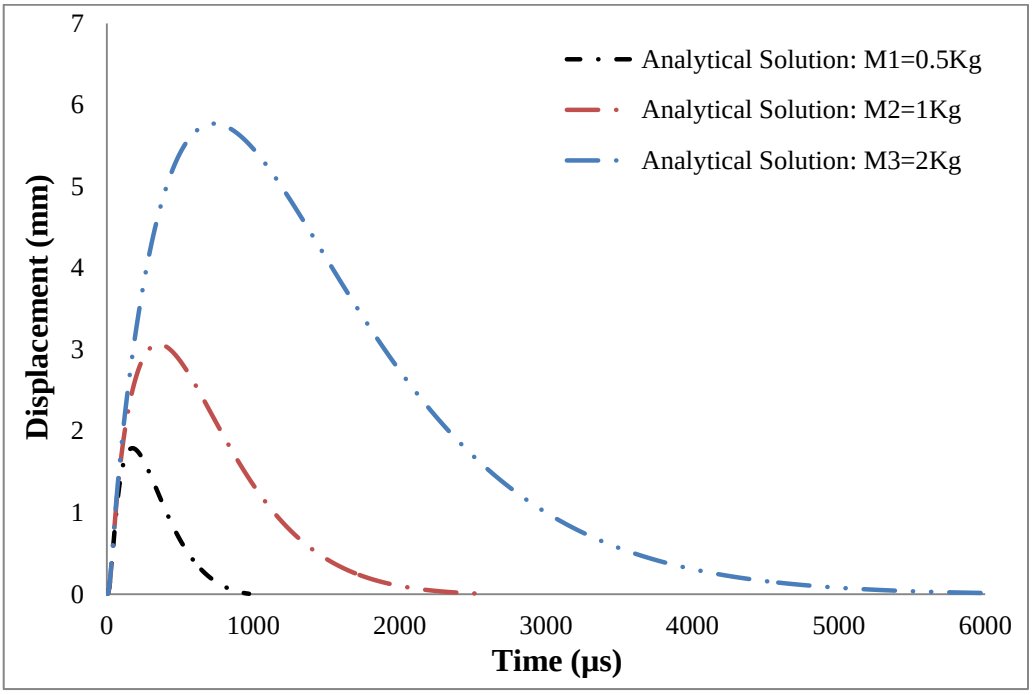

(b) Displacement– time history

Figure 3.5: Impact results for Case 3

Table 3.4 Summary of parametric studies using wave propagation method

Studied parameter	Maximum contact force (kN)		Max displacement (mm)
Impact velocity (m/s) Case 1	5	19.53	0.83
	20	82.01	3.07
	40	167.33	5.99
late thickness (mm) Case 2	12	82.01	3.05
	15	117.42	2.27
	18	153.32	1.86
Impactor mass (kg) Case 3	0.5	74.59	1.78
	1	82.01	3.03
	2	86.29	5.74

3.6 Low–velocity impact analysis of laminated safe glass plate using wave propagation method

The low-velocity impact response of laminated glass (LG) plate is also studied by using wave propagation analytical method. The LG plate consists of two or more glass plies bonded together with a PVB (polyvinyl butyral) interlayer, which has various geometric configurations for glass and PVB interlayers, respectively (Figure 3.6).

The length and width of the laminated glass plate are both 1 m and each glass ply thickness (t_g) are 6 mm, 8 mm, 10 mm, respectively and the PVB interlayer thickness (t_{pvb}) are 0.38 mm, 0.76 mm, 1.52 mm. The dimension details of LG plate and the studied parameters are summarised in Table 3.6. The glass, steel and PVB material properties are described in Table 3.3 and Table 3.5, respectively.

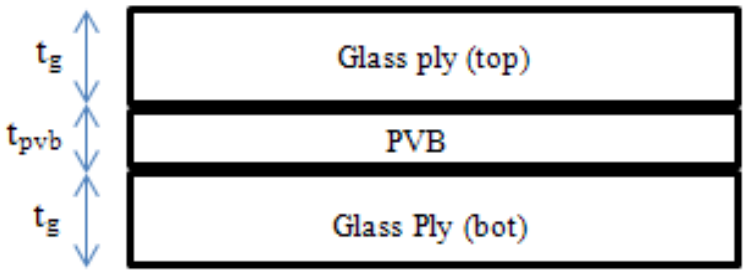

Figure 3.6**:** Sectional view of laminated glass plate

Table 3.5: Material properties of polyvinyl butyral (PVB)

Material Type	Young's modulus (MPa)	Poisson's ratio	Density (kg/m^3)
PVB	6.3	0.40	1100

The laminated glass is often treated as an equivalent monolithic glass by using effective geometric and material properties. Xu et al. (2009) proposed effective parameters of laminated glass plate namely, effective Young's modules E_e, Poisson's ratio ν_e, total plate thickness t_{total} and effective density ρ_e of the laminated glass plate. These relationships are given as;

$$E_e = \left(2t_g E_g + t_{pvb} E_{pvb}\right) \Big/ \left(2t_g + t_{pvb}\right) \tag{3.25}$$

$$v_e = \left(2t_g v_g + t_{pvb} v_{pvb}\right) \Big/ \left(2t_g + t_{pvb}\right) \tag{3.26}$$

$$t_{total} = 2t_g + t_{pvb} \tag{3.27}$$

$$\rho_e = \left(\rho_g t_g + \frac{1}{2}\rho_{pvb} t_{pvb}\right) / t_{total} \tag{3.28}$$

where E_g, ν_g, E_{pvb}, ν_{pvb} are the Young's modulus and Poisson's ratio of the glass and PVB materials and the density and ply thickness of the glass and PVB materials use symbols of ρ_g ,t_g and ρ_{pvb}, t_{pvb}, respectively. The effective material properties of laminated glass plate (E_e, ν_e, t_{total}, ρ_e) are used to calculate the stiffness (Kc) from Eq.3.6, plate mobility factor (λ) from Eq.3.22, the plate flexural rigidity ($D = \frac{E_e h^3}{12(1-\nu_e^2)}$,h = t_{total}), the density and mass required in wave propagation method. M_i is the mass of the impactor.

The arrangement for parametric analysis for the laminated glass plate is described in Table 3.6, which shows four cases with different parametric conditions such as impact velocity (Case 4), glass ply thickness (Case 5), impactor mass (Case 6) and PVB inter layer thickness (Case 7).

Table 3.6: Arrangement of parametric studies for laminated glass plate

Case 4	LG plate size :1 mx 1 m x 0.01276 m; ($t_g/t_{PVB}/t_g$) :6 mm/0.76 mm/6 mm; M_i = 1kg ; K_c = 1.328E10 GPa, D = 12918.04 Nm^3 **Studied parameter** : The impact velocity V_1 = 5 m/s , V_2 = 20 m/s , V_3 = 40 m/s
Case 5	LG plate size : length = 1 m x 1 m , t_{PVB} = 0.00076 m; Impact velocity : 20 m/s M_i = 1kg ; **Studied parameter** : The glass ply thickness (t_g), g = 1,2,3 ; (t_g/0.76/t_g) 6 mm/0.76 mm/6 mm ; t_1 = 6 mm ; K_c = 1.328E10 GPa, D = 12918.04 Nm^3 8 mm/0.76 mm/8 mm ; t_2 = 8 mm ; K_c = 1.343E10 GPa, D = 29679.62 Nm^3 10 mm/0.76 mm/10 mm ; t_3 = 10 mm; K_c = 1.351E10 GPa, D = 56879.53 Nm^3
Case 6	LG plate size : 1 m x 1 m x 0.01276 m; Plate thickness ($t_g/t_{PVB}/t_g$) : 6mm/0.76mm/6mm Impact velocity (V_{impact}) : 20m/s **Studied parameter** : The impactor mass M_i, i= 1, 2, 3 M_1 = 0.5Kg ; K_c = 1.204E10 GPa, D = 12918.04 Nm^3 M_2 = 1Kg ; K_c = 1.328E10 GPa, D = 12918.04 Nm^3 M_3 = 2Kgm ; K_c = 1.513E10 GPa, D = 12918.04 Nm^3
Case 7	LG plate size :1 m x 1 m; Impact velocity : 20 m/s, M_i = 1kg **Studied parameter** : The PVB layer thickness (t_{PVBi}), i = 1.2,3; (6 mm/ t_{PVB} /6 mm) 6mm/0.38mm/6mm; t_{PVB1} = 0.38 mm ; K_c = 1.357E10 GPa, D = 12130.51 Nm^3 6mm/0.76mm/6mm; t_{PVB2} = 0.76 mm: Kc = 1.329E10 GPa, D = 12918.04 Nm^3 6mm/1.52 mm/6mm; t_{PVB3} = 1.52 mm; Kc = 1.276E10 GPa, D = 14569.47 Nm^3

3.6.1 Low-velocity impact analysis results of laminated glass plate

For LG plate glass, the contact force-time histories are shown in Figures 3.7(a), 3.8(a), 3.9(a) and 3.10(a). It can be seen that the contact force-time curves are not symmetric for the all four cases. The figures also indicate that the peak contact forces are higher with larger impact velocity and glass ply thickness. The increase in impact velocity generates large contact force on laminated glass plate.

The plate central displacement-time histories are also shown for laminated plate glasses in Figures 3.7(b), 3.8(b), 3.9(b) and 3.10(b). All the displacement-time curves have un-symmetric nature. It can be seen that the central displacements for LG plate significantly increase with increasing impact velocity and mass, and with decreasing glass ply and PVB interlayer thicknesses.

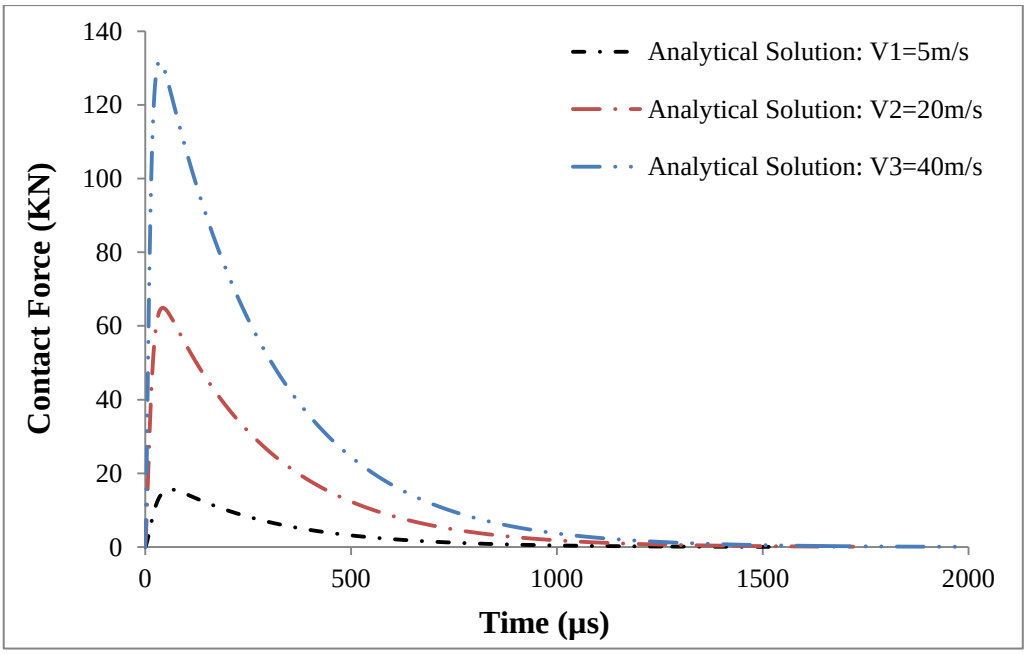

(a) Contact force-time history

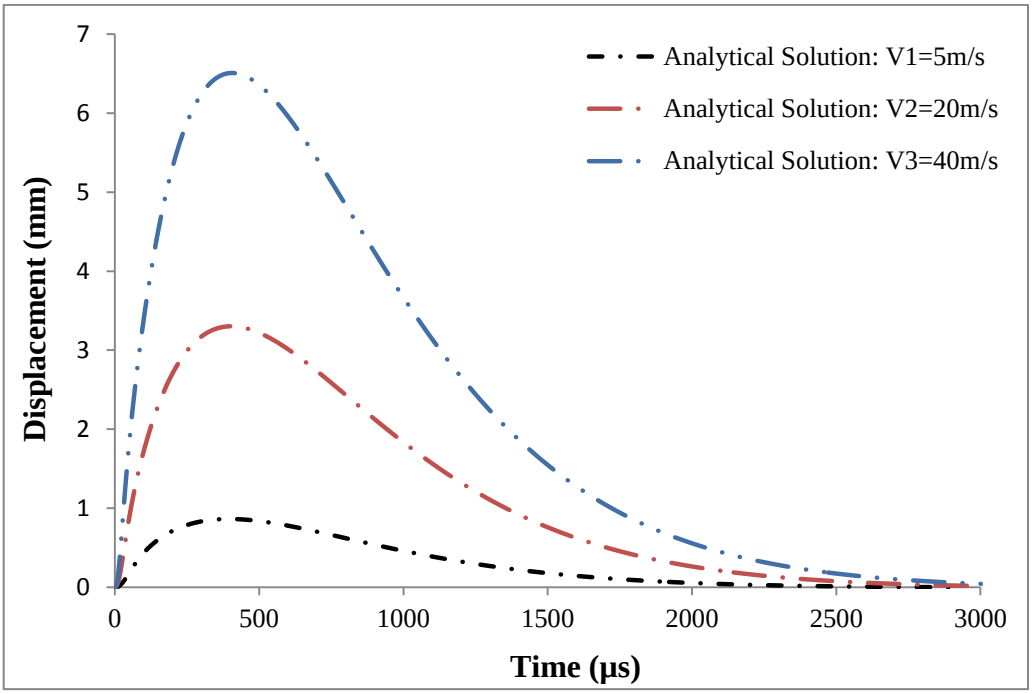

(b) Displacement–time history

Figure 3.7: Impact results for Case 4

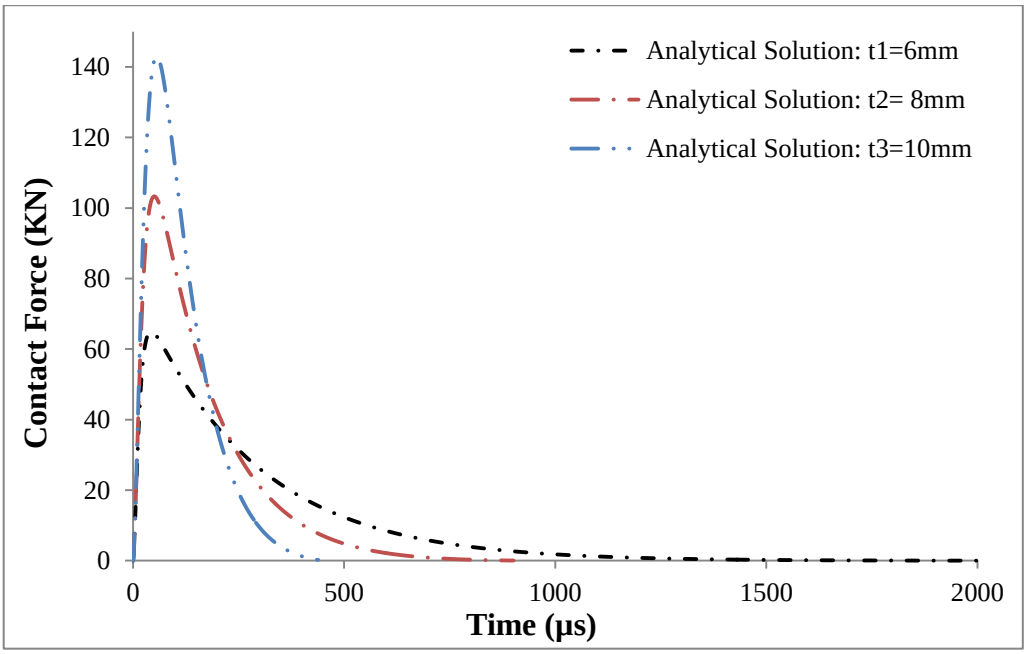

(a) Contact force-time history

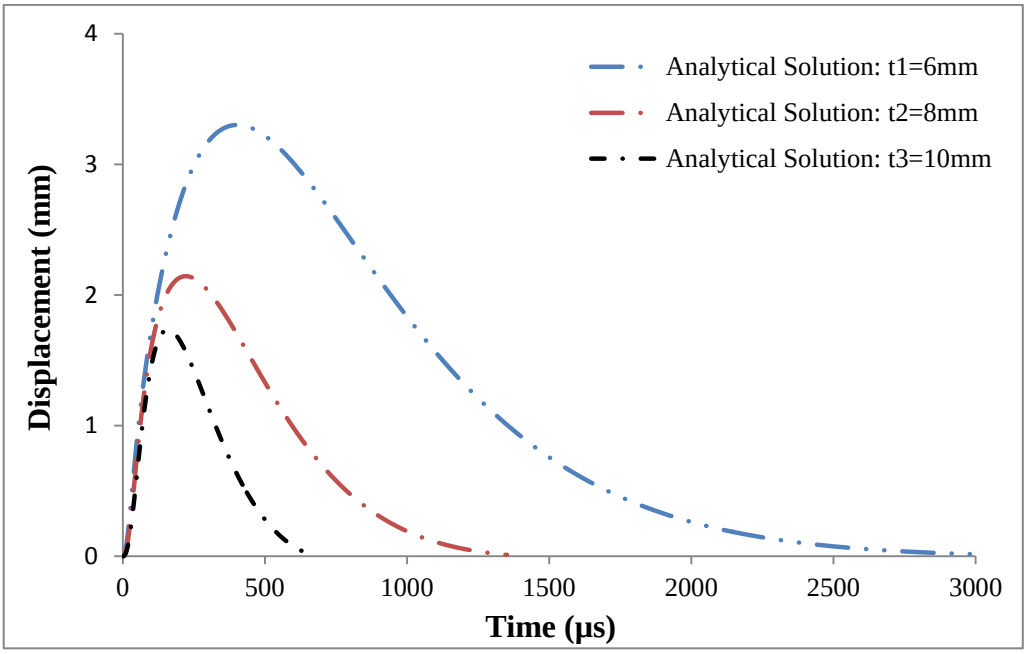

(b) Displacement–time history

Figure 3.8: Impact results for Case 5

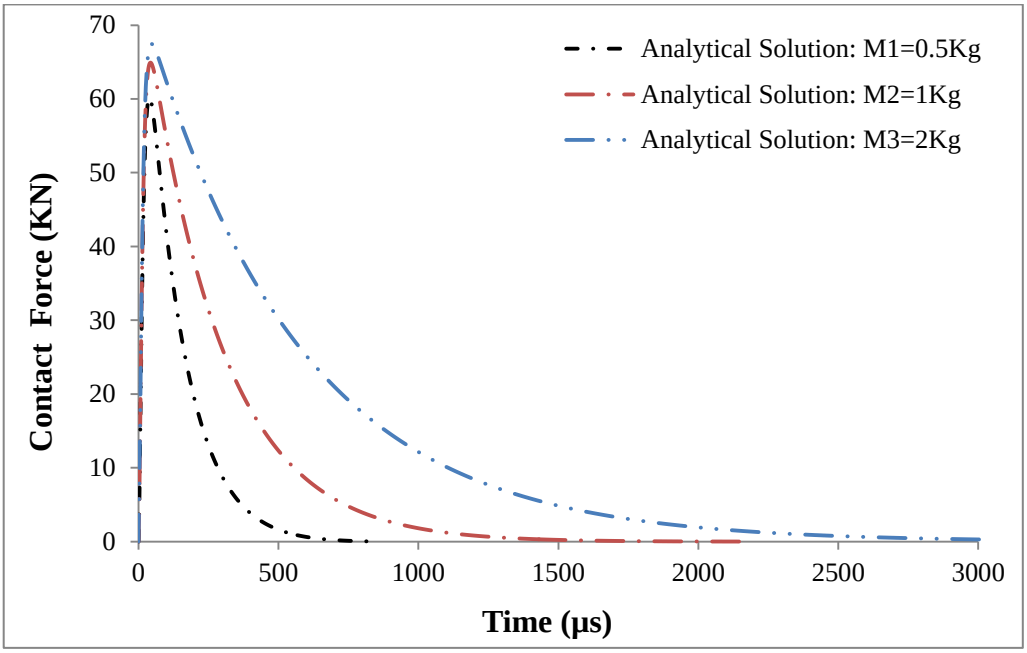

(a) Contact force-time history

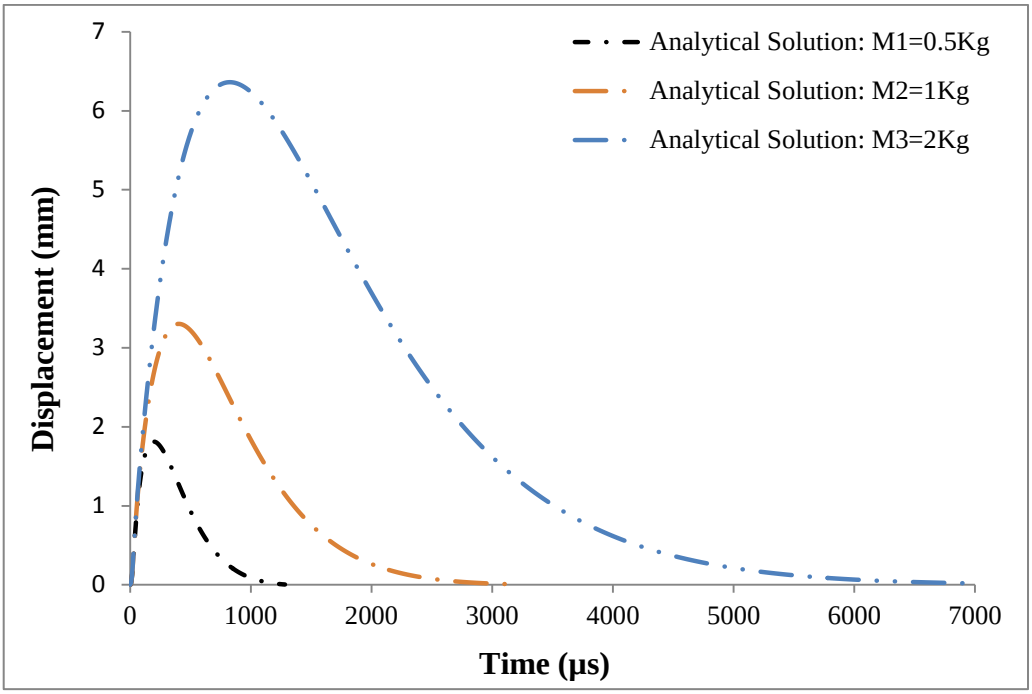

(b) Displacement–time history

Figure 3.9 Impact results for Case 6

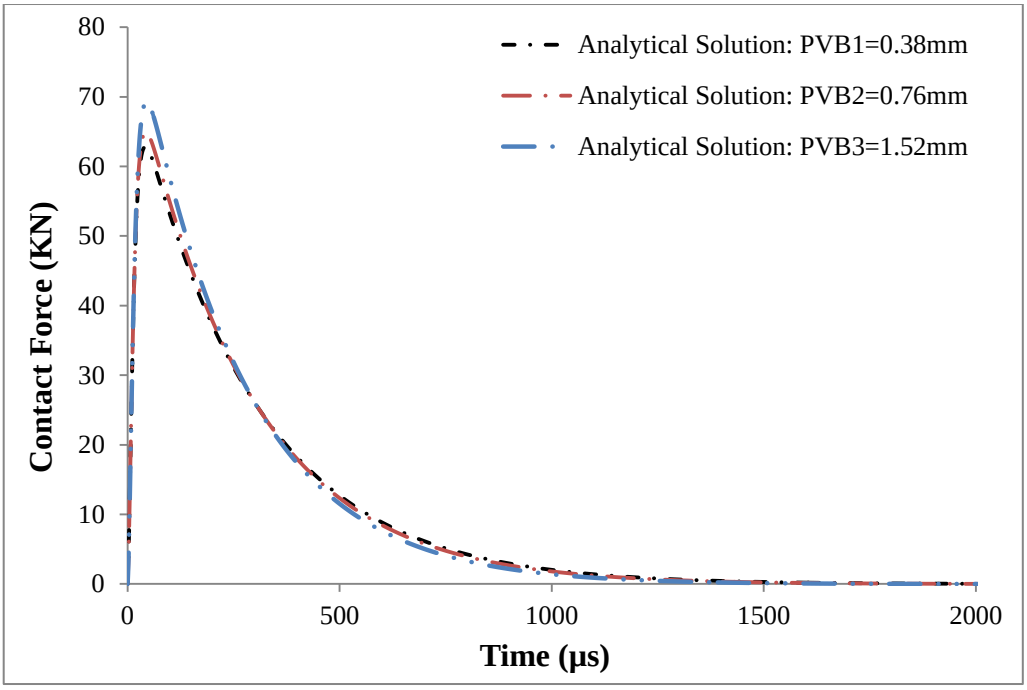

(a) Contact force-time history

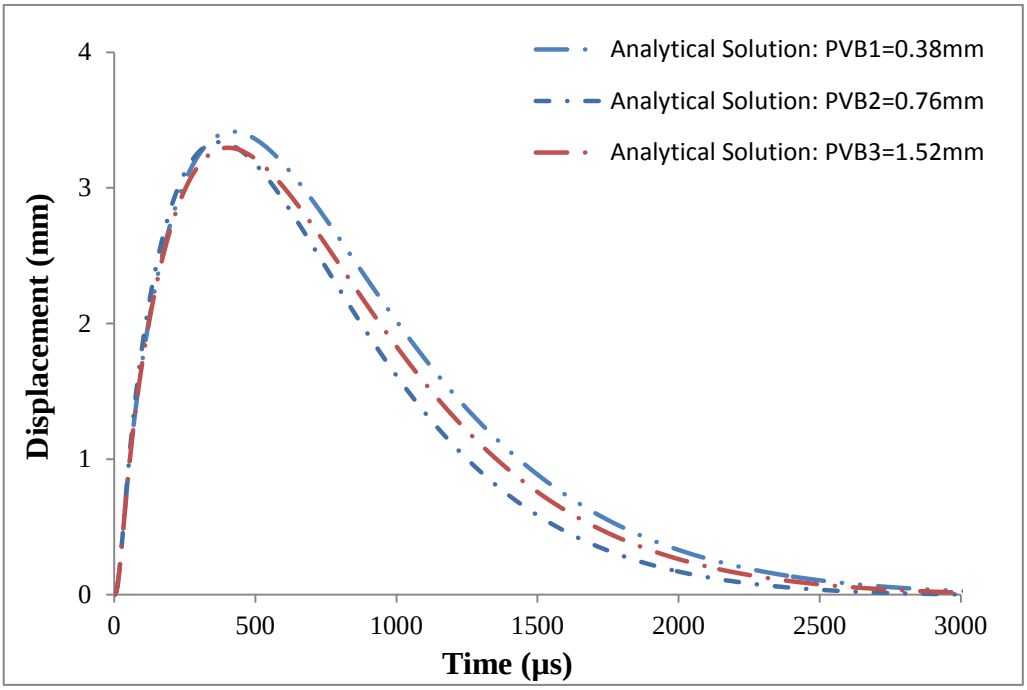

(b) Displacement–time history

Figure 3.10: Impact results for Case 7

Under various parametric conditions, the peak contact force and displacement results of the LG plate are summarised in Table 3.7.

Table 3.7: Summary of parametric studies using wave propagation method (LG plate)

Studied parameter		Maximum contact force (kN)	Maximum Displacement (mm)
Impact velocity (m/s) Case 4	5	15.63	0.86
	20	64.92	3.34
	40	131.83	6.46
Each lass ply thickness (mm) Case 5	6	64.92	3.34
	8	103.28	2.13
	10	142.93	1.71
Impactor mass (kg) Case 6	0.5	60.21	1.72
	1	64.92	3.34
	2	67.45	6.36
PVB interlayer thickness (mm) Case 7	0.38	68.81	3.41
	0.76	64.92	3.34
	1.52	69.24	3.29

3.7 Analytical prediction of contact area for monolithic and laminated glass plates subject to impacts

As discussed in Chapter 2 (section 2.10), the impactor's geometry, impact location, impact angle play an important role in the resulting impact response. One of the effected result is the contact area. The main purpose of this section is to study the contact area on the plate during the impact. For contact area or contact radius, different types of analytical relationships have been proposed for the spherical projectile and impactor (Langitan and Lawn, 1968, Knight et al., 1977 , Kirchner and Gruver, 1977, Kirchner and Gruver, 1978).

In this Chapter, the obtained predicted peak contact forces are used to evaluate the maximum contact area and contact radius of the monolithic and LG plates. The overall relationship between the contact area and the geometry of impactor and plate has been described by Aryaei et al. (2010). The effective radius (R^*) between spherical impactor and infinite plate of thickness can be expressed as:

$$\frac{1}{R^*} = \left(\frac{1}{R_1} + \frac{1}{R_2} \right) \quad R_2 = h_{plate} = \infty \tag{3.29}$$

The rearrangement of the above equation yields

$$R^* = R_1 \tag{3.30}$$

where R_1 is the radius of the impactor, h $_{\text{plate}}$ is the thickness of plate. Then the radius of contact area (a) given by

$$a = \sqrt[3]{\frac{3F}{4}\left(\frac{R^*}{E^*}\right)} \tag{3.31}$$

In equation 3.31, $E^*=E$ is the effective Young's modulus between two contact objects, which is calculated from equation 3.4 and F is the maximum contact force found from wave propagation method (Eq.3.24). For the contact radius subjected to laminated glass plate, the effective Young's modulus and Poisson's ratio were calculated by equation 3.25 and 3.26.

3.7.1 Results of contact radius and area for the monolithic glass plate

The previously discussed three cases with various parametric conditions have been used to evaluate the contact radius and contact area for monolithic glass plate and results are summarized in Table 3.8. It is suggested that the plate contact radius increases with impact velocity, impact mass and plate thickness.

Table 3.8: Summary of peak contact radius and area on monolithic glass plates under various parametric conditions

Studied parameter		Contact radius (a) (mm)	Contact area (A) (mm^2)
Impact velocity (m/s) Case1	5	1.90	12.48
	20	3.21	32.44
	40	4.07	52.16
Each glass ply thickness (mm) Case2	12	3.21	32.44
	15	3.63	41.29
	18	3.96	49.32
Impactor mass (kg) Case3	0.5	2.89	26.23
	1	3.21	32.44
	2	3.54	39.29

3.7.2 Results of contact radius and area for the laminated glass plate

For Case 4 to Case 7, the results of contact radius and area for laminated glass plates are summarised in Table 3.9. The results show that the contact radius of laminated glass plate increases with impact parameters such as impact velocity, glass ply thickness, impactor mass and PVB interlayer thickness. It is noticed that the influence of glass ply thickness is

significant. However, a limited degree of contact radius variation is shown for laminated glass plate with different PVB interlayer thicknesses.

Table 3.9: Summary of peak contact radius and area on laminated glass plates under various parametric conditions

Studied parameter		Contact radius (mm)	Contact area (mm^2)
Impact velocity (m/s) Case 4	5	1.88	11.05
	20	3.01	28.53
	40	3.82	45.74
Each glass ply thickness (mm) Case 5	6	3.01	28.53
	8	3.51	38.73
	10	3.90	47.97
Impactor mass (kg) Case 6	0.5	2.73	23.36
	1	3.01	28.53
	2	3.30	34.26
PVB interlayer thickness (mm) Case 7	0.38	2.96	27.54
	0.76	3.01	28.53
	1.52	3.12	30.55

3.8 Summary

Analytical models for analysing the dynamic impact response of plate structures are presented in this chapter.

An impact case from existing literatures is used to verify the proposed analytical models, which include linear spring-mass, energy-balance and wave propagation method, respectively. Analytical results were further compared with published data and good agreement has been observed.

Under difference parametric arrangement, the impact responses of monolithic and laminated plate glasses were predicted by using wave propagation analytical method. The impact velocity, impactor mass, plate thickness and PVB interlayer thickness were set as the studied parameters in this study. The behaviour of the laminated glass plate was calculated by adopting effective parameters, such as effective Young's Modulus (E_e), Poisson's ratio (ν_e), total thickness (t_{total}) and effective density (ρ_e). The contact force, plate central displacement and contact radius were predicted responses for the monolithic and laminated glass plate glasses. In general, the influence of impact velocity and overall plate thickness were identified more significant on the impact response. Same parametric details (e.g. plate type, dimension and impact's properties) will be used in next Chapter to carry out further comparative studies

CHAPTER 4: NUMERICAL MODEL FOR LOW-VELOCITY IMPACT OF MONOLITHIC AND LAMINATED GLASS PLATE

4.1 Introduction

Commercial tools (e.g. ABAQUS, ANSYS and LS-DAYAN) are widely available nowadays to analyse and design structures by using various numerical methods, e.g. finite element method (FEM), finite different method (FDM), and discrete element method (DEM).

In this study, a finite element method based commercial software package of ABAQUS is utilized to model and analyse the low-velocity dynamic impact response of monolithic and laminated plate glasses. The process of modelling is presented, which includes the selection of material models, model verification, convergence studies and results interpretations.

4.2 Numerical model preparation

For both types of plate glasses, ABAQUS package 6.10 and dynamic explicit module have been used to model and simulate the low-velocity impact responses. By using the embedded graphical interface module ABAQUS/CAE, a 3D finite element model with the following options is created:

- The part and section (3D) verification (deformable or rigid)
- Type of mesh and element

- The physical and mechanical property of material
- Assign the material and section properties
- The part assembling
- Define analysis module (Abaqus/Explicit) and step time (time increment)
- Define boundary and initial conditions
- Create and assign the job

In this investigation, three parts, namely, a steel spherical impactor, a monolithic glass plate and a PVB inter layer, is considered and created. The deformable option was used to model glass plate and PVB interlayer, respectively. The monolithic and laminated glass plates with a planer dimension of 1000 mm x 1000 mm, but only a quarter symmetric section with a dimension of 500 mm x 500 mm (see Figure 4.1) was considered.

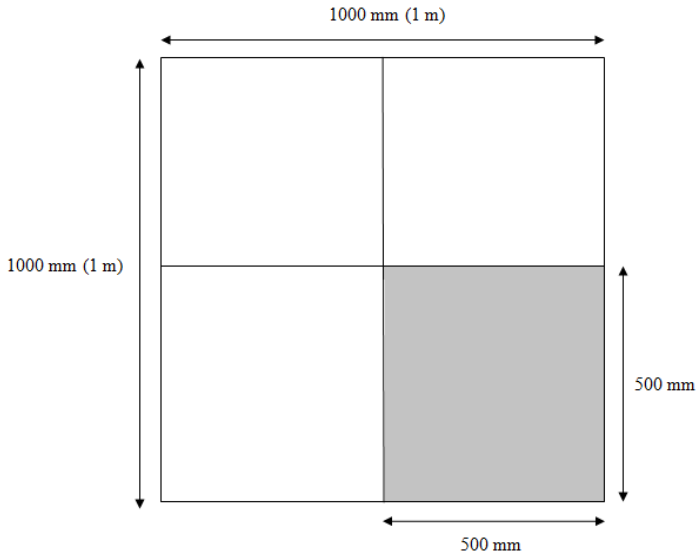

Figure 4.1: A quarter section of full plate model

The purpose of using quarter section is to minimise the computational time for the simulation. A circular partition section was used in order to create a finer mesh around the impact region (see Figure 4.2a and Figure 4.2b). The single layer monolithic glass plate thicknesses were 12 mm, 15 mm, 18 mm, respectively and in the laminated glass plate, the top and bottom glass ply thicknesses were 6 mm, 8 mm, 10 mm. The PVB inter layer thickness was 0.38 mm, 0.76 mm and 1.52 mm.

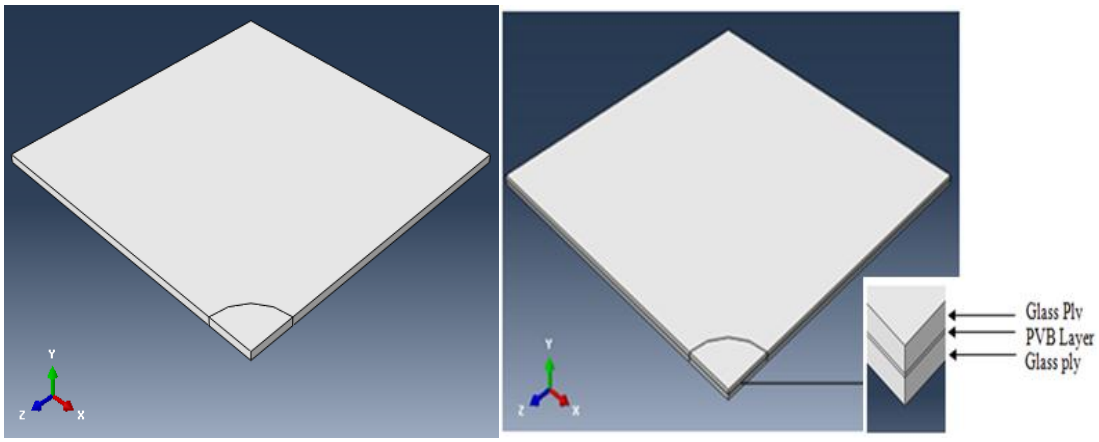

(a) Monolithic glass plate (b) Laminated glass plate

Figure 4.2: Quarter geometric parts

The steel spherical impactor was also created in a 3D solid form with three different mass of 0.5, 1kg and 2kg. It is worth noting that the majority of impact events have used a stiff material to create a projectile or impactor and the impact object behaviour is assumed as a rigid body during the investigation (Liu and Liaw, 2009 and Khalili et al., 2011). This means that the amount of deformation is negligible during the impact process. In this investigation, the elastic stiffness of steel is approximately three time larger than glass; therefore, the rigid body behaviour was considered for the steel spherical impactor (steel ball). In the numerical

model, a quarter symmetric section of impactor was constructed with a rigid body option. Similarly, a reference point was introduced in the steel ball in order to assign the boundary conditions (see Figure 4.3).

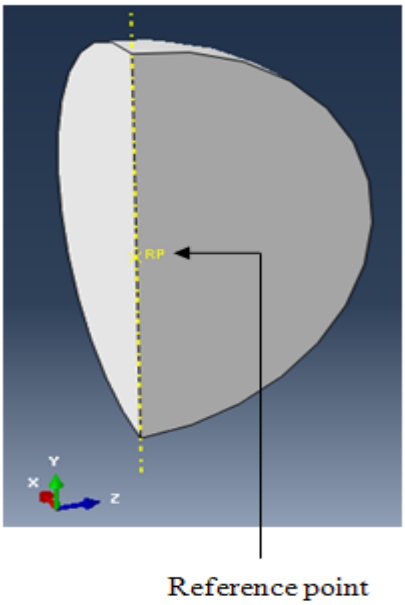

Figure 4.3: Quarter geometric part of steel ball (impactor)

A hexahedral element and structural mesh pattern was applied for plate glasses, impactor and PVB interlayer, respectively. Furthermore, the three dimensional eight nodes continuum solid elements (C3D8R) was applied element type for each components mesh with reduced integration method. C3D8R element is designed with three degrees of freedoms per node which means only the displacement degrees of freedom are available. It is recommended for the nonlinear large deformation analysis. The mesh and elements arrangement of each components are shown in Figure 4.4.

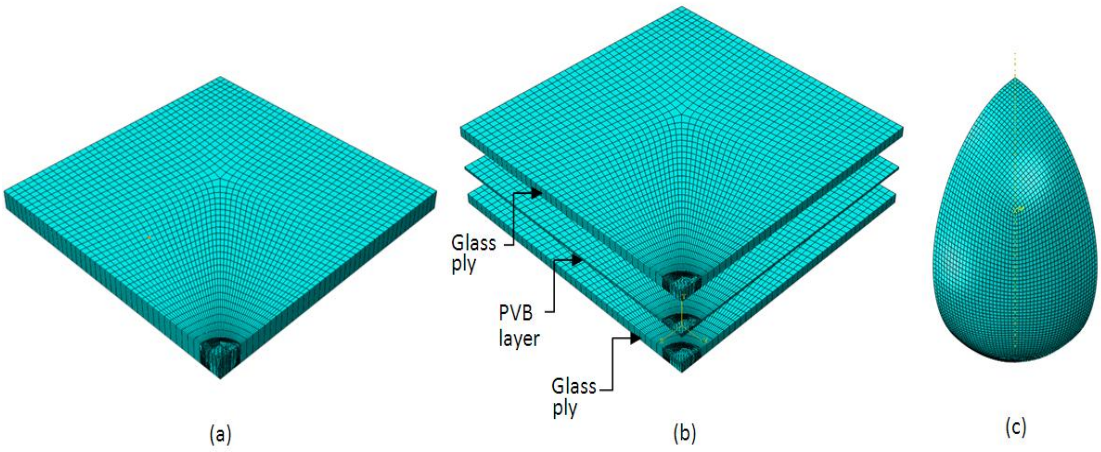

Figure 4.4: Mesh of (a) Monolithic glass plate (b) laminated glass plate with PVB inter layer and (c) impactor

The applied physical and mechanical properties of glass, PVB, steel are listed in Table 4.1.

Table 4.1: Overview of mechanical and physical properties of glass, PVB and steel materials

Material	Density ρ [kg/m^3]	Young's modulus E (GPa)	Poisson's ratio v
Glass	2500	74.4	0.24
Steel	7800	210	0.33
PVB	1100	0.0063	0.40

The quarter sections of both glass plates were assigned with the symmetric boundary conditions or containments in the X and Z directions. The XSYMM boundary condition for the X direction and ZSYMM boundary condition for the Z direction were applied (see Figure 4.5 and 4.6) were assigned

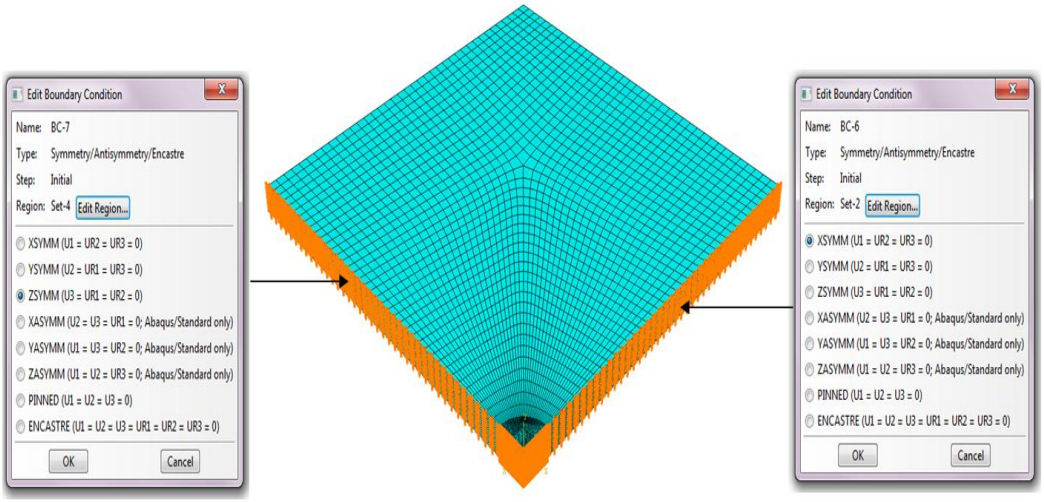

Figure 4.5: Symmetric boundary condition of monolithic glass plate in X and Z directions

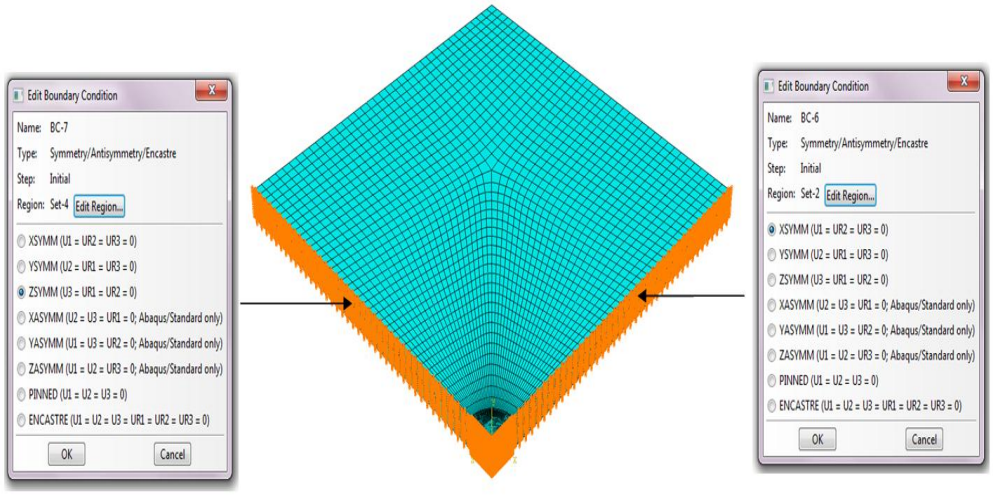

Figure 4.6: Symmetric boundary condition of laminated glass plate in X and Z directions

In order to model the plate support conditions, a fully-fixed boundary condition was applied along the free edges of the monolithic and laminated plate glasses. These constraints will fix all three degrees of freedoms (DOFs) as indicated in Figure 4.7.

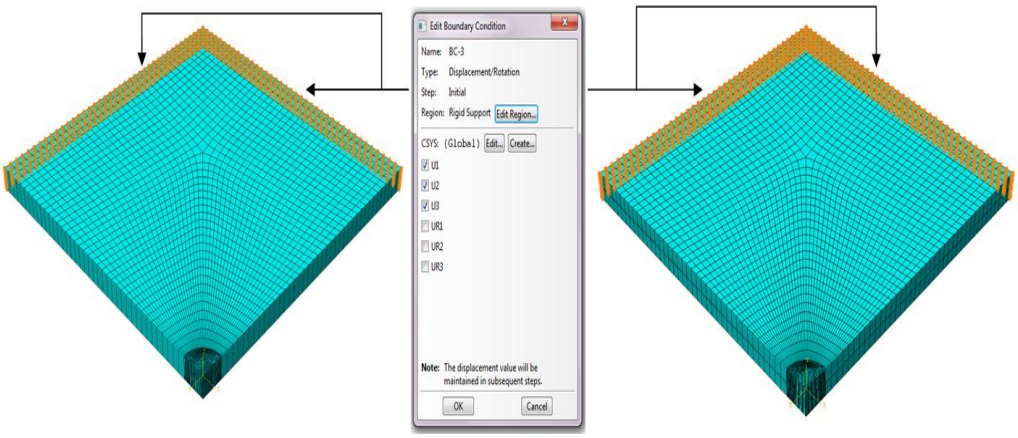

Figure 4.7: Fixed support monolithic glass plate (left) and laminated glass plate (right) boundary conditions

Furthermore, a symmetric section of steel ball (impactor) was used in this simulation with rigid body response. In this model, the whole rigid body is controlled by a single point called as reference point and the symmetric boundary conditions is in the X and Z directions and the impact velocity are also assigned at that point in this simulation (Figure 4.8).

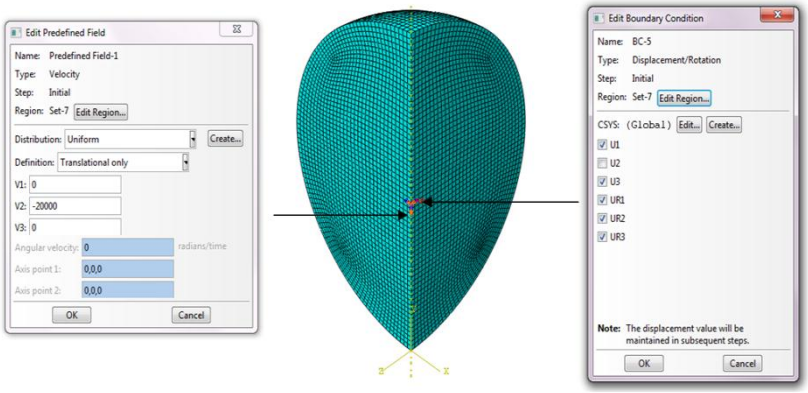

Figure 4.8: Arrangement of Symmetric boundary condition and pre-define initial impact velocity for impactor

Impact occurs in a very short duration of time, which means that most impact reposes (e.g. damage, energy dissipation, forces, displacements and stresses) vary with time. Also, impact may be executed normal or oblique to the target structures. In order to model a transient impact problem with ABAQUS, it is possible to choose a suitable algorithm. In this study, a dynamic explicit algorithm (ABAQUS/Explicit) was chosen. For all simulations, the total contact duration varies approximately within the range of 300 μs 1200 μs.

A surface based contact algorithm (*surface-to-surface) with frictionless contact behaviour was used to model the contact surfaces. For the contact surfaces, the stiffer steel ball surface and resilient glass plate surface were assumed as master and slave, respectively. In the laminated glass plate, a perfect bond behaviour was assumed between the PVB interlayer and glass plies and the contact relationship between surfaces was developed by tie-constrain (Wu et al., 2010 and Khalili et al., 2011).

4.3 Material models in ABAQUS

ABAQUS has a large collection of material models for homogenous, non-homogenous and composite materials. But not all specific material models are pre-built in the package. In this study, it involves two different material models that will be described in the following sections.

4.3.1 Linear elastic material model

A linear elastic materials model was chosen to simulate the elastic impact response, which only needs the input of material density (*p*), Young's modulus (*E)* and Poisson's ratio (v). However, results do not provide any information on the impact damage or failure.

4.3.2 Brittle fracture model

The brittle fracture material model is included in ABAQUS for modelling concrete material failure, in particular, the tension zone. It can also be used for brittle glass and ceramic. The impact damage initiation, evolution and failure patterns can be obtained by using this material model. When this material model is used for concrete crack modelling, smeared crack model is often used. As a result, the model does not track individual cracks but rather takes into account the effect of their presence by degrading the material stiffness in the constitutive calculations at the appropriate material points.

Brittle fracture model has been considered for damage analysis, such as the damage initiation, damage evolution and ultimate failure. Firstly, a Mode I fracture criteria is used to determine the damage initiation of the brittle structure. The damage initiation is captured when the maximum principal stress exceeds a certain cracking failure stress (σ_{tu}^{I}), which is an input parameter of the model.

The damage evolution is included mode I and mode II post-cracking behaviour. The post-crack mode I behaviour is also called tension softening. This behaviour is originally governed

by fracture energy (G_I^f). For brittle materials, fracture energy means the amount of energy in order to progress crack and this material property can be directly specified in ABAQUS. The stress-displacement relation of fracture model is shown in Figure 4.9 and a linear loss in stress is assumed after the first cracks initiation.

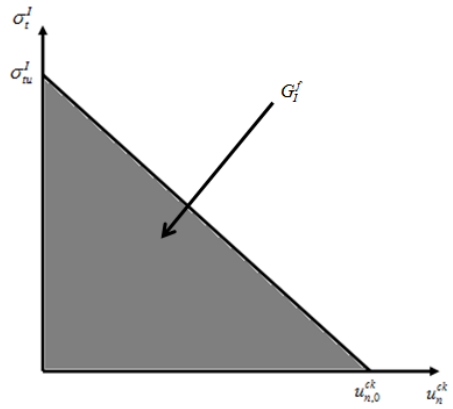

Figure 4.9: Post-failure stress displacement curve

The main parameters of fracture energy model are material cracking failure stress (σ_t^I) and cracking failure displacement (u_n^{ck}) and it is expressed by Eq.4.1.

$$u_{n,0}^{ck} = \frac{2G_I^f}{\sigma_{tu}^I} \tag{4.1}$$

where σ_{tu}^I and $u_{n,0}^{ck}$ are direct cracking failure stress and direct cracking failure displacement which can be specified mode I fracture energy.

For this analysis, the fracture energy of brittle glass is applied 4.0 N/m (Mecholsky et al., 1974 and Wiederhorn and Lawn, 1977) and the direct cracking failure stress of 74.0 MPa (Bouzid et al., 2001). Finally, the direct cracking failure ($u_{n,0}^{ck}$) displacement calculated by equation 4.1 and it was 1.081E-7 m.

The mode II post-cracking behaviour is established in relation to material shear modulus (G) and this shear modulus is reduced with crack slides. The post-cracking mode II function can be directly specified by shear retention model and the related function expressed by equation 4.2.

$$G_c = \rho\left(e_{nn}^{ck}\right)G \tag{4.2}$$

where G_c, and e_{nn}^{ck} are material post-cracked shear modulus and crack opening strain.

The factor of $p(e_{nn}^{ck})$ is called shear retention factor and it can be specified by power law and expressed in Eq.4.3.

$$\rho\left(e_{nn}^{ck}\right) = \left(1 - \frac{e_{nn}^{ck}}{e_{\max}^{ck}}\right)^{p} \tag{4.3}$$

The power law technique only needs to consider two non-zero material parameters in order to model post-failure mode II behaviour in ABAQUS brittle cracking model. For this study, it is assumed non-zero parameters are p = 2 and , $e_{max}^{ck} = 0.002$ respectively.

The final part of this model is brittle failure. By default, when at least one local direct cracking displacement component at a material point reach the direct cracking failure displacement u_{max}^{ck} model parameter, the material point is considered to have failed.

4.4 Convergence study and verification of FE model

To verify the impact model, a previously published case of a rigid sphere impact on a steel plate was modelled (Wu and Chang, 1989). In this case, the material properties, boundary conditions and plate dimension were described in Chapter 3 (section 3.4). The author used the uniform mesh across the steel plate, which includes the eight elements in length and width directions and four elements in plate thickness direction. The average element size was 25 mm x 25 mm x 2 mm. However, this mesh pattern and element sizes are upgraded in the present numerical study. The steel plate and rigid sphere were meshed by using the structural mesh pattern and C3D8R element, which is, an 8-nodes three dimensional continuum solid element with reduce integration method.

For modelling this impact case, a quarter symmetric sections of the steel plate and steel impactor were used with special mesh arrangement, i.e. a finer mesh pattern in contact zone and a coarse mesh out of the contact zone. It is well known that the mesh density plays an important role in the simulation. Therefore, the refine mesh technique was applied in that contact zone. The steel plate and impactor element arrangements are shown in Figures 4.10(a), 4.10(b), 4.11(a), and 4.11(b), respectively.

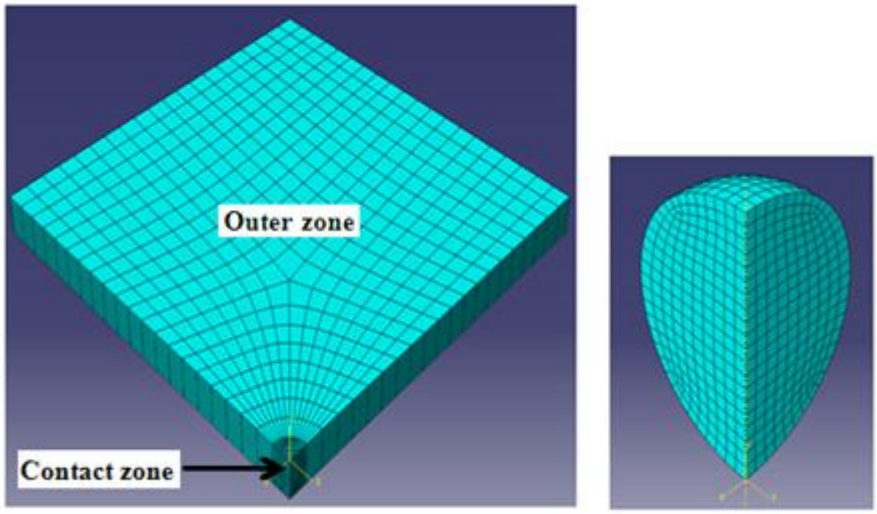

(a) Steel plate (b) Steel impactor

Figure 4.10: 3D FE quarter model with mesh

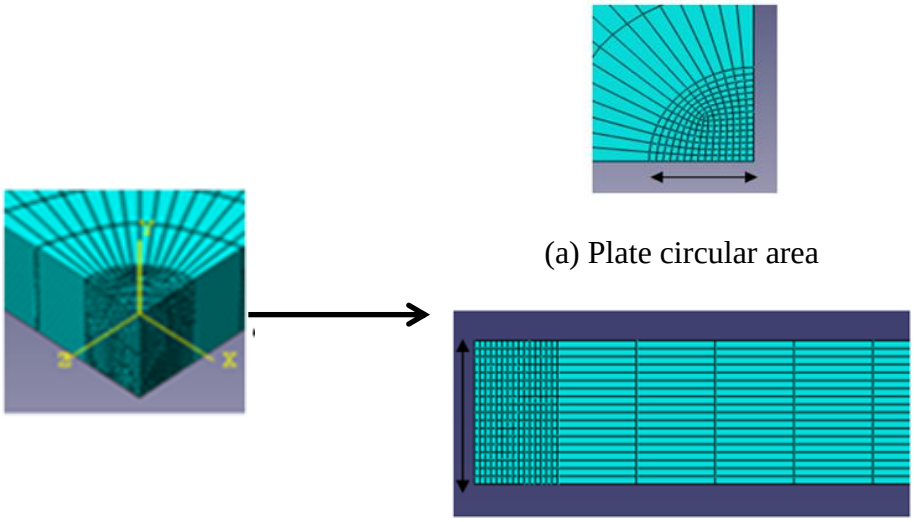

(a) Plate circular area

(b) Plate thickness direction

Figure 4.11: Element preparation of convergence study

The convergence analysis results of the steel plate subject to low-velocity impacts are shown in Figure 4.12 and 4.13. They are based on different element size in circular contact area and in plate thickness direction. The responses of peak contact force and plate centre displacement were considered in the convergence analysis.

The contact force and displacement results converges when the contact zone mesh becomes finer, however one of the mesh pattern shows best agreement with published results (Wu and Chang, 1989). In this case, the mesh arrangement in the contact zone (see Figure 4.10a) was 15 x 15 x 8, which means 15 elements in plate length and width directions and 8 elements along the plate thickness direction. The element size was 0.333 mm x 0.333 mm x 1 mm (Figure 4.14a). The outer zone (see Figure 4.10a) of the steel plate was discretised into 21 x 21 x 8 with twenty one elements in length and width direction and 8 elements in plate thickness direction; the optimum element size in that zone was 4.75 mm x 4.75 mm x 1 mm (Figure 4.14a). The steel sphere's (rigid impactor) diameter is 20 mm (radius = 10 mm). Roughly 10 elements (Figure 4.10b) from the centre in each direction were created and the element size was 1mm x 1mm x 1mm (Figure 4.14b). For future modelling of impacts, the recommended optimum element sizes details are shown in Figures 4.14a and 4.14b. The comparison of contact force, displacement and impact velocity results are presented in Figures 4.15, 4.16(a) and 4.16(b) by using the optimum element sizes. A close agreement is obtained. The contact force results from the numerical modelling are compared with the analytical one by using wave propagation analytical method (Chapter 3 – section 3.4) and again results are close as indicated in Figure 4.15.

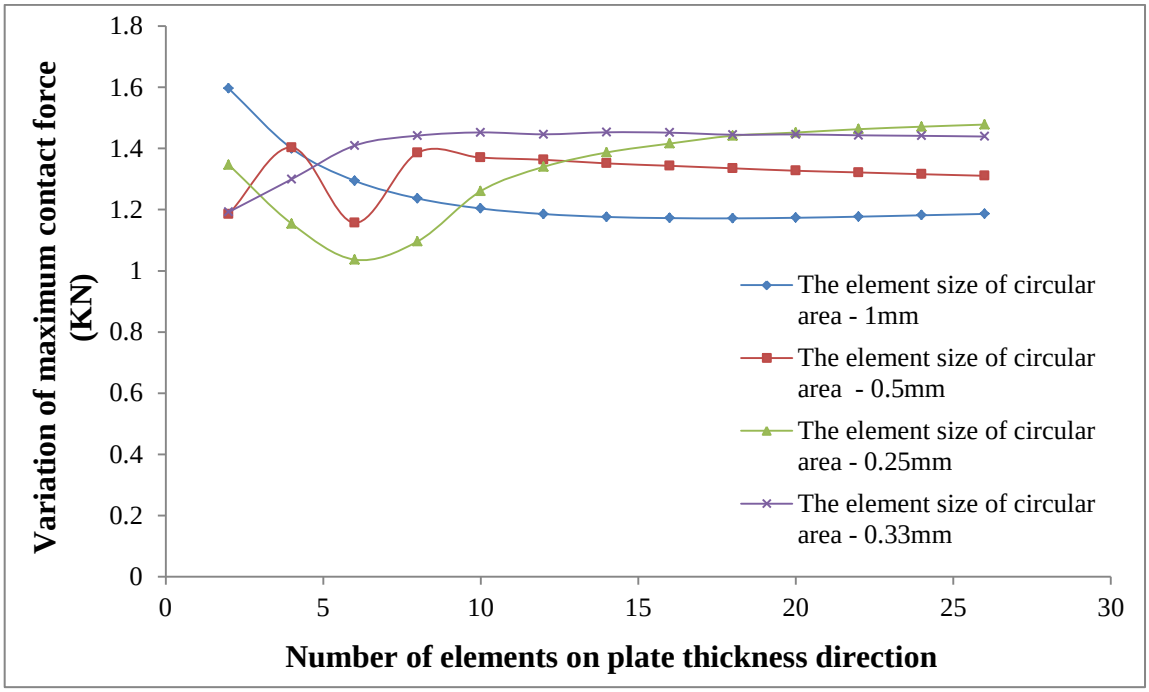

Figure 4.12: Convergence study - maximum contact force vs. number of elements along plate thickness direction

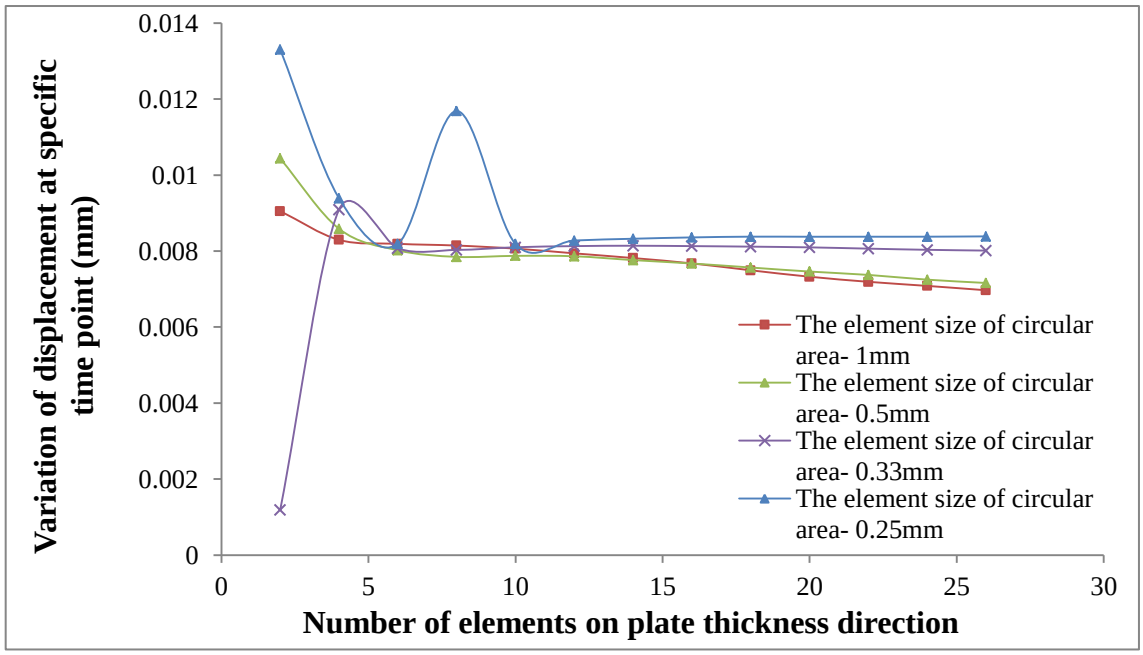

Figure 4.13: Convergence study – plate central displacement vs. number of elements along plate thickness direction

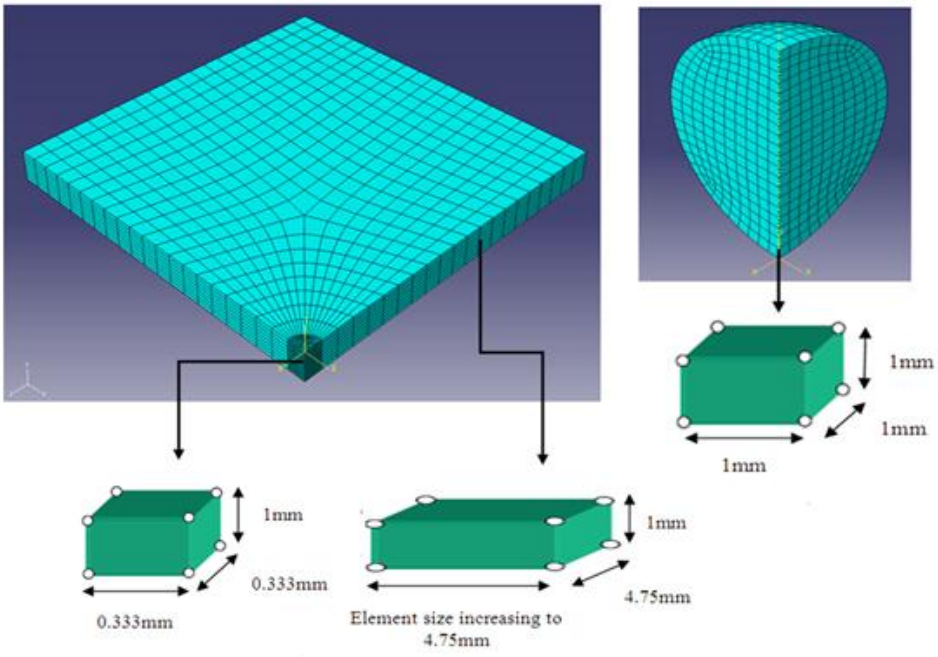

(a) The Plate (b) The impactor

Figure 4.14: Element size verification

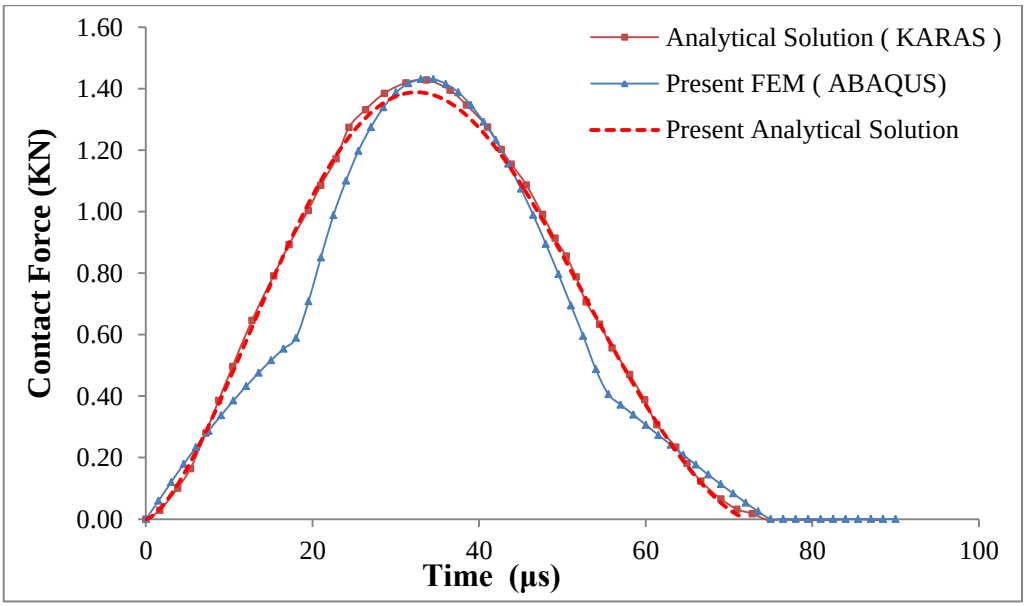

Figure 4.15: Comparison of contact force-time history with present FEM, analytical and previous data (Wu and Chang, 1989 - Karas study)

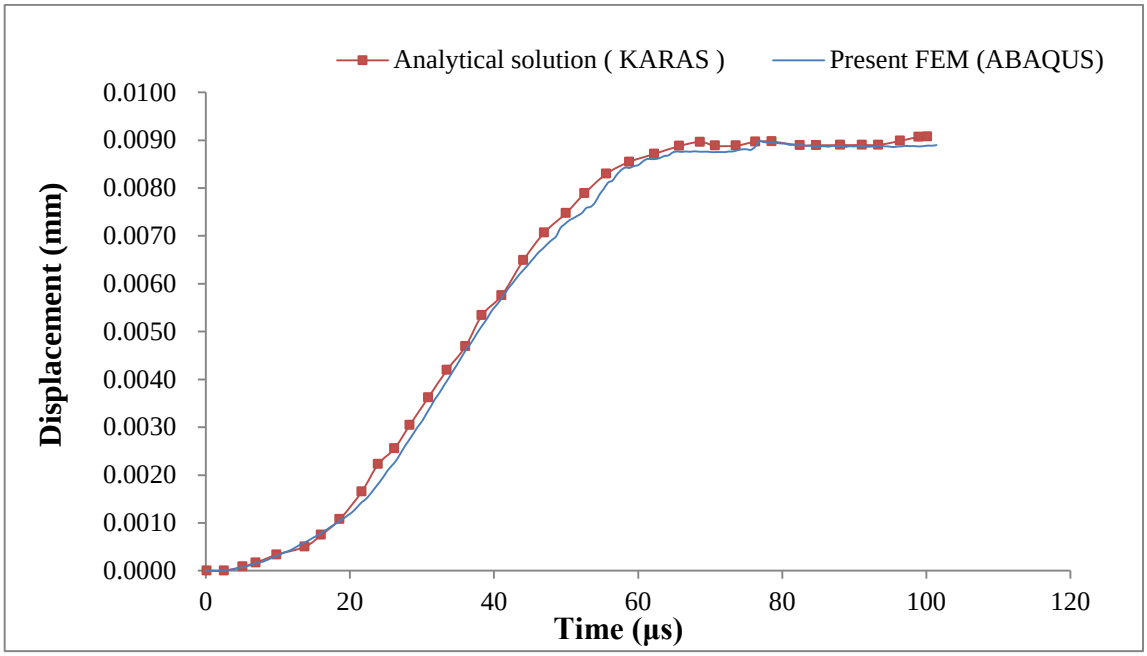

(a) The velocity-time history

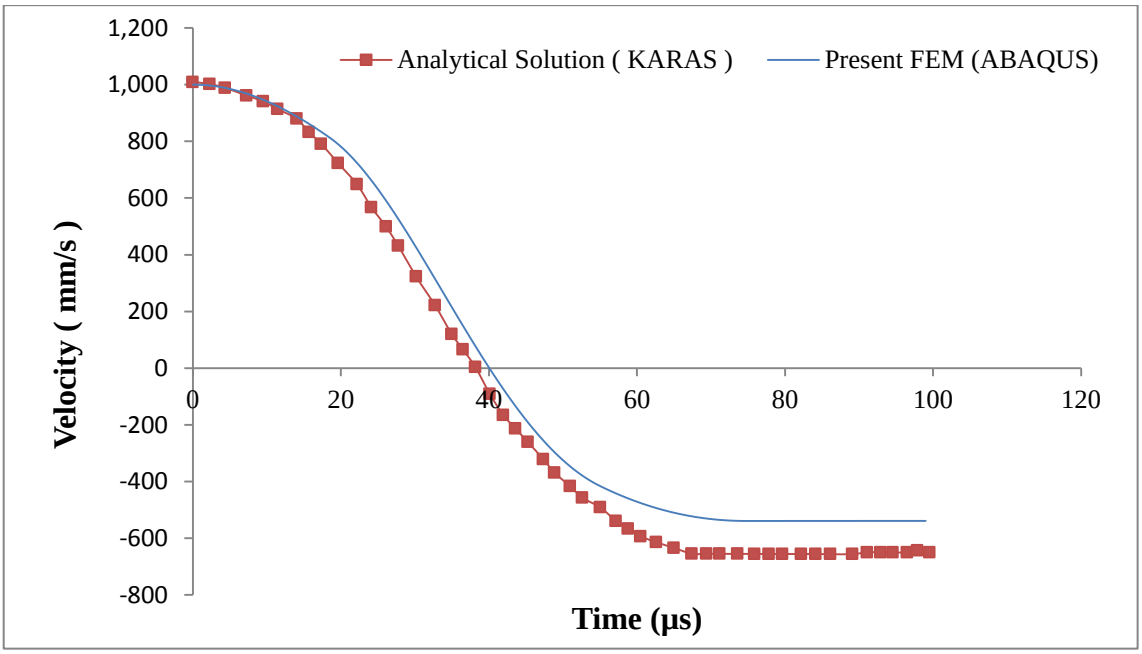

(b) The displacement–time history

Figure 4.16: FE results comparison with previous data (Wu and Chang, 1989)

4.5 Low – velocity impact numerical analysis of monolithic glass plate under various parametric conditions and comparison using an analytical method

Using the details listed in Table 3.2, the impact response of monolithic glass plate is numerically investigated in this section, which includes three cases from 1 to 3. While, the required material properties of numerical model are described in the Table 4.1. The quarter symmetric section of glass plate and impactor were created as three-dimensional form and the damping and friction effects between two objects were ignored during the analysis. For various plate thickness, the discretised monolithic glass plate nodes and elements details are outlined in Table 4.2 and it includes the optimum element size of 0.333 mm x 0.333 mm x 1 mm near contact zone and then gradually increase elements size of 4.75 mm x 4.75 mm x 1 mm in the outer zone (see Figure 4.14 a).

Table 4.2: Element and node summary of quarter symmetric monolithic glass plate

Plate size (1m x 1m)	Quarter model C3D8R	
	Nodes	Elements
0.012m thick plate	50739	45324
0.015m thick plate	62448	56655
0.018m thick plate	74157	67986

For damage analysis, it is necessary to consider the full plate numerical model, rather than the quarter of section. The damage initiation may occur in any direction with an irregular form for

the impacted glass plate, and this was the reason to select a full plate model. The highly dense mesh arrangement of full monolithic glass plate model is shown in Figure 4.17 and the element and node details are outlined in Table 4.3.

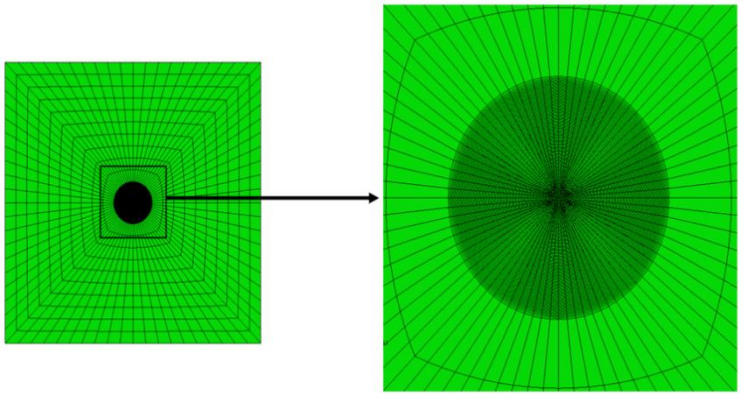

Figure 4.17 : Full plate model of monolithic glass plate (left) and expan view of damage initiate area (right)

Table 4.3: Element and node summary of monolithic glass plate full model

Plate size (1m x 1m)	Full model C3D8R	
	Nodes	Elements
0.012m thick plate	202956	182592
0.015m thick plate	249792	226620
0.018m thick plate	296628	271944

The contact force, displacement and velocity histories obtained from the numerical simulation by considering 5 m/s, 20 m/s and 40 m/s impact velocities for a 12 mm thick monolithic glass plate (Case 1) are shown in Figures 4.18(a), 4.18(b) 4.18(c), respectively. The time history

indicates the peak contact force is increasing with the increased impact velocity. It can also be seen that the first contact ending times are approximately equal for all three impact velocities. At the end of the first contact, the impactor started to reduce the initial impact velocity until zero with time and then, begins to rebound. The impactor rebounding velocities are 3.7 m/s, 15.1 m/s and 32.8 m/s, respectively. The velocity–time history also helps to identify the number of contacts between the plate and impactor. It can be found that maximum displacements at plate centre are 0.98 mm, 3.82 mm and 7.44 mm, respectively. Additionally, the displacement–time history curves help to estimate the total contact duration of the overall contact process, which included the impactor first contact, second contact and rebound responses, respectively.

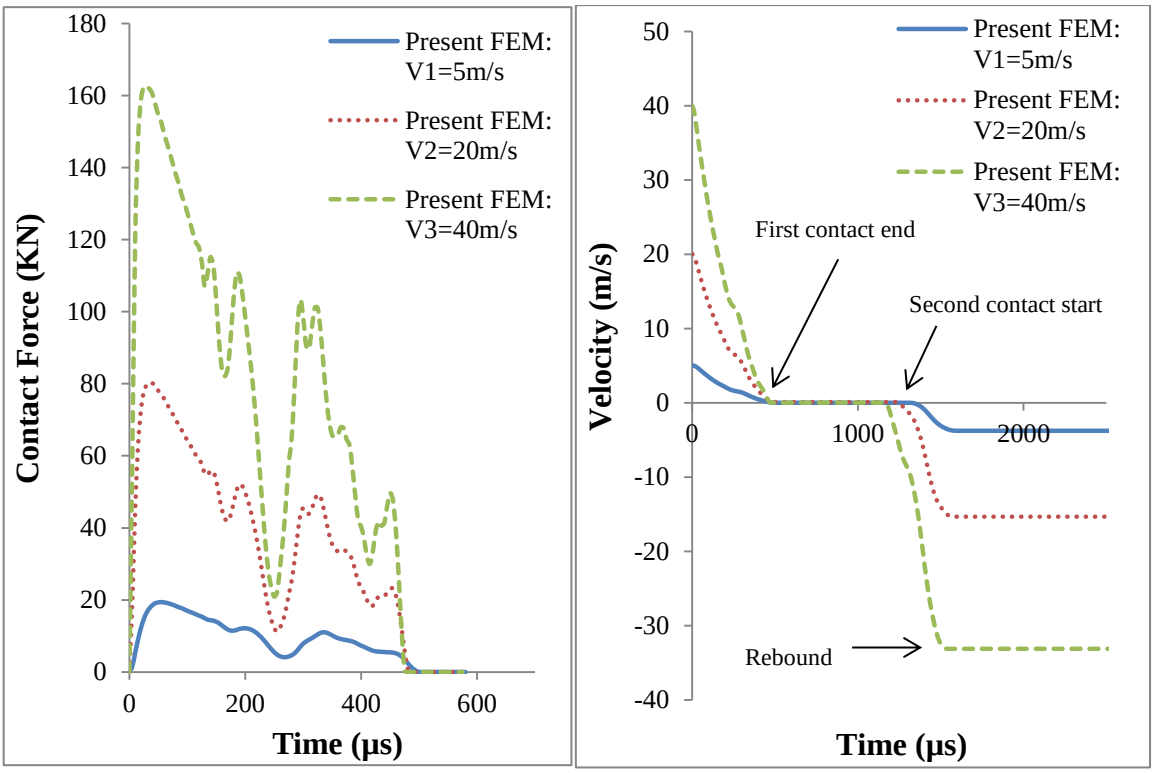

(a) Contact force-time history (b) Velocity-time history

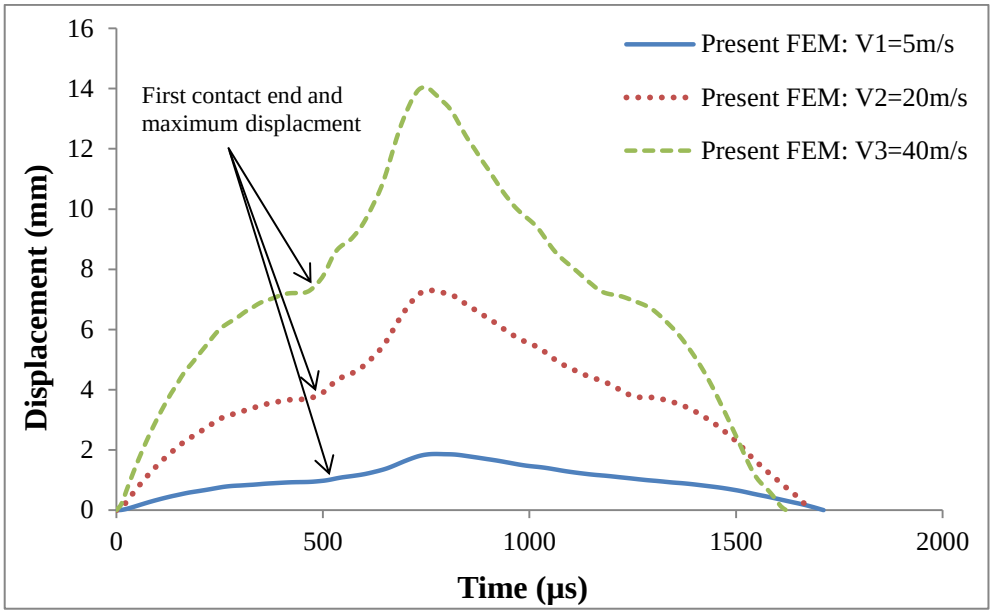

(c) Displacement-time history

Figure 4.18: Impact results for Case 1

Figure 4.19(a) presents the comparison of contact force history between present FEM and analytical method subject to the impact velocity. It can be seen that the peak contact forces, during the loading and unloading stages show close agreement between two methods. Figure 4.19(b) shows the displacement history comparison between the present numerical and analytical methods. It can be seen that the peak displacement results agree better at the impact velocity 5 m/s than the velocity of 20 m/s and 40 m/s. Table 4.4 summarises the peak contact force and displacement results with FEM and analytical methods. It is noted that the prediction of the peak contact forces can make a good agreement but not for peak displacements. It is also clear that the peak contact force is not directly proportional to the impact velocity.

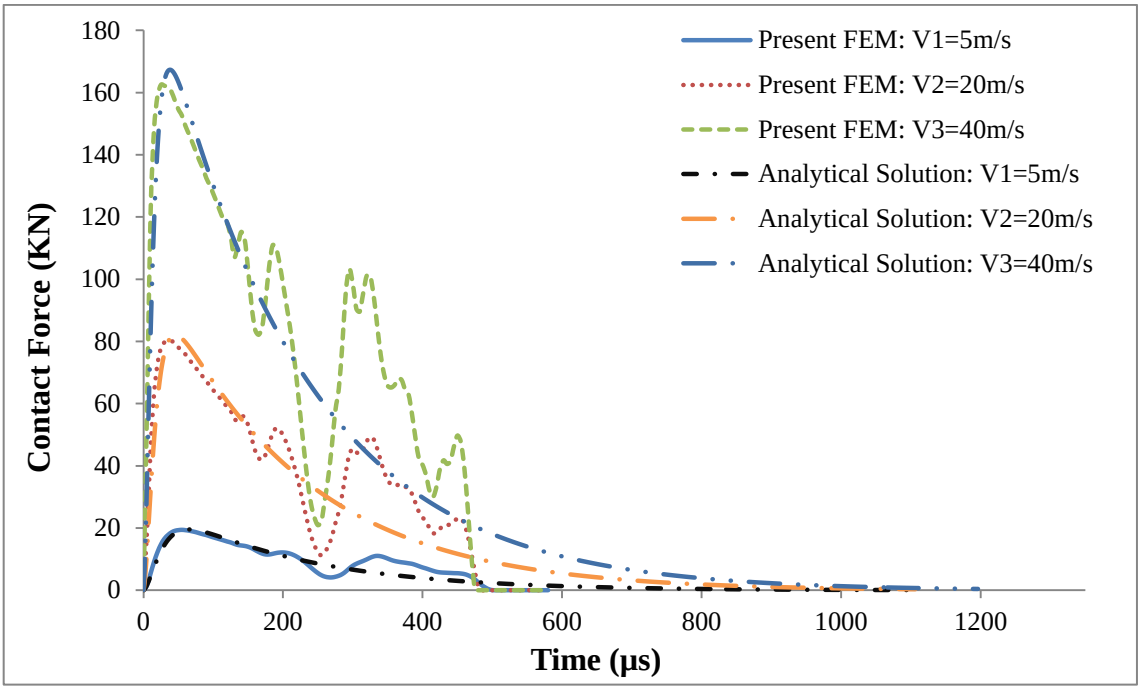

(a) Contact force-time history

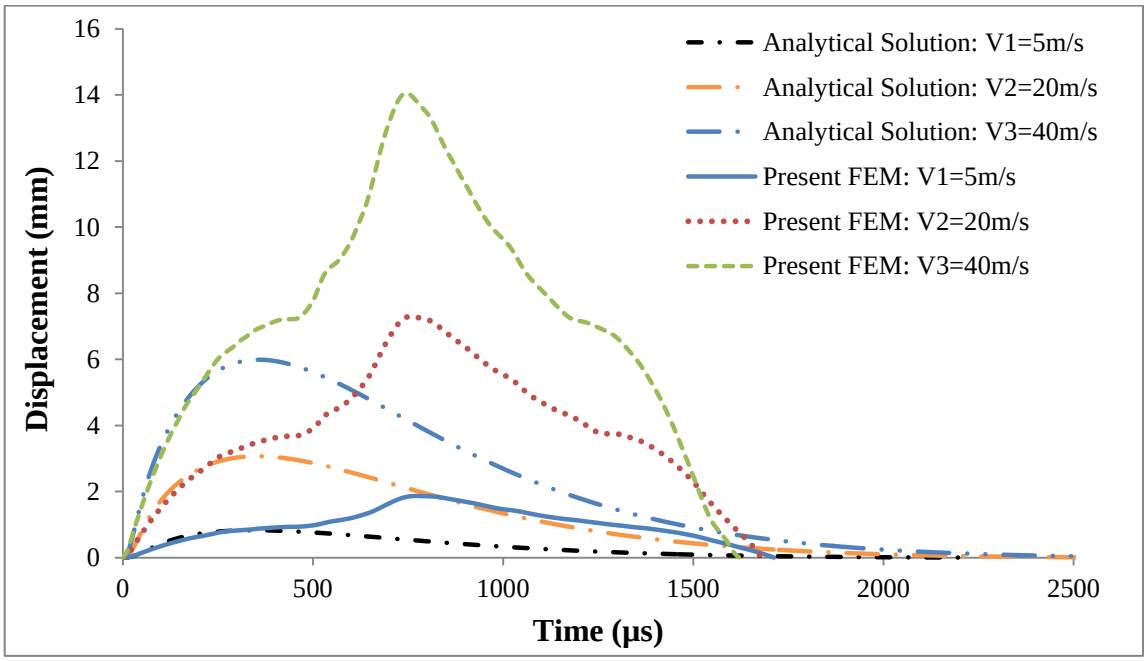

(b) Displacement time-history

Figure 4.19: Impact results comparison for Case 1

Figure 4.20 shows the impact damage response of monolithic glass plate using the force-time history results. The velocity 20m/s and 40m/s curves exhibited a sharp peak and a sudden drop while the velocity 5m/s curve obtained a smooth peak variation. Furthermore, the monolithic glass plate impact damage patterns are graphically summarised in Figure 4.21 and it included the glass plate rare or back surface damage initiation at contact force peak level (F_{peak}), time step before peak and finally contact ending time. It is clear that for the 12 mm thick glass plate, there is no damage initiation at velocity 5 m/s, but there are some star cracks appearing on the plate rare surface in loading and unloading stage at velocity 20 m/s and 40 m/s (Ball and McKenzie, 1994 and Bouzid et al., 2001).

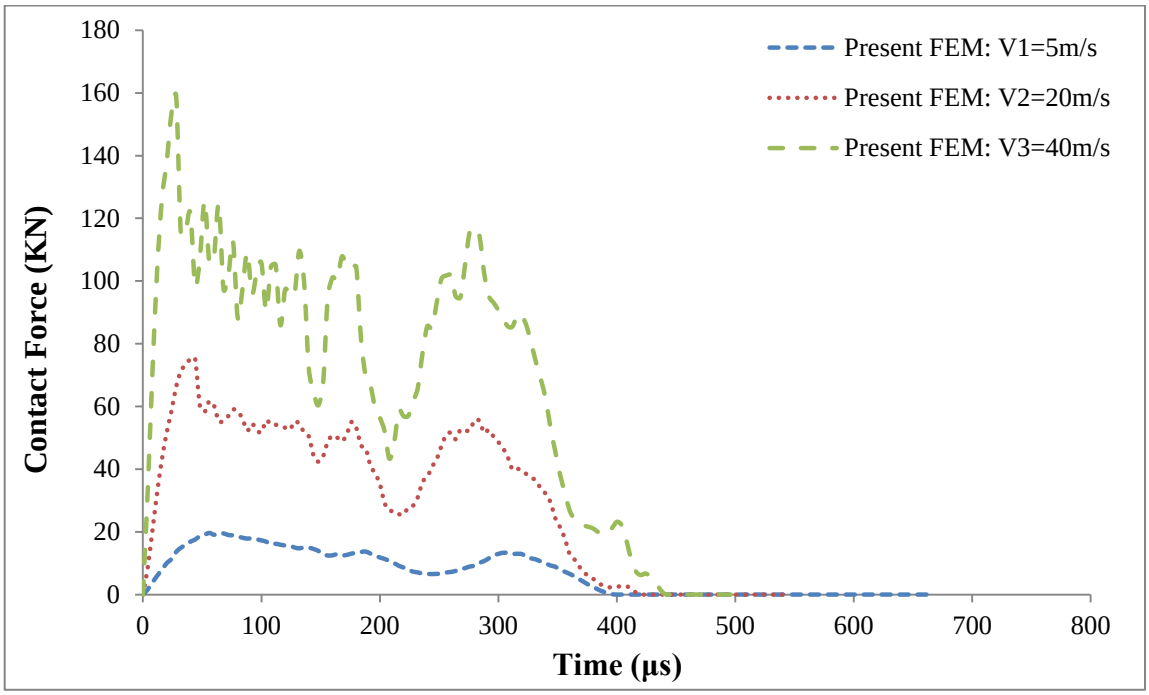

Figure 4.20: Contact force-time history damage prediction for Case 1

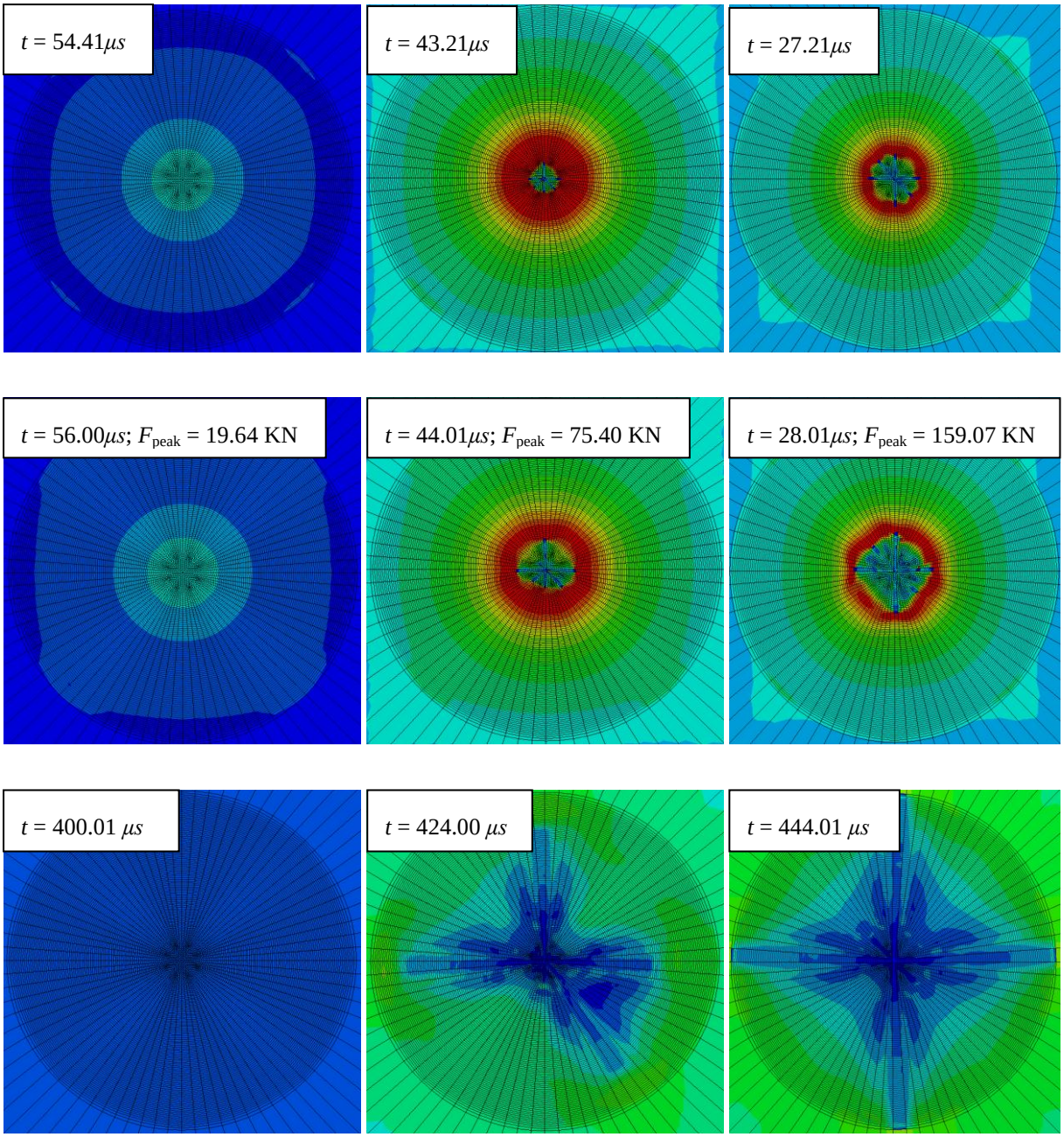

Figure 4.21: Impact damage response for Case 1

Table 4.5 summarises the peak contact force results by using the FE linear elastic and FE brittle cracking models. It is noted that the FE elastic material model and brittle cracking model results agree well for the impact velocity of 5 m/s and 40 m/s.

Table 4.4: Maximum contact force and displacement results comparison for Case 1

Studied Parameter		FEM (Elastic analysis)		Analytical method (wave propagation)		Difference	
		Peak contact force (kN)	Max. Displacement (mm)	Peak contact force (kN)	Max. Displacement (mm)	Peak contact force (%)	Max. Displacement (%)
Impact velocity (m/s) Case 1	5	19.40	0.98	19.53	0.83	-0.67	15.31
	20	80.35	3.82	82.01	3.05	-2.06	20.15
	40	162.49	7.44	167.33	5.99	-2.97	19.49

Table 4.5: FE elastic and FE damage models maximum contact force comparison for Case 1

Studied Parameter		FEM (Elastic analysis)	FEM (Damage model)	Difference
		Peak contact force(kN)	Peak contact force (kN)	(%)
Impact velocity (m/s) Case 1	5	19.40	19.67	-1.40
	20	80.35	75.40	6.16
	40	162.49	159.07	2.10

In Case 2, the contact force, velocity and displacement histories FE analysis results are shown in Figures 4.22(a), 4.22(b) and 4.22(c). The increasing in plate thicknesses can lead to an increases in overall contact force while decreasing the plate centre impact displacement and reducing the contact duration. The maximum contact force and displacement at the plate centre are 80.35, 116.65, 154.22 kN and 3.82, 2.48, 1.88 mm, respectively. The velocity plot is also used to predict the impactor movement during the analysis. It is clear that the plate thickness does control the impactor rebounding time and rebound velocity. The rebound velocity of 12mm, 15mm and 18 mm thickness glass plates are 15.3 m/s, 13.9 m/s and 12.9 m/s, respectively.

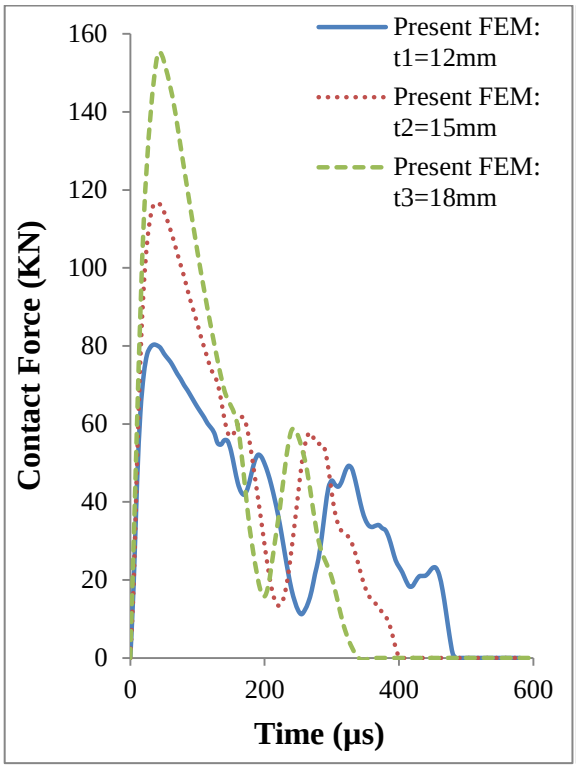

(a) Contact force-time history

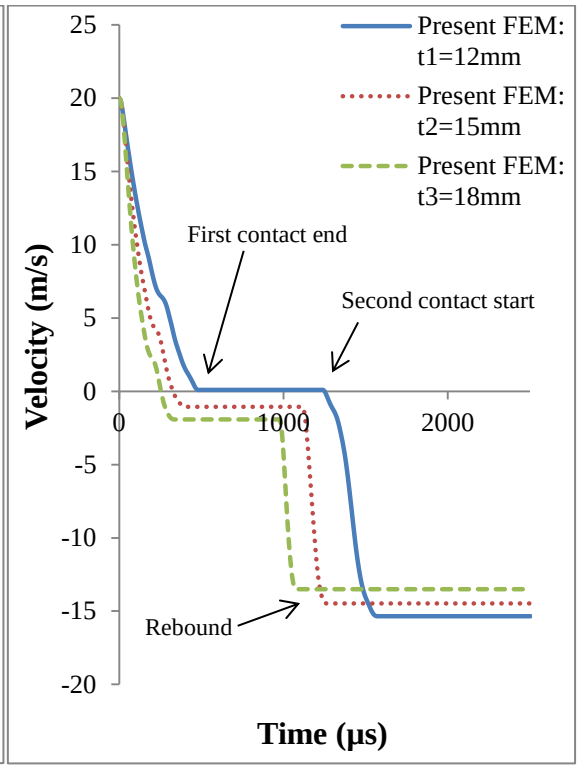

(b) Velocity-time history

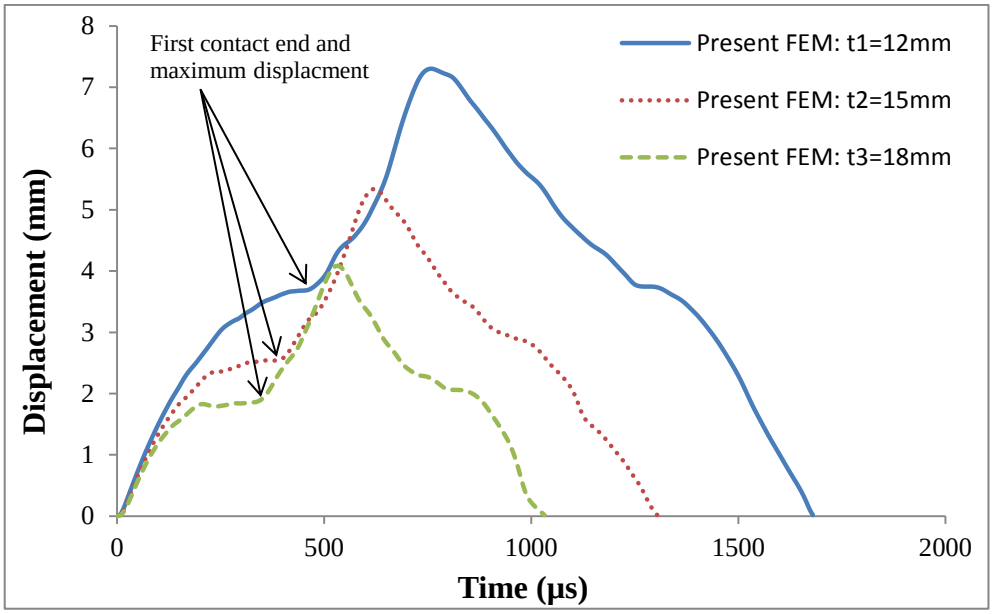

(c) Displacement-time history

Figure 4.22: Impact results for Case 2

Figures 4.23(a) shows the contact force-time history comparison between the FEM and wave propagation analytical method. It should be noted that both methods yield relatively close results. It can be also seen that the first contact ending times are significantly reduced when plate thickness increases. The first contact ending time is close with 18mm thick plate, but not for the 12 mm and 15 mm thick plates. The peak displacement results comparisons are illustrated in Figure 4.23(b). The comparison of the maximum contact force and maximum displacement results are summarised in Table 4.6. It is noted that the numerical prediction of the contact forces are in very good agreement with the analytical results. The 12 mm and 15 mm thickness plates shows less agreement for the peak displacement and the maximum over-prediction is 20.16%.

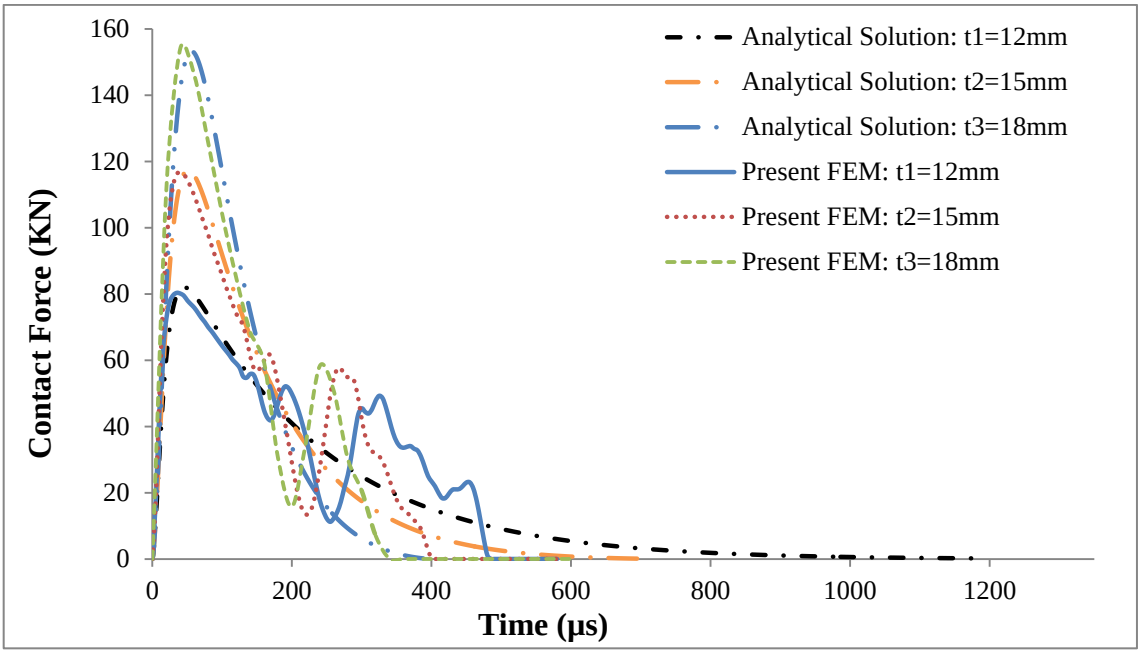

(a) Contact force-time

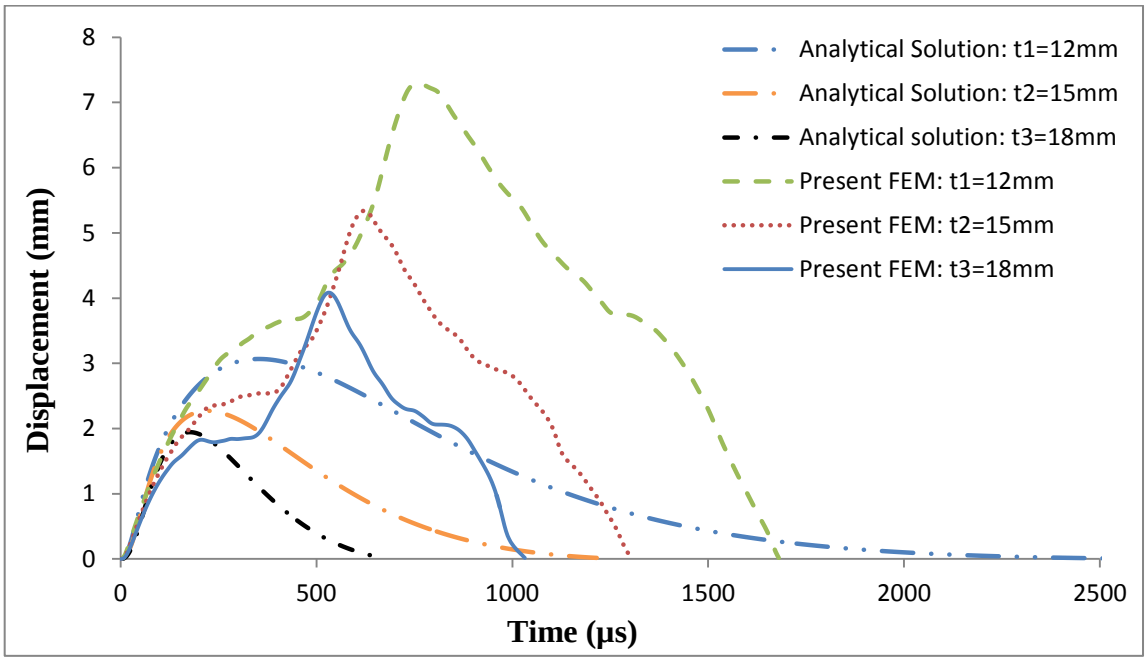

(b) Displacement-time

Figure 4.23: The results comparison for Case 2

Table 4.6: Maximum contact force and displacement results comparison for Case 2

Studied Parameter		FEM (Elastic analysis)		Analytical method (wave propagation)		Difference	
		Peak contact force (kN)	Max. Displacement (mm)	Peak contact force (kN)	Max. Displacement (mm)	Peak contact force (%)	Max. Displacement (%)
Top/bottom Glass ply thickness (mm) Case 2	12	80.35	3.82	82.01	3.05	-2.07	20.16
	15	116.65	2.48	117.42	2.27	-0.66	8.46
	18	154.22	1.88	153.32	1.86	0.59	1.07

In Case 2, the impact damage behaviours are illustrated in Figure 4.24. A sharp sudden drop was observed from the contact force curve. It can be seen that the 12 mm and 15 mm thick glass plates experience sharp drops immediately after the peak contact force and there is no sudden sharp drop for the monolithic glass plate with thickness 18 mm. The impact damage response of monolithic glass plate is graphically outlined in Figure 2.25. It is also noticed that the star shape cracks appear on the rare surface of 12 mm thick plate before the contact force approaches the peak level and but slightly after the peak contact force for the 15 mm thick glass plate. Also, there is no damage obtained in 18 mm thick glass plate during the analysis.

Table 4.7 summarises the peak contact force results from the FE linear elastic and FE brittle cracking models. It is noted that the results of the linear elastic material model slightly over-predicts the impact response when compared with the brittle cracking model results.

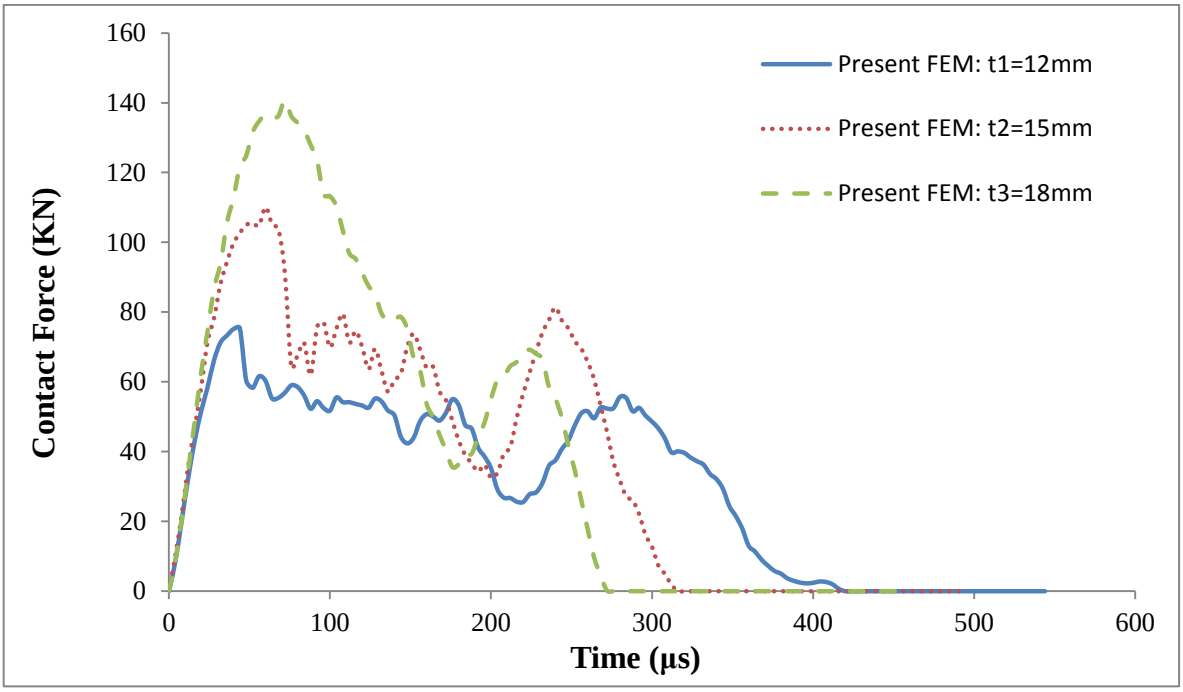

Figure 4.24: Contact force-time history damage prediction for Case 2

Table 4.7: FE elastic and FE damage models maximum contact force comparison for Case 2

Studied Parameter		FEM (Elastic analysis)	FEM (Damage model)	Difference
		Peak contact force (kN)	Peak contact force (kN)	(%)
Top/bottom Glass ply thickness (mm) Case 2	12	80.35	75.40	6.17
	15	116.65	110.09	5.63
	18	154.22	140.66	8.80

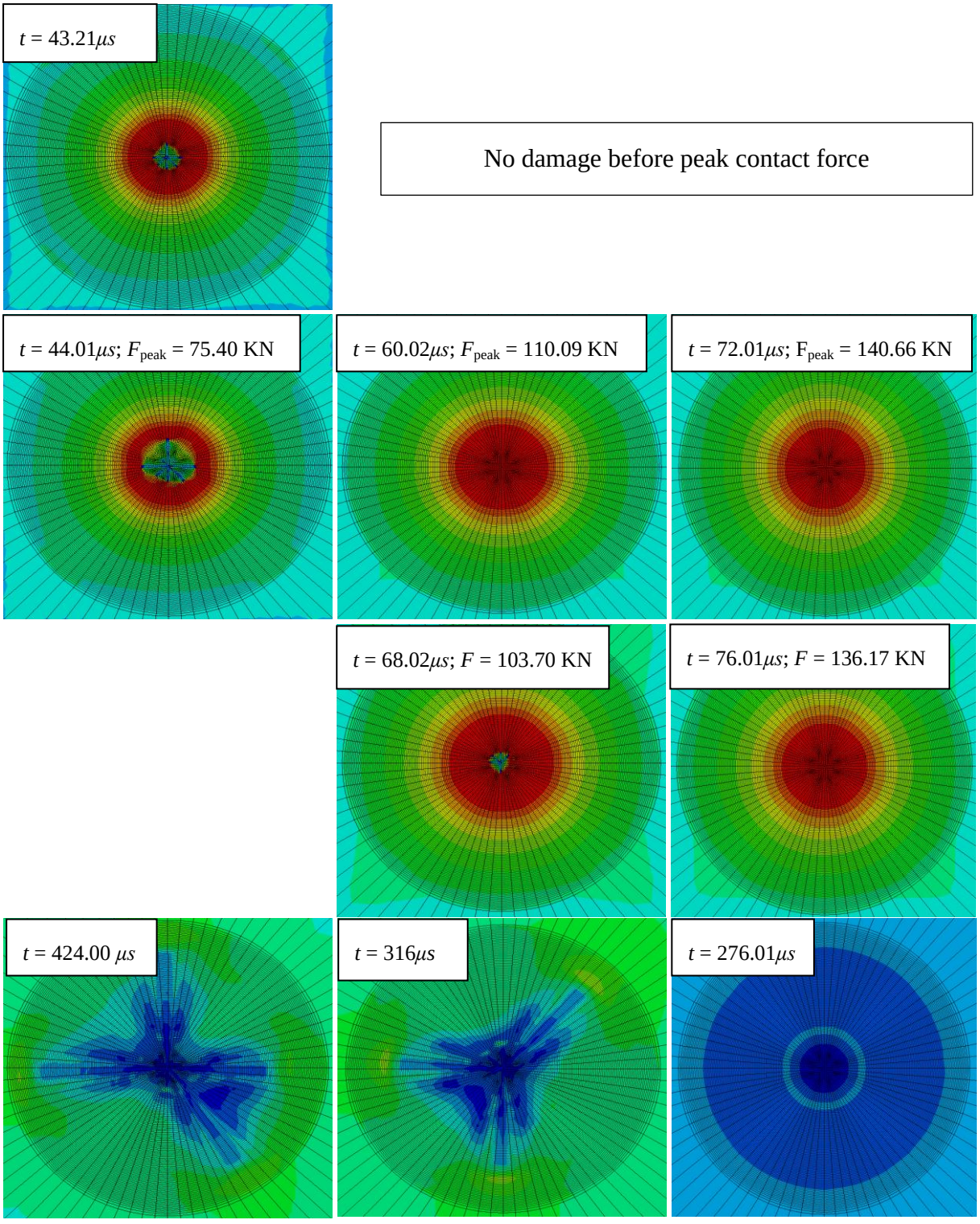

Figure 4.25: Impact damage response for Case 2

A variation of force, displacement and velocity with time for a 12 mm thick monolithic glass plate subjected to impact of various masses (0.5, 1 and 2Kg) are shown in Figures 4.26(a), 4.26(b) and 4.26(c), which is Case 3. The linear variation of loading stage is identical in the force-time history curves. The increased impactor masses can slightly increase the contact force response, but the difference is not significant compared to the contact force curves of Case 1 and Case 2. For each impactor masses, the initial impact velocity is 20 m/s and the rebound velocities are 8.75m/s, 15.30 m/s and 14.30 m/s, respectively. The velocity-time history shows some difference in rebound velocity for the impactor mass of 1Kg and 2Kg. The maximum plate centre displacement is observed from displacement-time history curves. It is evident that the plate centre displacement is increasing with impact mass and the maximum displacements are 1.98 mm, 3.82 mm and 5.98 mm, respectively.

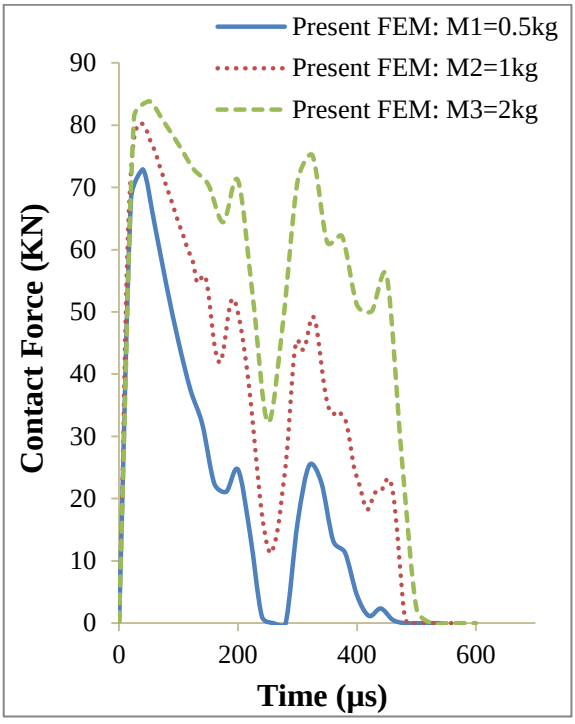

(a) Contact force-time history

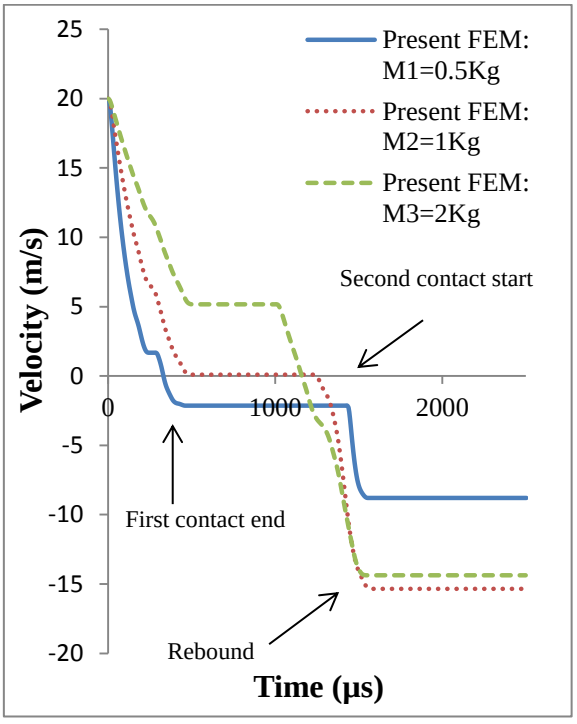

(b) Velocity-time history

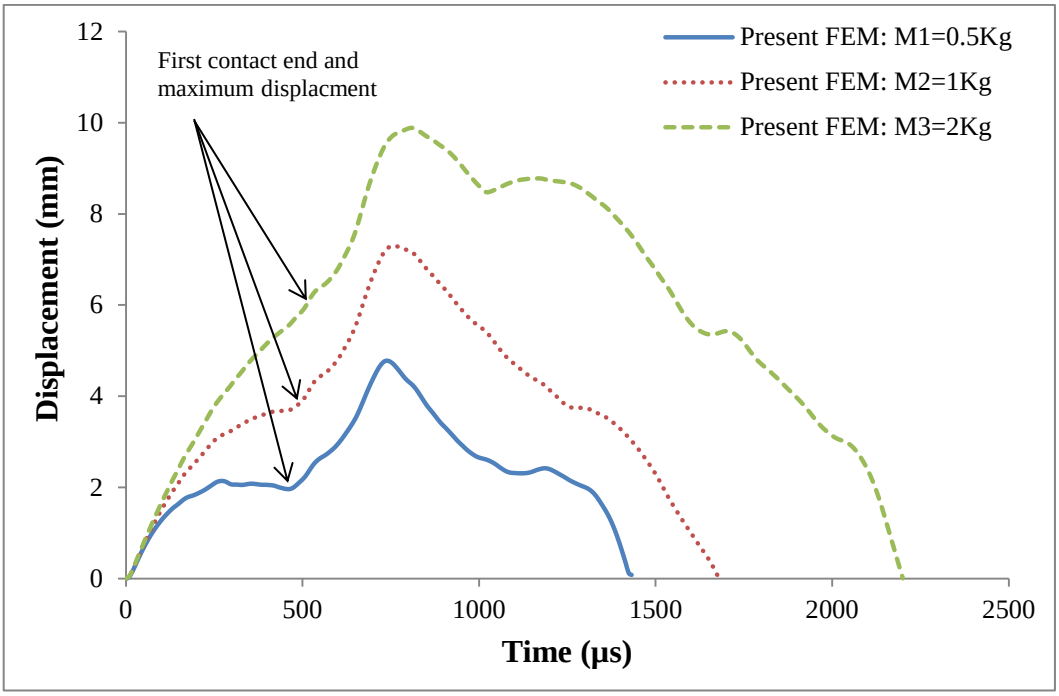

(c) Displacement-time history

Figure 4.26: Impact results for Case 3

Figure 4.27(a) shows the contact force comparison between FEM and wave propagation analytical methods. It is evident that the contact force response is increasing very slowly with impact mass. The peak contact force results of all impact masses are summarised in Table 4.8. Although the results provide less agreement for the peak contact force in comparison with the central plate displacement, but the differences are acceptable. The analytical method over-predicts the first contact ending time for the impactor mass of 1 Kg and 2 Kg but under-predicts it for the impact mass of 0.5 Kg. Figure 4.26(b) shows the comparison of the plate centre displacements between the numerical and analytical. The peak displacements are s summarised in Table 4.9.

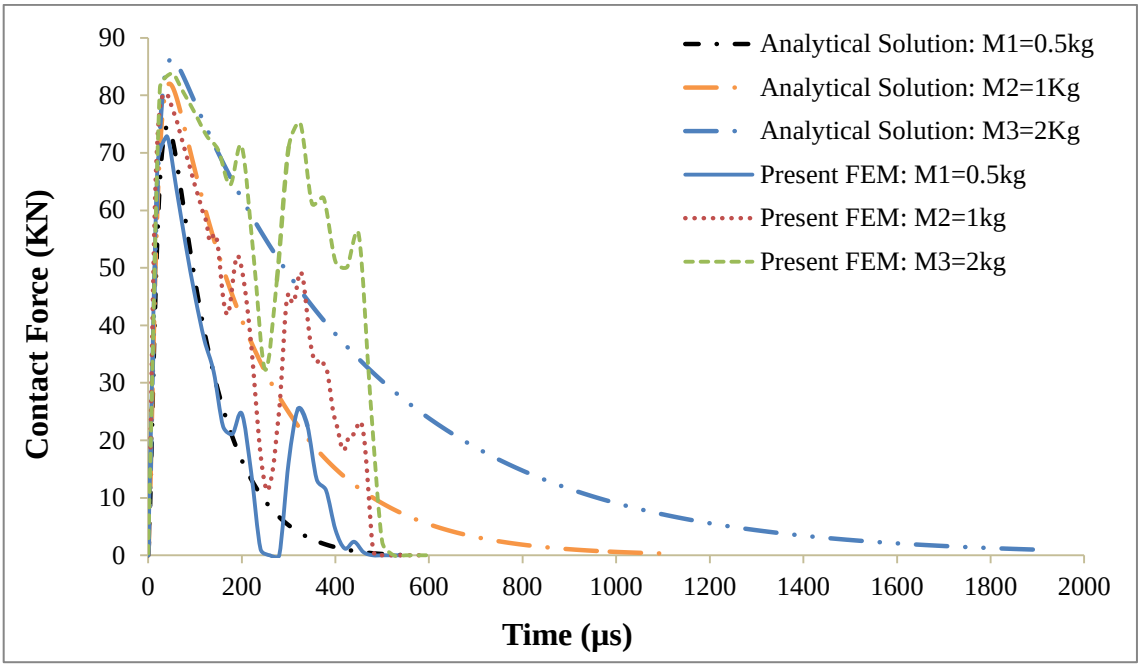

(a) Contact force-time history

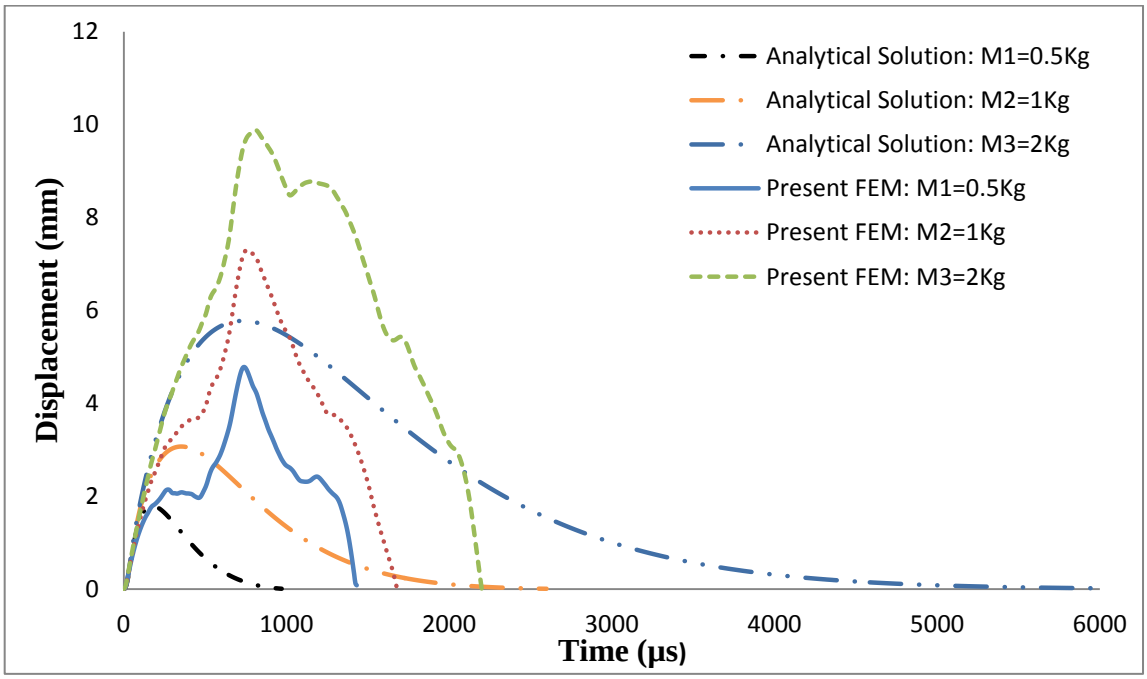

(b) displacement-time history

Figure 4.27: The results comparison for Case 3

Table 4.8: Maximum contact force and displacement results comparison for Case 3

Studied Parameter		FEM (Elastic analysis)		Analytical method (wave propagation)		Difference	
		Peak contact force (kN)	Max. Displacement (mm)	Peak contact force (kN)	Max. Displacement (mm)	Peak contact force (%)	Max. Displacement (%)
Impactor mass (Kg) Case 3	0.5	72.89	1.98	74.54	1.78	-2.27	10.10
	1	80.35	3.82	82.01	3.05	-2.06	20.15
	2	83.85	5.98	86.29	5.74	-2.91	4.02

Figure 4.28 shows the FE damage model contact force–time history for the Case 3. The contact force plot shows the two significant sharp drops for the 1 kg and 2 kg impact masses at peak force, but the 0.5 kg impact mass occurred as a sharp drop a small time step later from peak contact force. This response is graphically summarized in the Figure 4.29.

The peak contact force comparison between the present FE elastic and brittle cracking models are summarised in the Table 4.9. The result shows small mass impactor (0.5 Kg) is in good agreement for the both models. The 1Kg and 2Kg masses show less agreement and the over-predictions are occurred by the FE elastic material model.

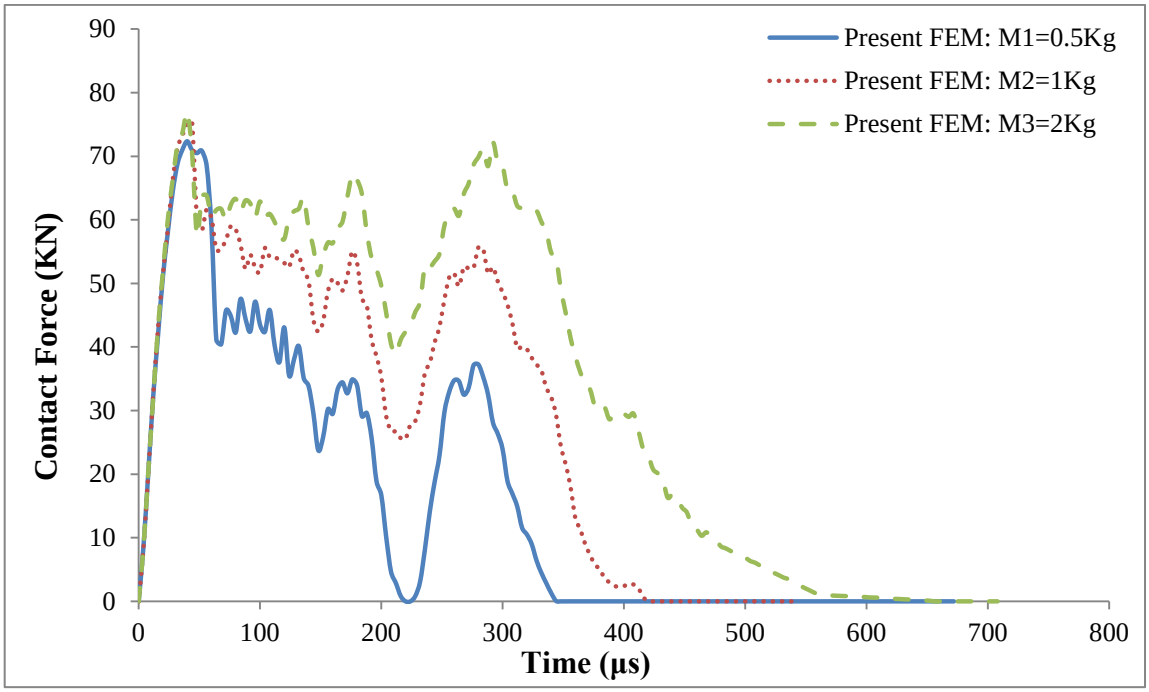

Figure 4.28: Contact force history damage response of monolithic glass plate with various impactor masses – Case 3

Table 4.9: FE elastic and FE damage models maximum contact force comparison for Case 3

Studied Parameter		FEM (Elastic analysis)		Analytical method (wave propagation)		Difference	
		Peak contact force (kN)	Max. Displacement (mm)	Peak contact force (kN)	Max. Displacement (mm)	Peak contact force (%)	Max. Displacement (%)
Impactor mass (Kg) Case 3	0.5	72.89	1.98	74.54	1.78	-2.27	10.10
	1	80.35	3.82	82.01	3.05	-2.06	20.15
	2	83.85	5.98	86.29	5.74	-2.91	4.02

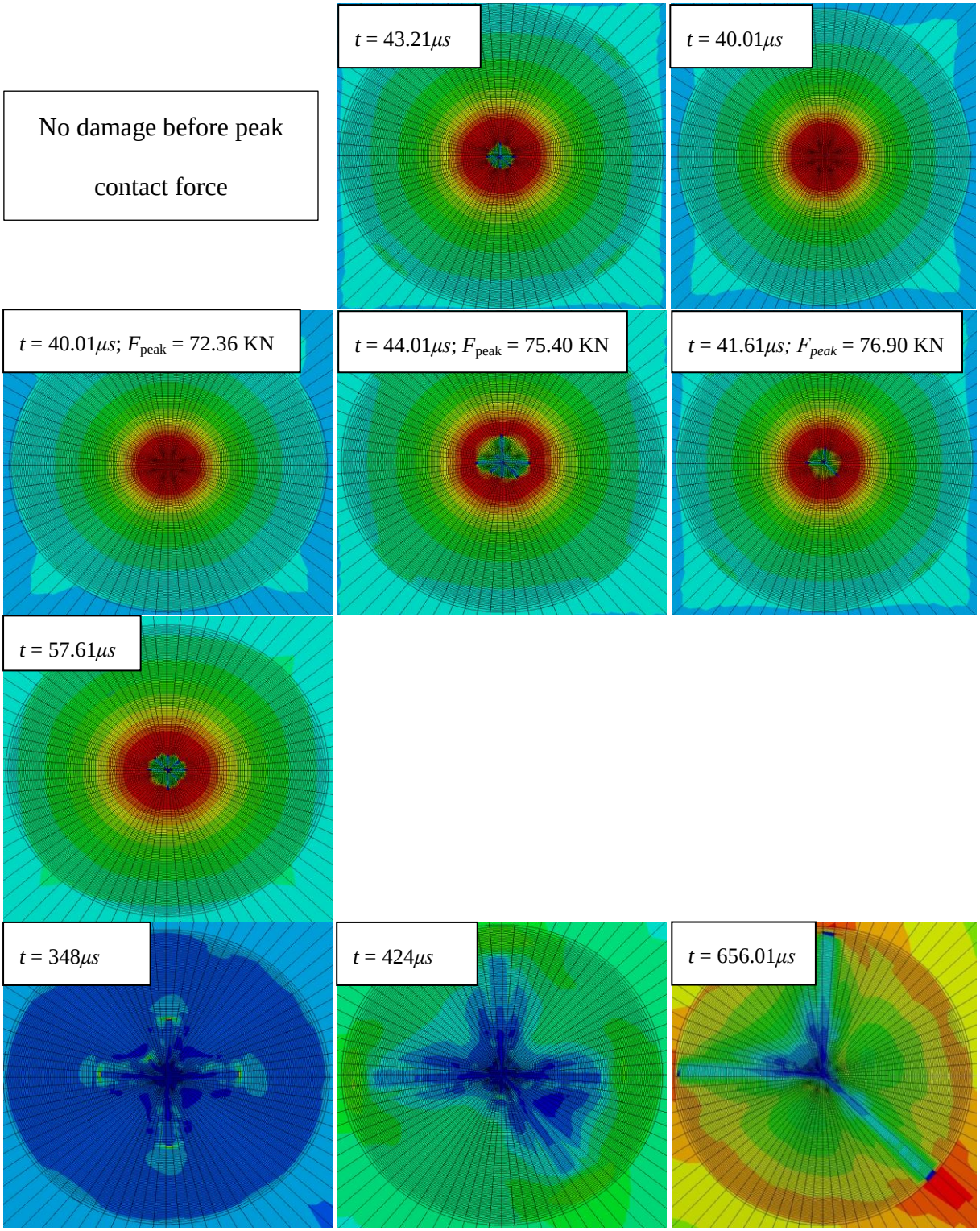

Figure 4.29: Impact damage response for Case 3

4.6 Low – velocity impact numerical analysis of laminated glass plate under various parametric conditions and comparison using an analytical method

Elastic response of laminated glass (LG) plate was simulated in this section under low-velocity impact loading. The required dimensions and study parameters of LG plate were previously described in section 3.6, Table 3.6. It was outlined typical four cases, such as Case 4- the impact velocity, Case 5- the glass ply thickness, Case 6- the impactor mass and finally Case 7- the PVB inter layer effect. These four cases correspond to elastic impact and no damage or failure responses of the LG plate. For the numerical model, the required material properties were previously described in the Table 3.3 and 3.5. The quarter symmetric section of laminated glass plate and impactor were generated as three-dimensional form and it was indicated in Figure 4.4(b) and 4.4(c). The discretised laminated glass model consisted element and node details are outlined in Table 4.10. As we discussed in section 4.4, exactly the same element type and size were used to mesh the LG plate top/bottom glass plies and PVB interlayer, such as near impactor contact zone element size of 0.333 mm x 0.333 mm x 1mm and outer zone element size of 4.75 mm x 4.75 mm x 1 mm (see Figure 4.14).

Table 4.10: Element and node summary of quarter symmetric laminated glass plate

Laminated glass 1m x 1m	Quarter model C3D8R					
	Glass top		PVB		Glass bottom	
$h_{glass}/h_{pvb}/h_{glass}$ (mm)	Nodes	Elements	Nodes	Elements	Nodes	Elements
6.0/0.76/6.0	27321	22662	11709	7554	27321	22662
8.0/0.76/8.0	35127	30216	11709	7554	35127	30216
10.0/0.76/10.0	42933	37770	11709	7554	42993	37770

It is worth noting that all time history curves exhibits smooth variation. For Case 4, the numerical results for contact force, velocity and displacement with three different impact velocities are shown in Figures 4.30(a), 4.30(b) and 4.30(c). The peak force and displacement responses increase with increasing impact velocity. The first contact durations are approximately the same for all three impact velocities. The velocity-time history is also used to identify the first and second contacts and rebound response of the impactor. The rebound velocities are 4.55 m/s, 18.20 m/s and 35.80 m/s.

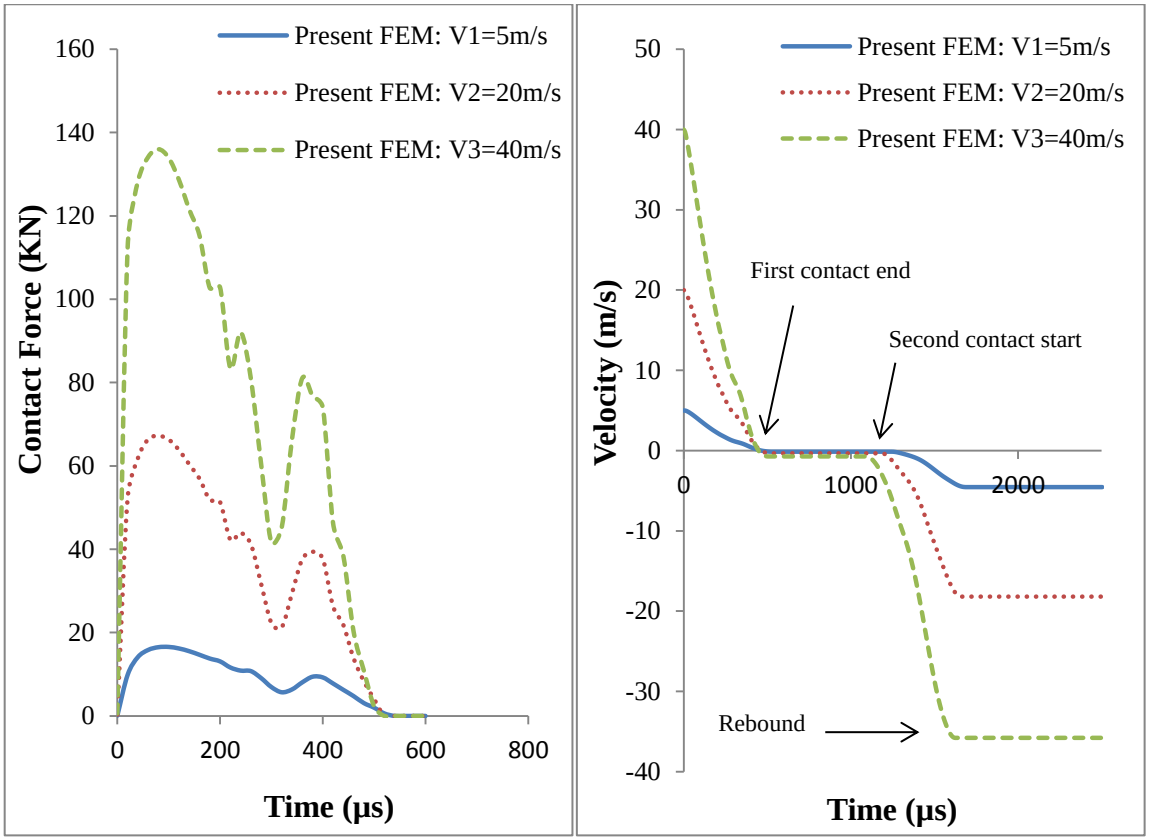

(a) Contact force-time history (b) Velocity-time history

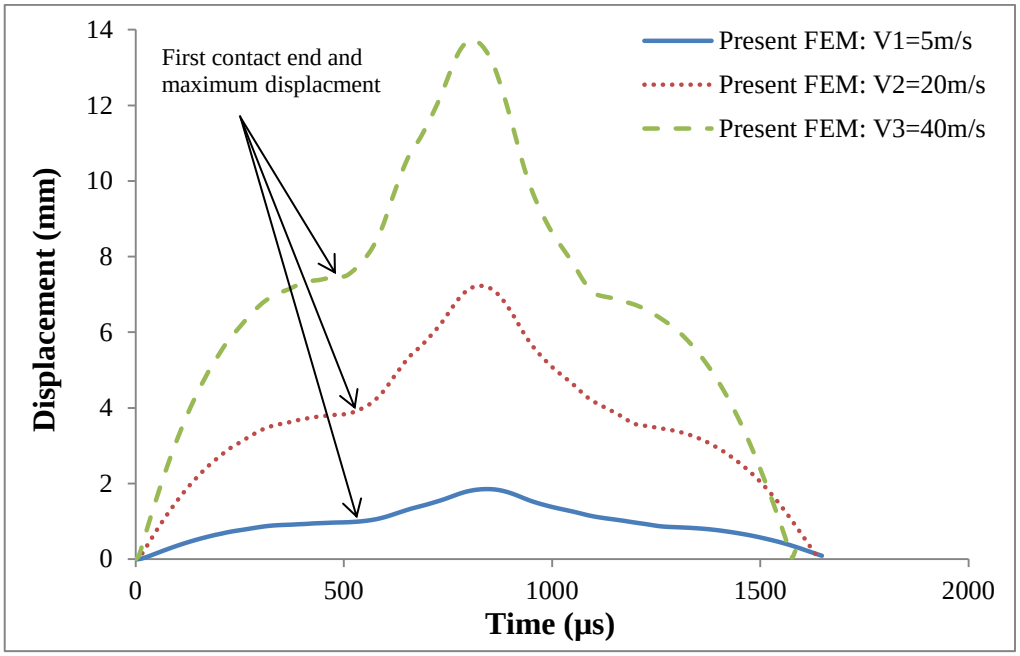

(c) Displacement-time history

Figure 4.30: Impact results for Case 4

For Case 4, the comparison of results for LG plate between the FE and wave propagation analytical methods are illustrated in Figure 4.31(a) and Figure 4.31(b). It includes the contact force and plate centre maximum displacement. The contact force curves show that a close agreement can be observed in the loading stage until the peak level and the discrepancy will occur during the unloading stage. From the same figure, one can see that there is an evident difference in the first contact ending times between two methods. The comparison of the peak contact force and maximum displacement are summarised in Table 4.11. It is noted that the peak contact force prediction of the FE and analytical methods are in good agreement with the impact velocity of 40 m/s. The peak displacement results, however, show a less agreement and an over-prediction from the numerical method.

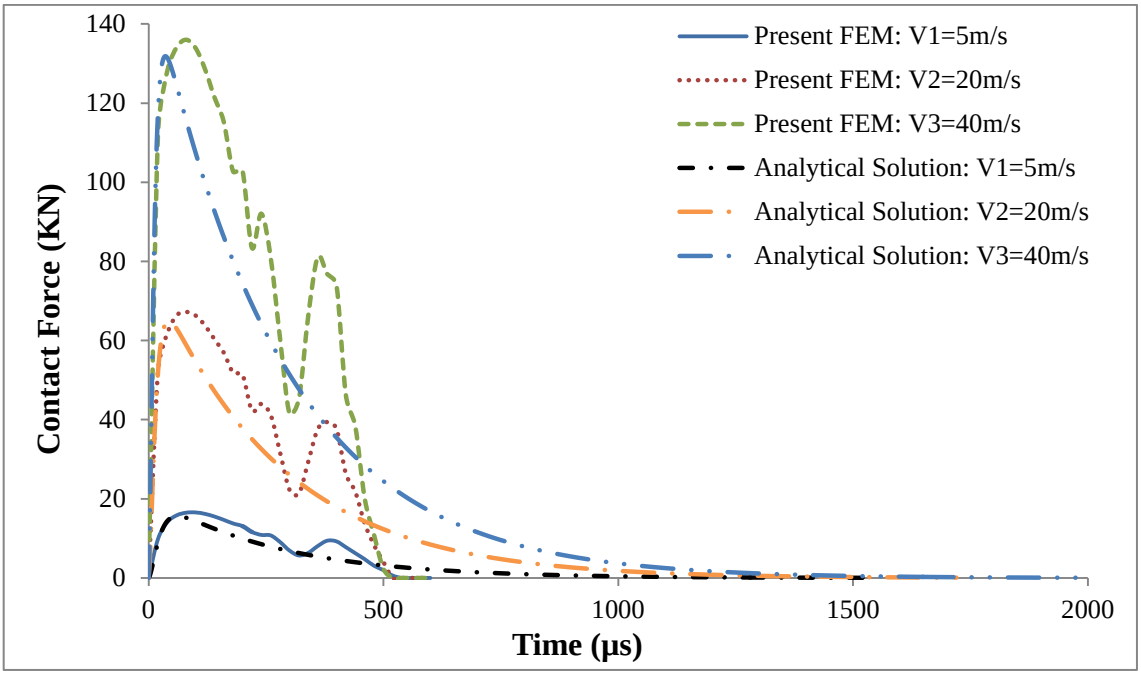

(a) Contact force-time history

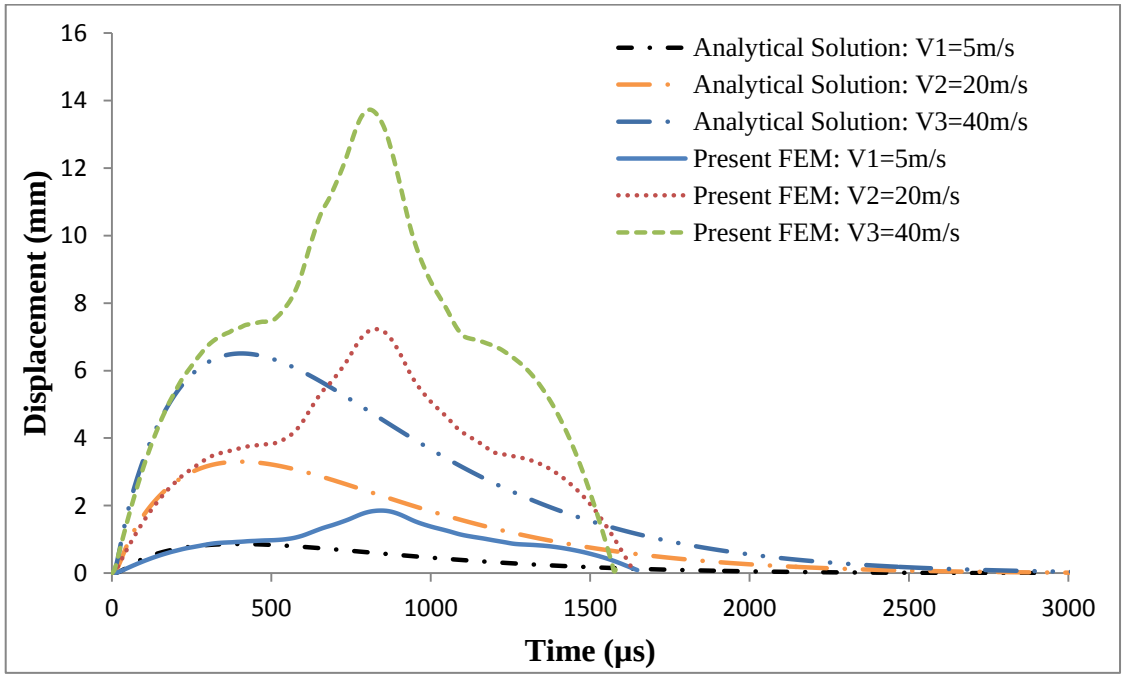

(b) Displacement-time history

Figure 4.31: The results comparison for Case 4

Table 4.11: Maximum contact force and displacement results comparison for Case 4

Studied Parameter		FEM (Elastic analysis)		Analytical method (wave propagation)		Difference	
		Peak contact force (kN)	Max. Displacement (mm)	Peak contact force (kN)	Max. Displacement (mm)	Peak contact force (%)	Max. Displacement (%)
Impact velocity (m/s) Case 4	5	16.57	0.95	15.63	0.86	5.68	9.47
	20	67.22	3.80	64.92	3.34	3.43	12.11
	40	134.14	7.45	131.83	6.46	1.73	13.28

The low-velocity impact response for the LG plates of various thicknesses is presented in Figures 4.32(a), 4.32(b), 4.32(c), which corresponds to Case 5. The contact force curves indicate that the overall response of laminated glass plate increases with increasing top/bottom glass ply thickness. Also, the first contact duration is decreased when the thickness of the glass ply is increased. The impact velocity curves indicates that the impactor's first, second contact and rebound velocities varies significantly while the top/bottom glass ply thicknesses is changed. The impactor's initial velocity is 20 m/s and the impactor rebound velocities are 18.20, 15.90 and 11.60 m/s. The first contact ending times is used to predict the maximum plate centre displacement using displacement–time history curves. It can be seen that the peak displacement results for LG plate decreases with increasing top/bottom glass ply thickness. The maximum displacements of LG plates are 3.80, 2.43 and 1.68 mm.

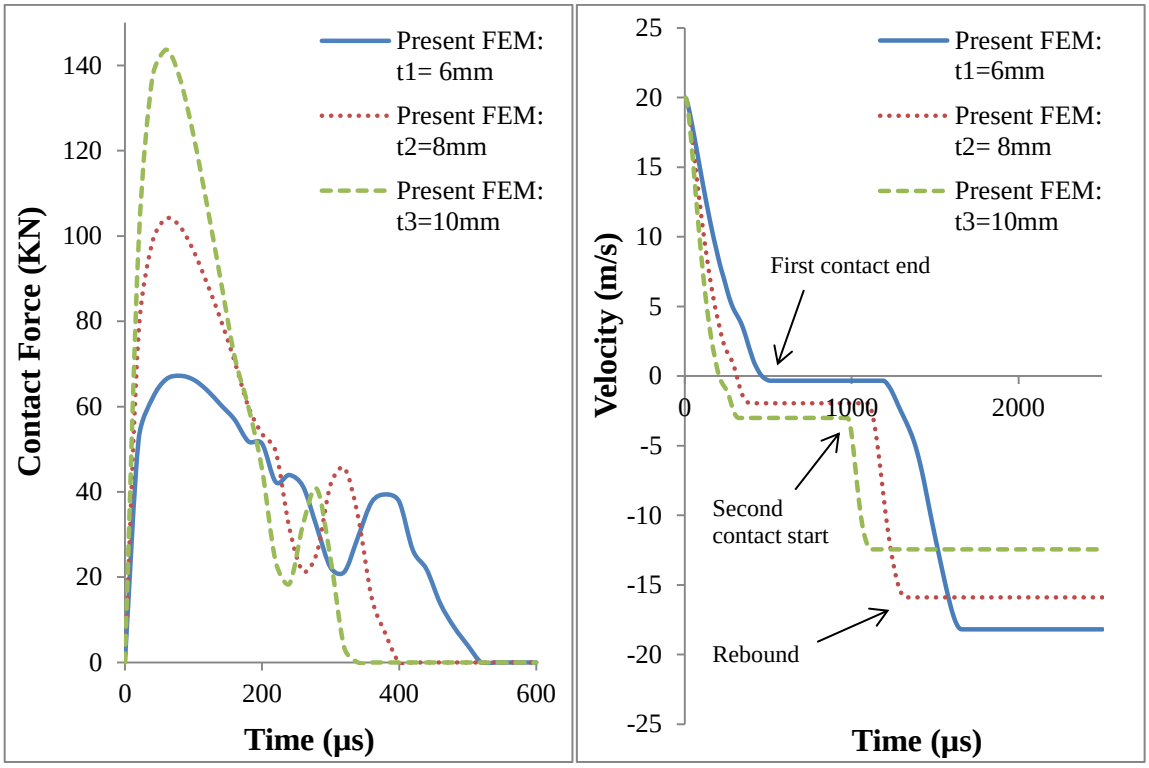

(a) Contact force-time history (b) Velocity-time history

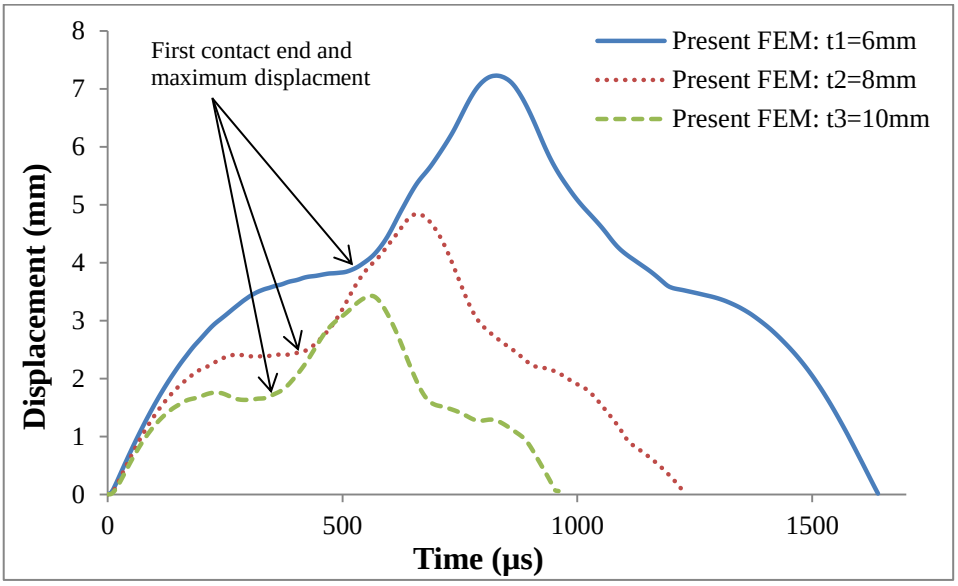

(c) Displacement-time history

Figure 4.32: Impact results for Case 5

Figure 4.33(a) presents the comparison of contact force history between present FEM and wave propagation analytical method subject to the top/bottom glass ply thickness. The peak contact force was observed and it is summarised in Table 4.12. It is noted that the peak contact force results are in extremely good agreement with the 8 mm and 10 mm top/bottom ply thicknesses when compared to the 6 mm top/bottom ply thickness. Additionally, the contact force plot shows the loading portions are co-incident with all three ply thicknesses, but the unloading portion slightly vary for the top/bottom ply thickness 6 mm LG plate. Figure 4.33(b) shows a comparison of LG plate central displacement using the numerical and wave propagation analytical methods and the results are also illustrated in Table 4.12. The results show the peak displacements are in good agreement with the 6 mm and over-prediction for the 8 mm and 10 mm top/bottom ply thicknesses.

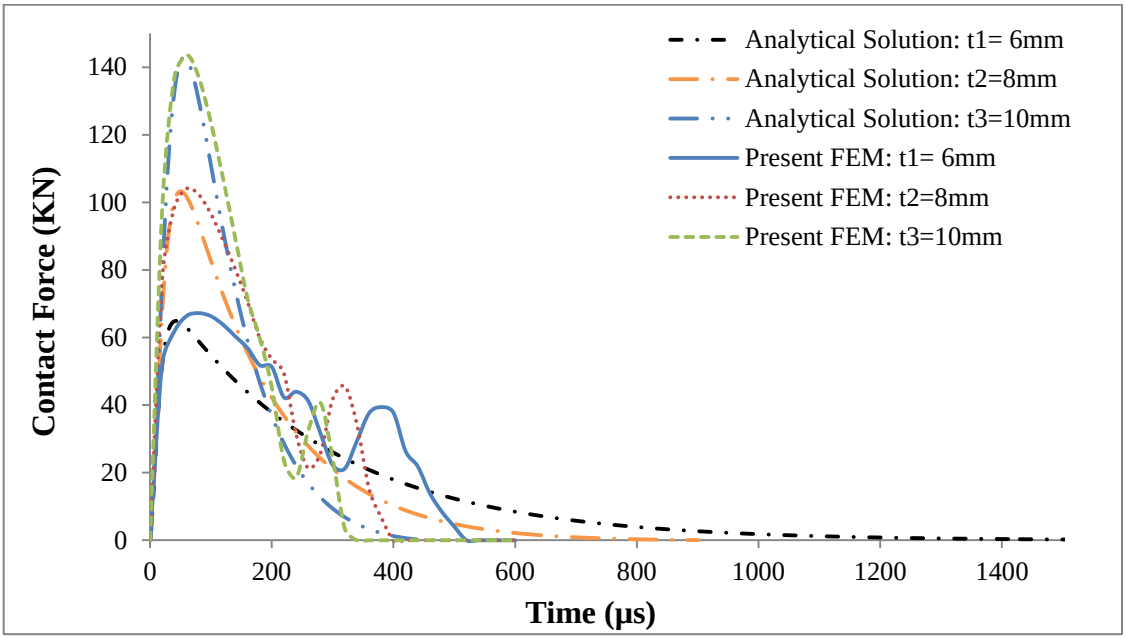

(a) Contact force-time history

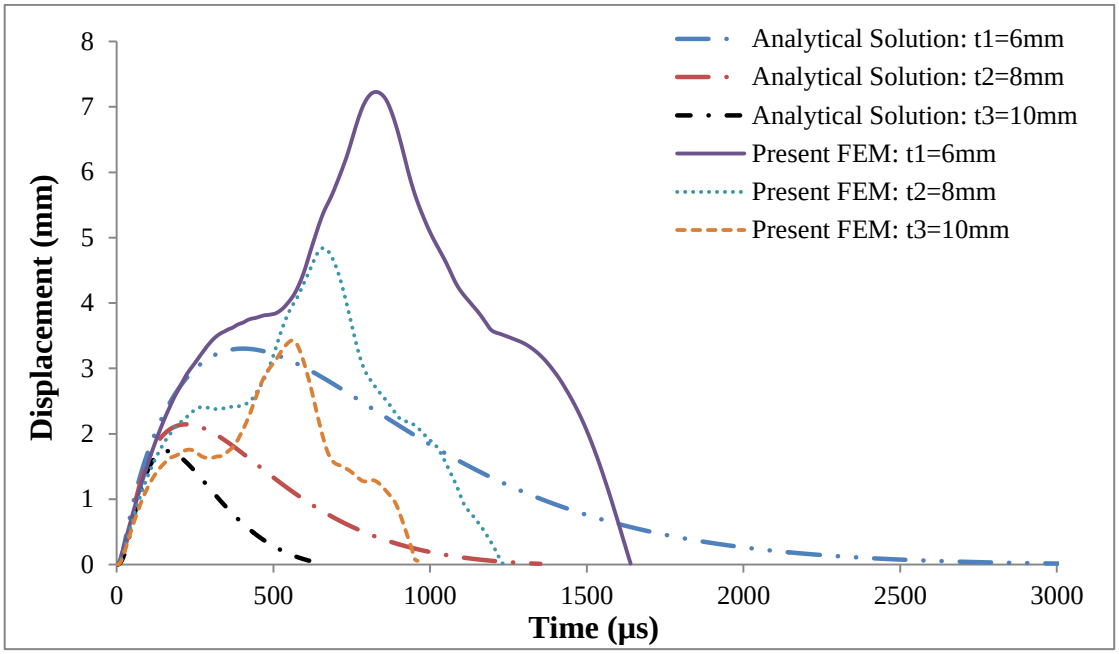

(c) Displacement-time history

Figure 4.33: The results comparison for Case 5

Table 4.12: Maximum contact force and displacement results comparison for Case 5

Studied Parameter		FEM (Elastic analysis)		Analytical method (wave propagation)		Difference	
		Peak contact force (kN)	Max. Displacement (mm)	Peak contact force (kN)	Max. Displacement (mm)	Peak contact force (%)	Max. Displacement (%)
Glass ply Thickness (mm) Case 5	6	67.22	3.80	64.92	3.34	3.42	12.11
	8	104.07	2.43	103.28	2.13	0.76	12.35
	10	143.67	1.68	142.93	1.70	0.52	-1.20

In Case 6, the responses of contact force, velocity and plate central displacement subject to the different impactor masses are shown in Figures 4.34(a), 4.34(b) and 4.34(c). It can be seen that the contact force, first contact ending time and plate centre displacement are increased when the impact masses are increased. The variation of LG plate velocity-time history is approximately similar to Case 3.

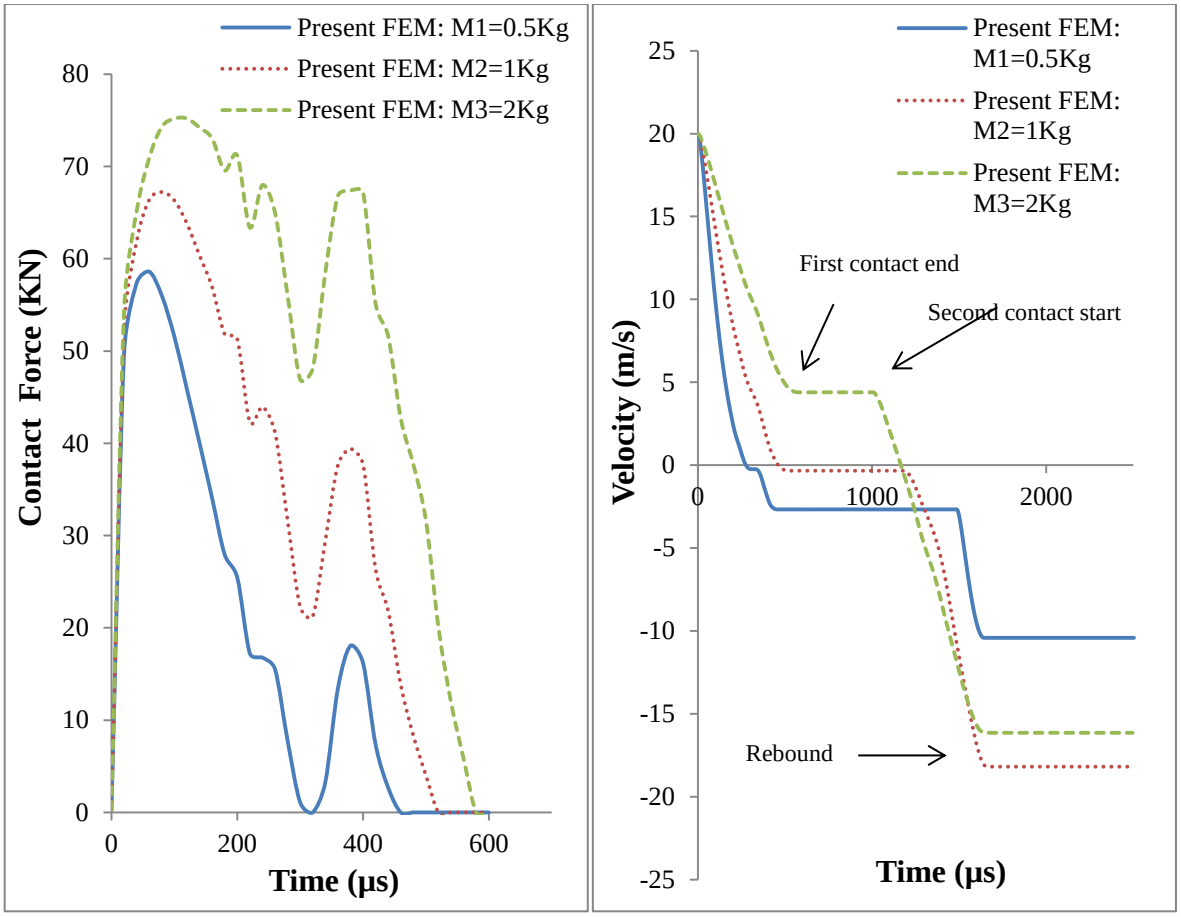

(a) Contact force-time history (b) Velocity-time history

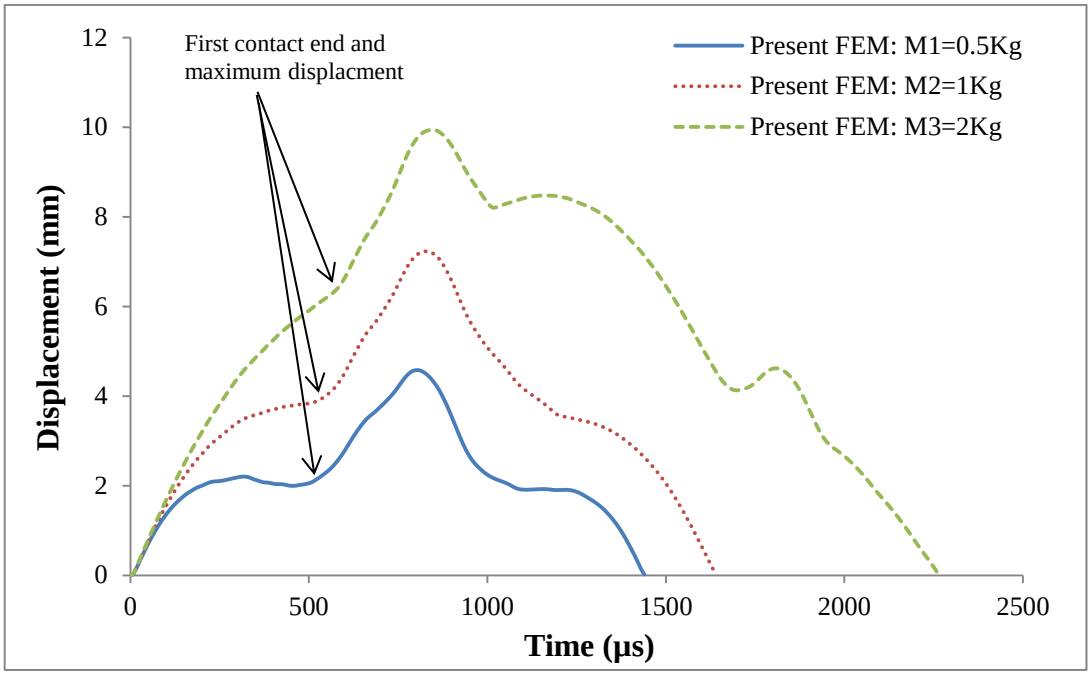

(c) Displacement-time history

Figure 4.34: Impact results for Case 6

The comparisons of the effect of impact mass on the contact force and plate central displacement are shown in Figures 4.35(a) and 4.35(b). The numerical and analytical results show that the contact force increases very slowly with impact mass and the impact mass has an insignificant effect on the impact response in the loading stage. The contact force curves also indicate over-predictions for the first contact ending time from the wave propagation analytical method.

Table 4.13 summarises the peak contact force and displacement results from the FEM and analytical predictions. It is noted that the FEM contact force results for the 0.5 Kg and 1 Kg masses and the displacement results for the 2Kg mass are in good agreement with analytical results.

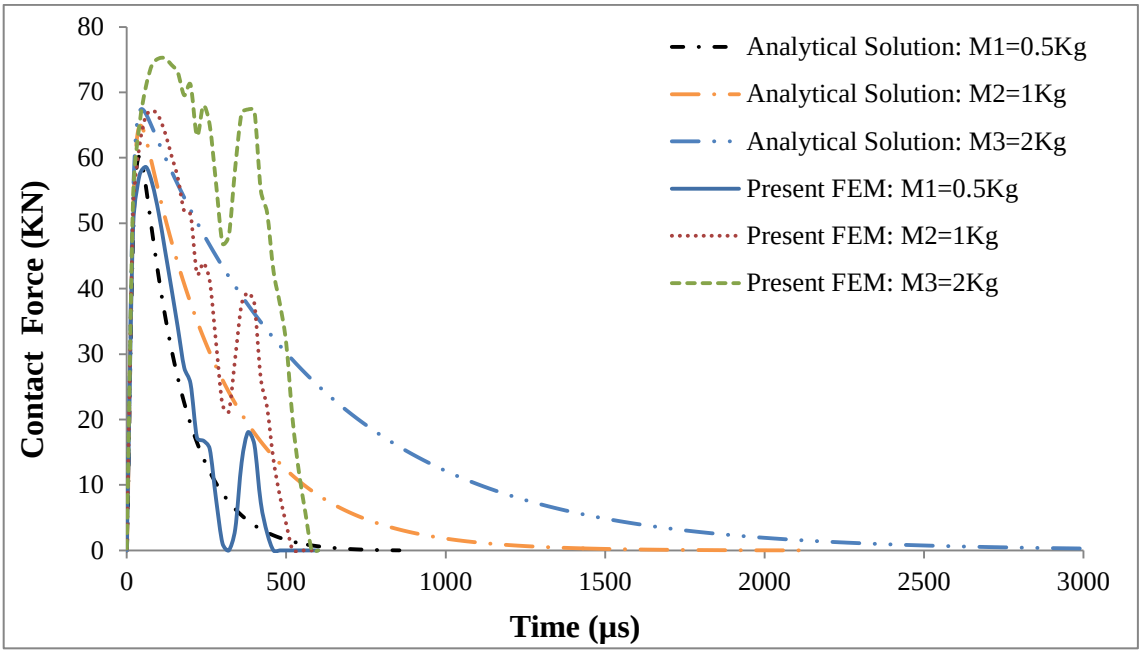

(a) Contact force-time history

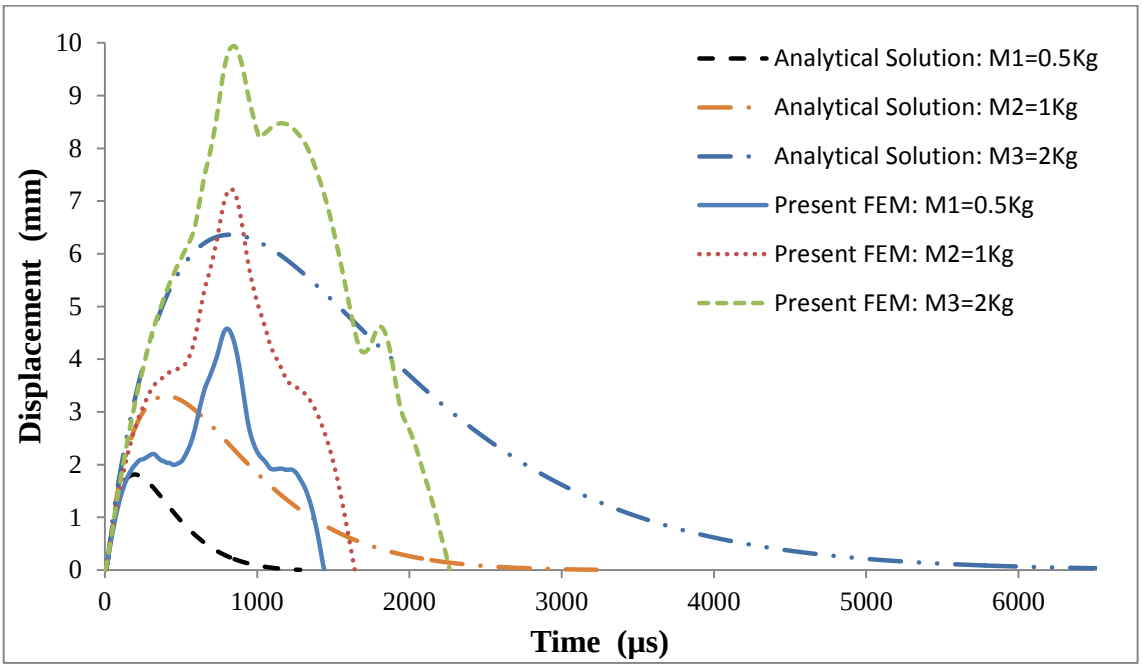

(b) displacement-time history

Figure 4.35: The results comparison for Case 6

Table 4.13: Maximum contact force and displacement results comparison for Case 6

Studied Parameter		Present FEM (Elastic analysis)		Analytical method (wave propagation)		Difference	
		Peak contact force (kN)	Max. Displacement (mm)	Peak contact force (kN)	Max. Displacement (mm)	Peak contact force (%)	Max. Displacement (%)
Impactor mass (Kg) Case 6	0.5	58.60	2.07	60.21	1.72	-2.75	16.91
	1	67.22	3.80	64.92	3.34	3.43	12.11
	2	75.19	6.30	67.45	6.36	10.30	-0.96

Figures 4.36(a), 4.36(b) and 4.36(c) show FE impact results from numerical modelling for Case 7. The PVB interlayer thickness effect was examined. It can be seen that the impact responses are not significantly affected by the PVB interlayer thickness. The velocity-time curves also show that the impactor rebound velocity are approximately equal for all PVB interlayer thicknesses and the impactor rebound velocity are 17.1, 17.4 and 17.7 m/s , respectively.

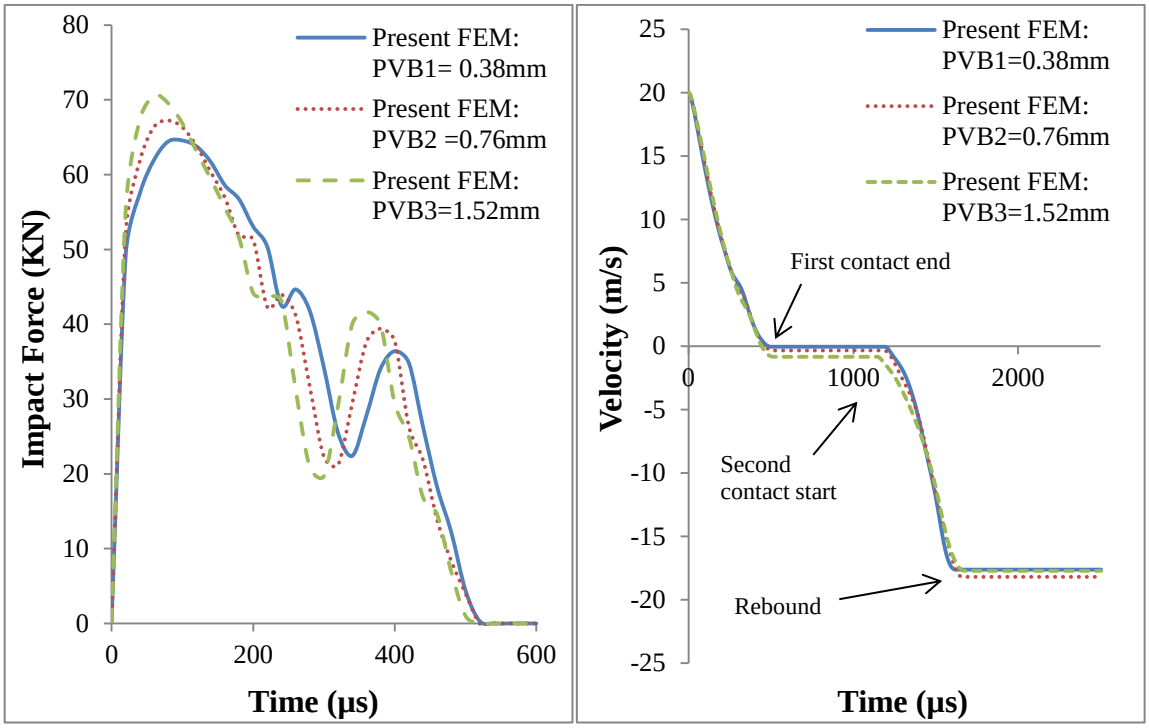

(a) Contact force-time history (b) Velocity-time history

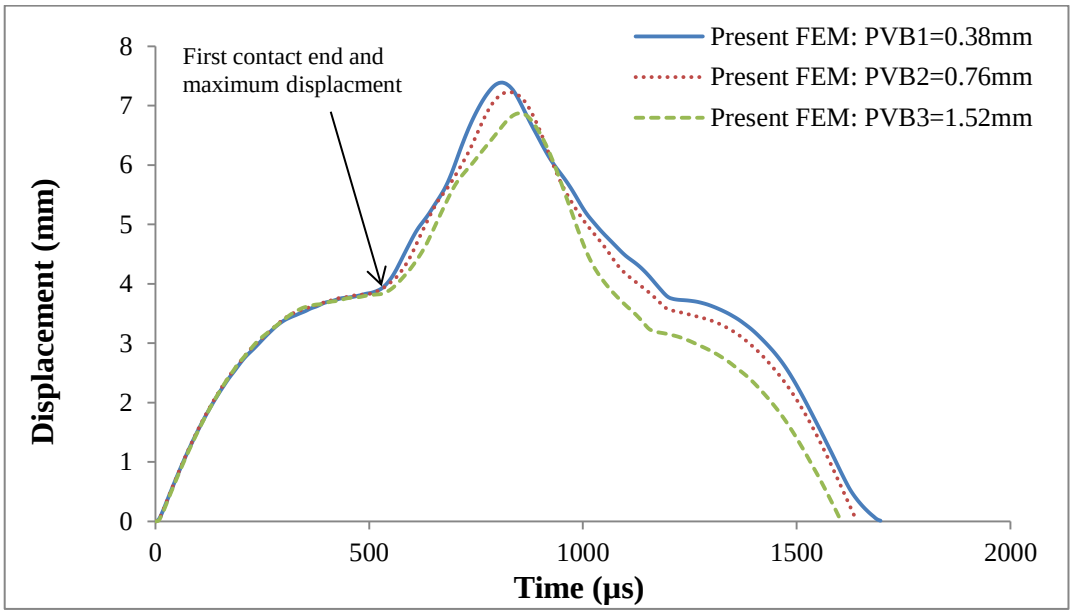

(c) Displacement-time history

Figure 4.36: Impact results for Case 7

By changing the PVB interlayer thickness, Figures 4.37(a) and 4.37(b) show the comparison of the contact force and displacement between the FEM and wave propagation analytical method. The linear variation of loading portions is identical for all PVB layer thicknesses as shown in the contact force figure. The wave propagation analytical method over-predicts the first contact ending time and the total contact time are also found from the contact force and displacement plots, respectively. Table 4.14 shows the peak contact force and displacement results predicted from the FEM and analytical method. The agreement of the peak contact forces between both methods is extremely good for the PVB thickness of 1.52 mm and 0.76 mm. However, the FEM peak displacement results do not agree with those from the wave propagation analytical method.

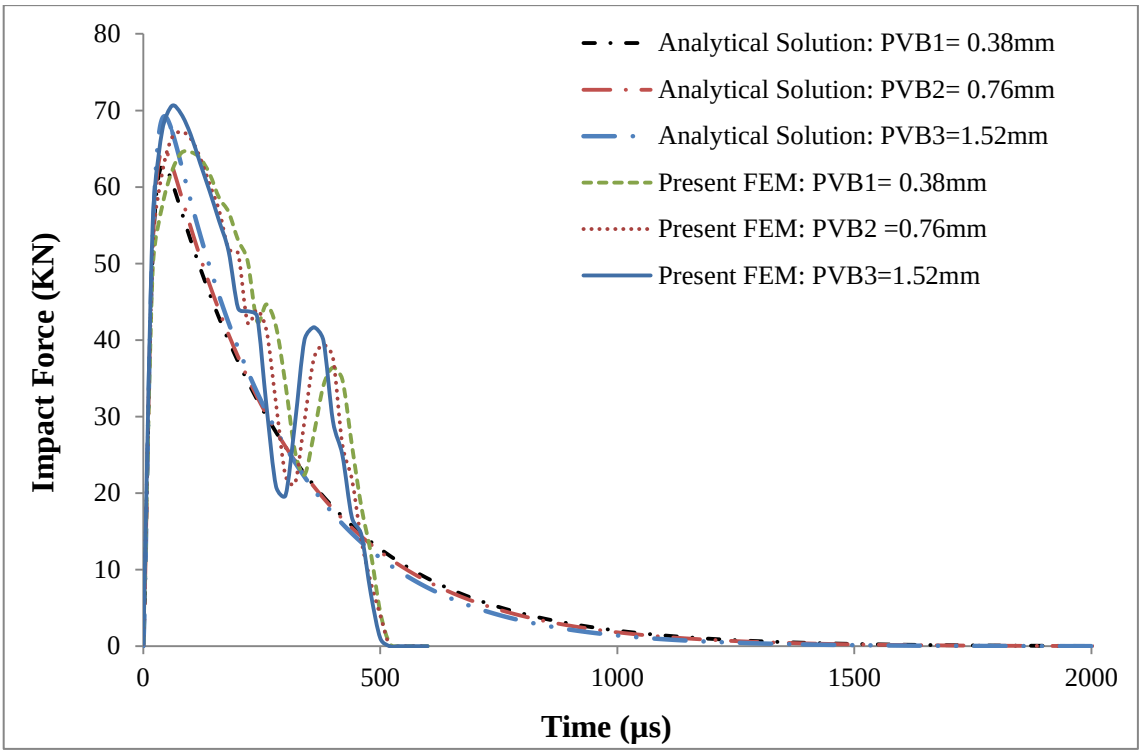

(a) Contact force-time

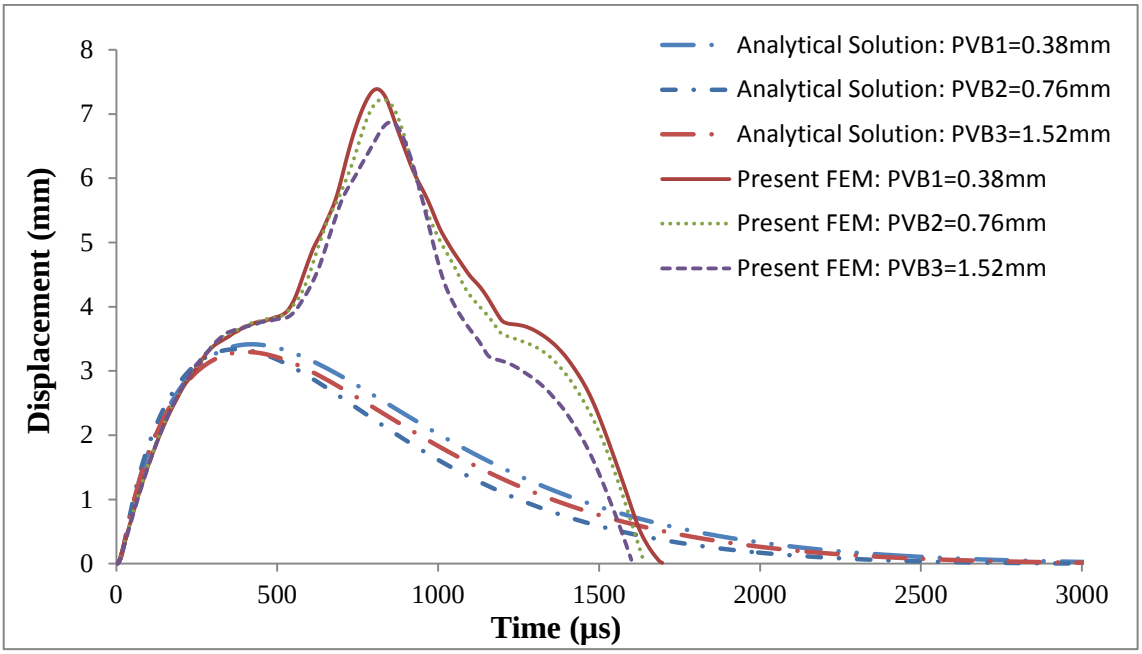

(b) Displacement-time history

Figure 4.37: The results comparison for Case 7

Table 4.14: Maximum contact force and displacement results comparison for Case 7

Studied Parameter		Present FEM (Elastic analysis)		Analytical method (wave propagation)		Difference	
		Peak contact force (kN)	Max. Displacement (mm)	Peak contact force (kN)	Max. Displacement (mm)	Peak contact force (%)	Max. Displacement (%)
PVB interlayer thickness (mm) Case 7	0.38	64.56	3.87	68.81	3.41	-6.59	11.89
	0.76	67.22	3.80	64.92	3.34	3.43	12.11
	1.52	70.58	3.78	69.24	3.29	1.90	12.97

4.7 Numerical analysis of contact radius of monolithic and laminated glass plates under various parametric conditions

For contact area analysis, a limited amount of investigation has been found analytically, but there is no literature found numerically. In this section, Case 1 to 3 for the monolithic and Case 4 to 7 for the laminated glass plates are used to analyse the contact area numerically. Again, a quarter symmetric section of each glass plate was used for contact area analysis and the plates mesh and elements arrangement are based on the scheme previously described in section 4.4 and Figure 4.14.

For evaluation purposes, a simplified symmetric section of the plate is shown in Figure 4.38. In that figure, the red dotted points represent the contact nodes of impacted plate at the peak contact force.

The optimum element size at the impactor contact zone is 0.333 mm (see Figure 4.14) and the calculated contact radius (r) can be expressed as:

The contact radius (r) = number of red dotted squares along symmetric edge x 0.333

where the optimum element size near the impactor contact zone = 0.333 mm

Using Equation 4.4 in section 3.8, the contact area (*A*) is given by;

$$A = \pi r^2 \tag{4.4}$$

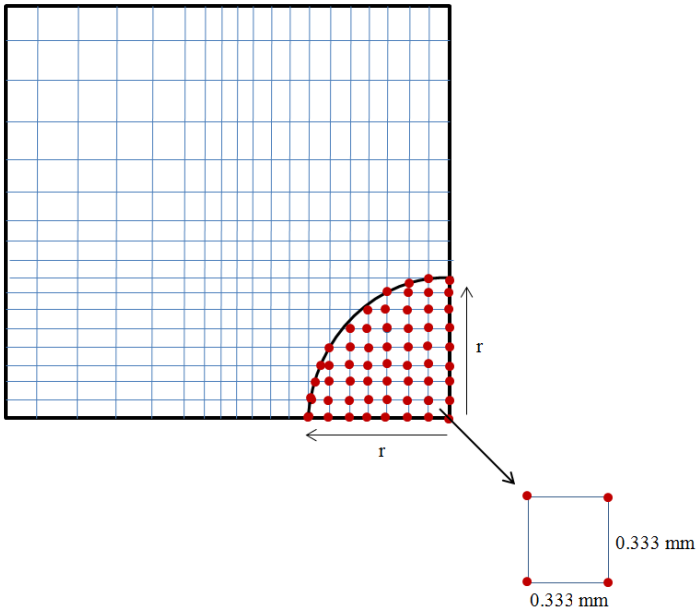

Figure 4.38: Section of a quarter-symmetric square plate for contact area calculation

As can be seen in sections 4.5 and 4.6, there are seven cases studied for parametric analysis purpose. All impact response curves are featured with a short loading and long un-loading section. It is well known that the end of the loading section and the beginning of the un-loading section represents the maximum contact force, which means a maximum number of contact nodes are engaged in contact at this moment.

For Case 1, Case 2 and Case 3, the engaged contact nodes for monolithic glass plates are presented in Figures 4.39, 4.40and 4.41. These figures show that the number of contact nodes at the peak contact force.

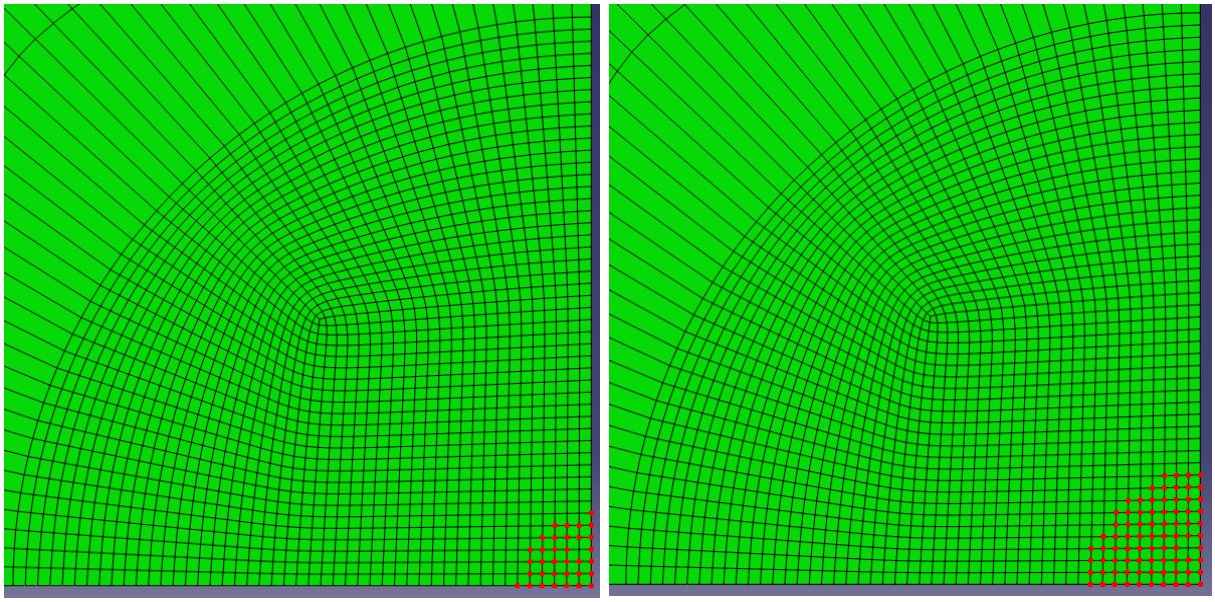

(a) V_1= 5 m/s ; contact radius (r) = 1.99 mm (b) V_2 = 20 m/s ; contact radius (r) = 2.99 mm

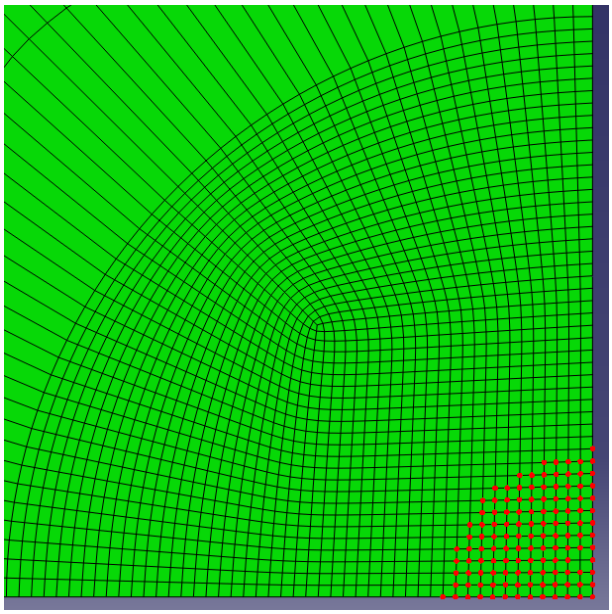

(c) V_3 = 40 m/s ; contact radius (r) = 3.99 mm

Figure 4.39: Engaged nodes in monolithic glass plate at peak contact force – Case 1

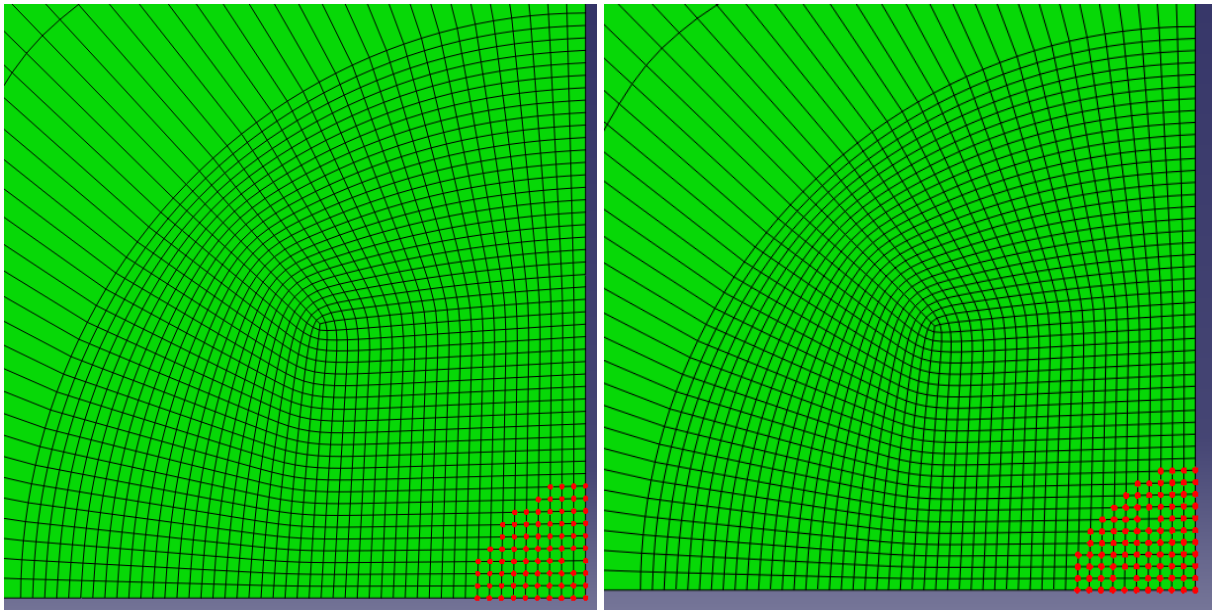

(a)t_1= 12 mm ; contact radius (r)= 2.99 mm (b) t_2= 15 mm ; contact radius (r)= 3.33 mm

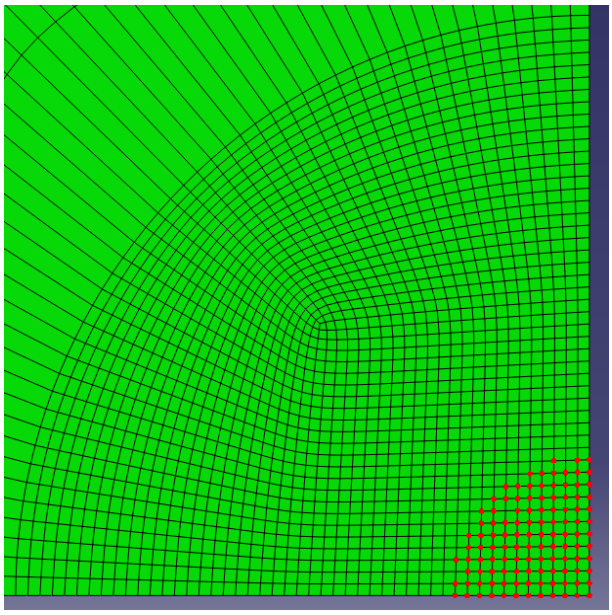

(c) t_3= 18 mm ; contact radius (r)= 3.67mm

Figure 4.40: Engaged nodes in monolithic glass plate at peak contact force – Case 2

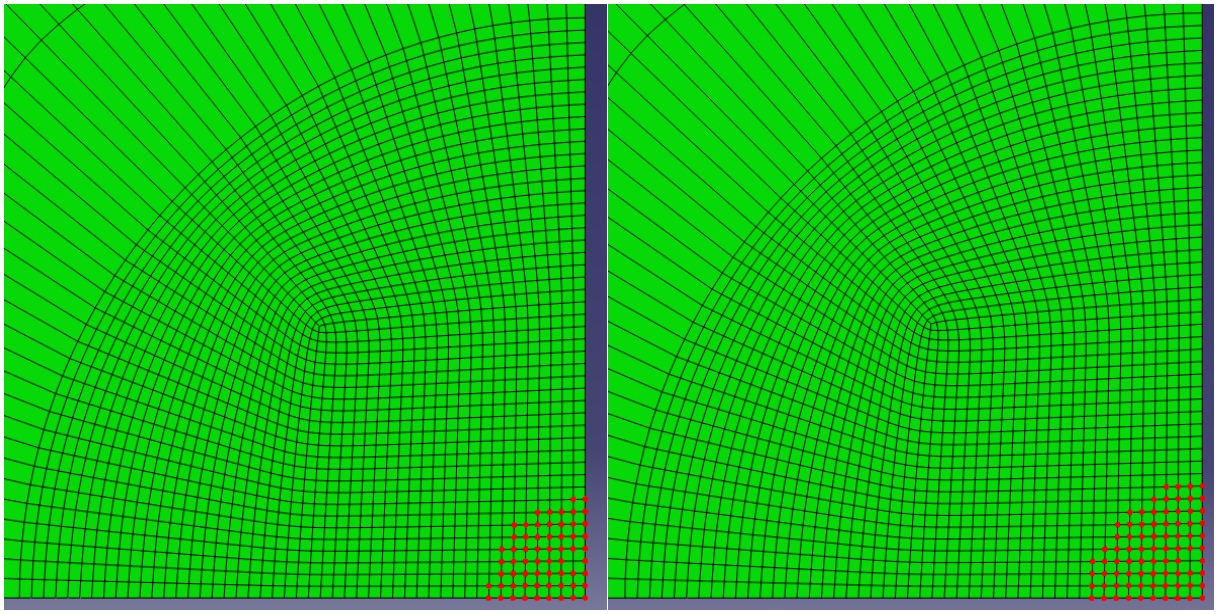

(a) M1= 0.5 Kg ; contact radius (r)= 2.67 mm (b) M2= 1 Kg ; contact radius (r)= 2.99 mm

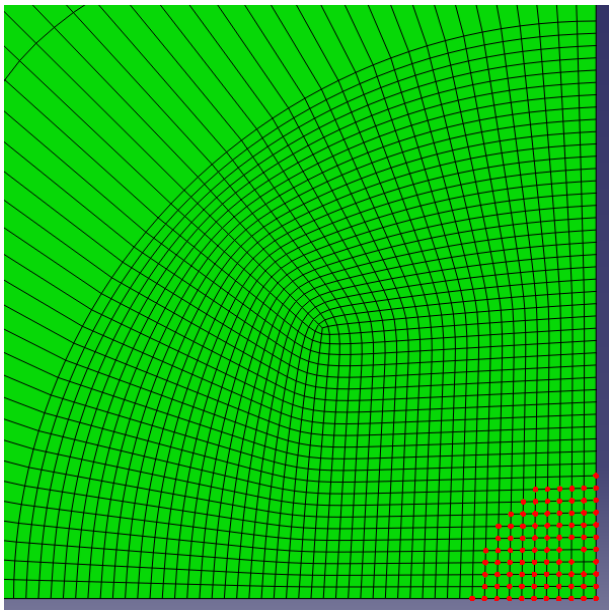

(c) M3= 2 Kg ; contact radius (r)= 3.33 mm

Figure 4.41: Engaged nodes in monolithic glass plate at peak contact force – Case 3

Table 4.15 provides the comparison of contact area for monolithic glass plates by FEM and analytical method.

Table 4.15: Numerical and analytical comparison of monolithic glass plate contact area

Studied parameter		Contact area = πr^2 (mm^2)		Difference
		Present FEM	Analytical Solution	(%)
Impact velocity (m/s) - Case 1	5	12.56	12.48	0.64
	20	28.27	32.44	-14.76
	40	50.26	52.16	-3.79
Glass plate thickness (mm) - Case 2	12	28.27	32.44	-14.76
	15	34.90	41.29	-18.31
	18	42.15	49.32	-17.02
Impactor mass (Kg) - Case 3	0.5	22.34	26.23	-17.42
	1	28.27	32.44	-14.76
	2	34.90	39.29	-12.58

The parameters of LG plate impacts were used to predict the contact radius and contact area response by FEM. At the peak stage of contact force, the impacted laminated glass plate node responses are presented in Figures 4.42, 4.43, 4.44 and 4.45. It is clear that from Case 4 to Case 6, the impacted LG plate contact node responses are increased with impact velocity,

glass ply thickness and impactor mass, but approximately unchanged contact node response is occurs by increased PVB interlayer thickness in Case 7.

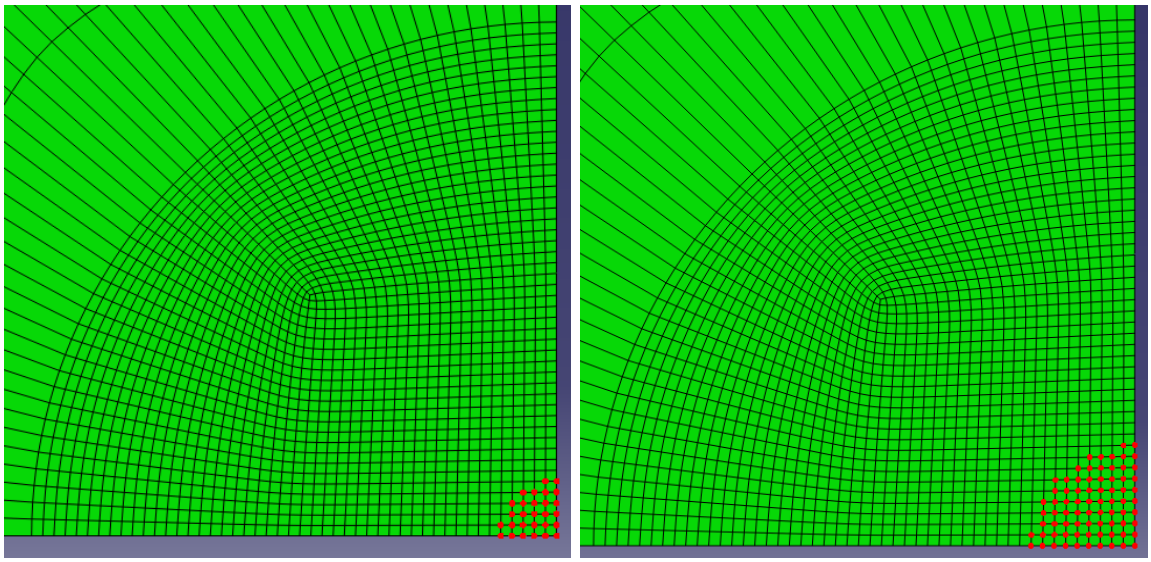

(a) V_1= 5 m/s ; contact radius (r) = 1.67 mm (b) V_2= 20 m/s ; contact radius (r) = 2.99 mm

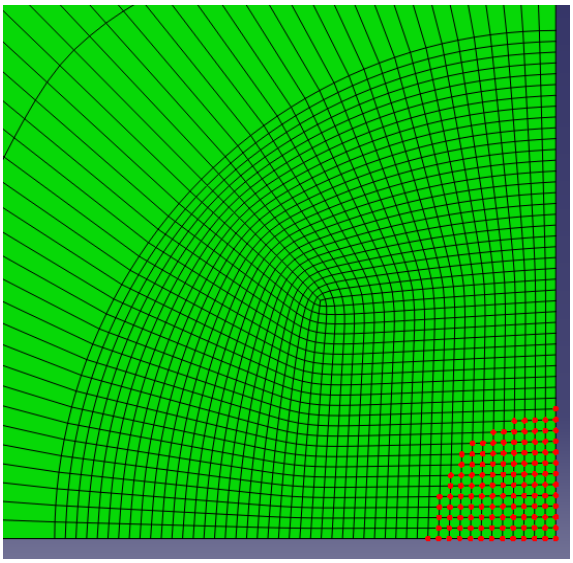

(c) V_3= 40 m/s ; contact radius (r)= 3.33 mm

Figure 4.42: Engaged nodes in monolithic glass plate at peak contact force - Case 4

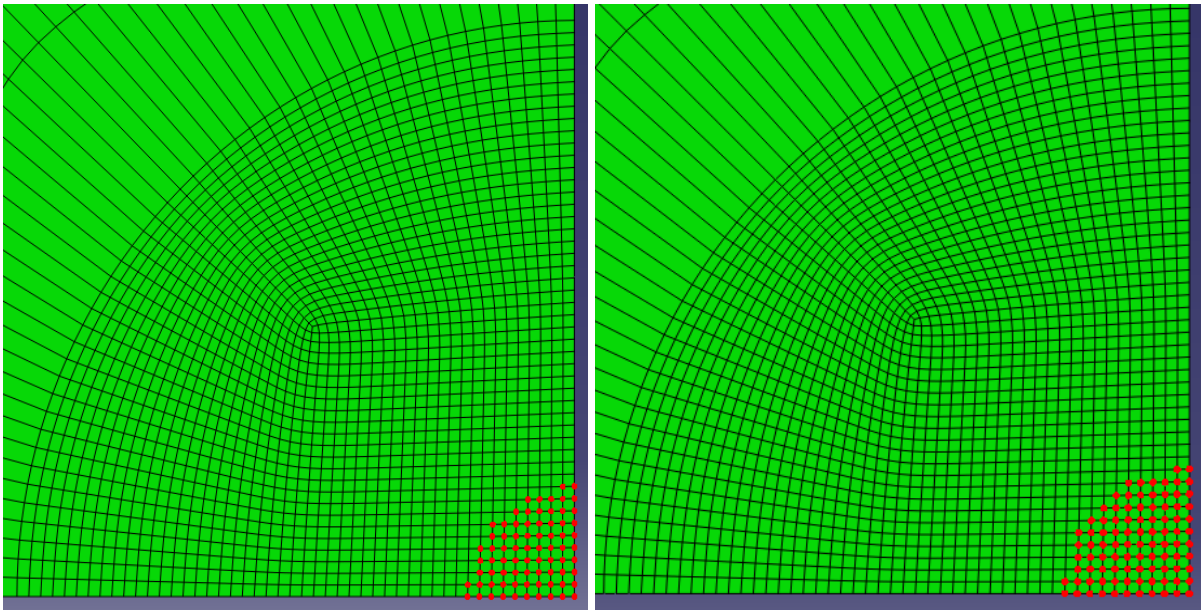

(a) 6 mm/0.76 mm/6 mm; t_1 = 6 mm
Contact radius (r)= 2.99 mm

(b) 8 mm/0.76 mm/8 mm; t_2 = 8 mm
Contact radius (r)= 3.33 mm

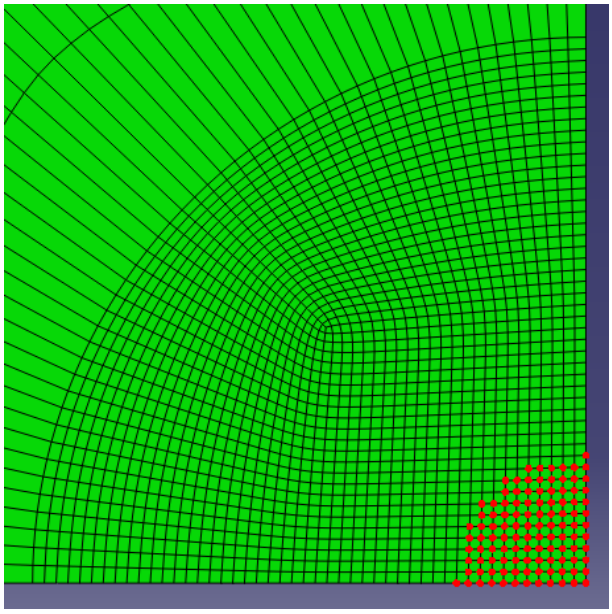

(c) 10 mm/0.76 mm/10 mm; t_3= 10 mm
contact radius= 3.67 mm

Figure 4.43: Engaged nodes in monolithic glass plate at peak contact force – Case 5

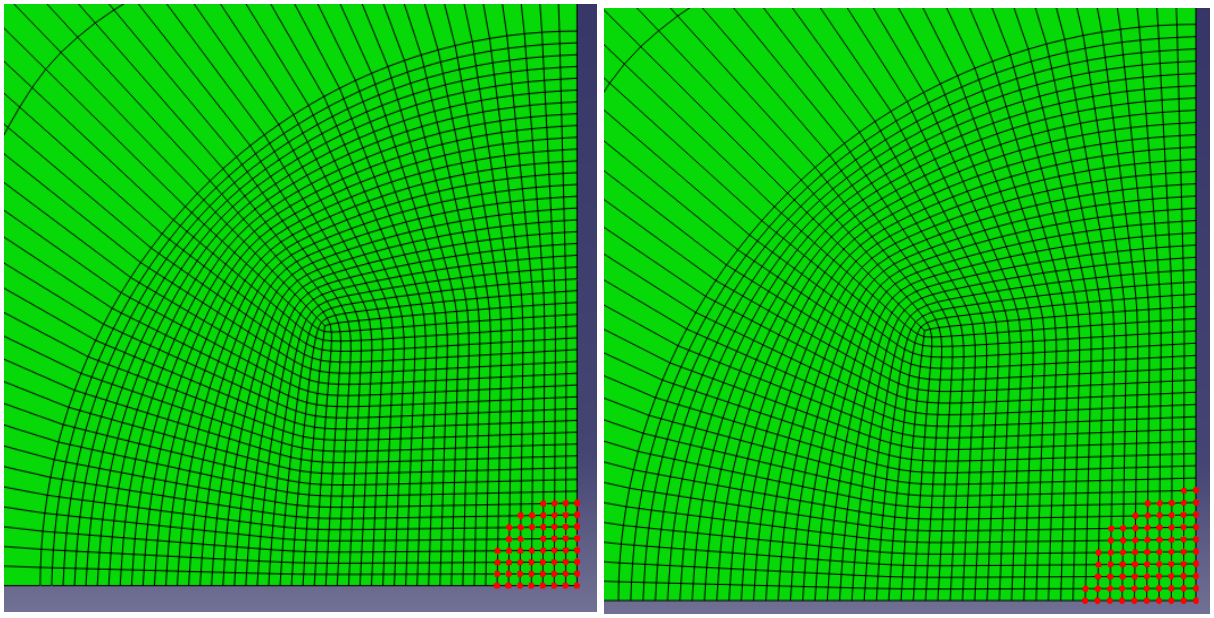

(a) M_1= 0.5Kg ; contact radius (r)= 2.33mm (b) M_2= 1Kg ; contact radius (r)= 2.99 mm

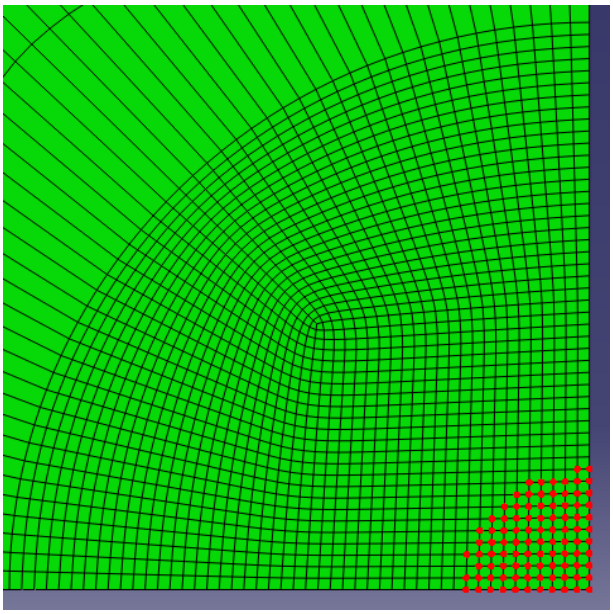

(c) M_3= 2Kg ; contact radius (r)= 3.33 mm

Figure 4.44: Engaged nodes in monolithic glass plate at peak contact force – Case 6

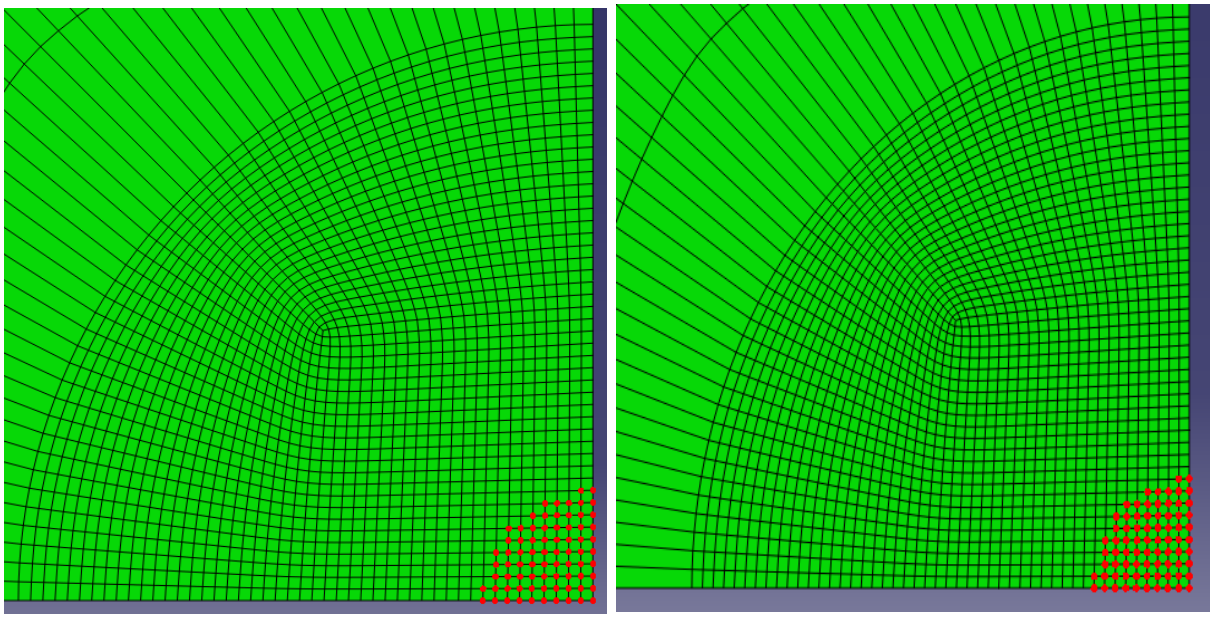

(a) PVB_1= 0.38 mm ;
Contact radius (r)= 2.99mm

(b) PVB_2= 0.76 mm ;
Contact radius (r)= 2.99 mm

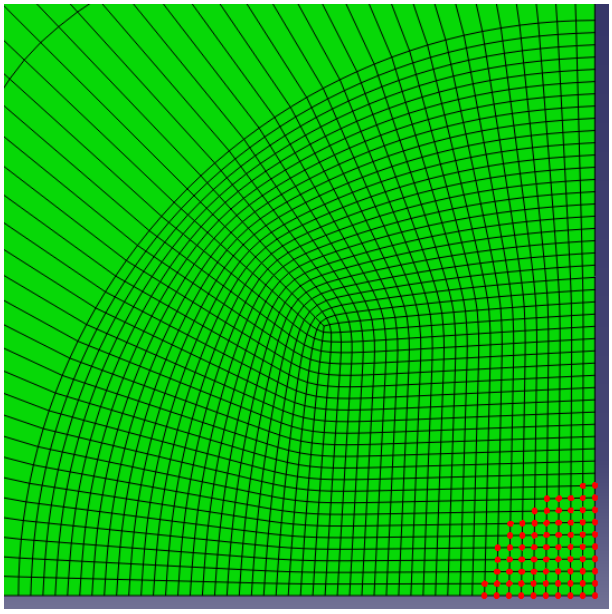

PVB_3= 1.52 mm ;

contact radius (r)= 2.99 mm

Figure 4.45: Engaged nodes in monolithic glass plate at peak contact force – Case 7

Table 4.16: Numerical and analytical comparison of laminated glass plate contact area

Studied parameter		Contact area = πr^2 (mm^2)		Difference
		Present FEM	Analytical Solution	(%)
Impact velocity (m/s) Case 4	5	8.71	11.05	9.05
	20	28.27	28.53	-0.92
	40	34.90	45.74	-31.06
Glass ply thickness (mm) Case 5	6	28.27	28.53	-0.92
	8	34.90	38.73	-10.98
	10	42.15	47.97	-13.81
Impactor mass (Kg) Case 6	0.5	17.07	23.36	-36.84
	1	28.27	28.53	-0.92
	2	34.90	34.26	1.83
PVB interlayer thickness (mm) Case 7	0.38	28.27	27.54	2.58
	0.76	28.27	28.53	-0.92
	1.52	28.22	30.55	-8.26

Table 4.16 summarises the comparison of the contact area for LG plates between FEM and analytical methods. It can be seen that in some parametric cases, good agreement between two

methods can be achieved, e.g. the impact velocity of 20m/s, the top/bottom glass ply thickness of 6mm, the impactor mass of 1Kg and 2Kg and the PVB interlayer thickness of 0.38 mm and 0.76 mm. It is interesting to note that the contact area or radius is not very sensitive to the LG plate interlayer thickness, as compared to other parameters such as impact velocity, mass and glass ply thickness

4.8 Summary

Numerical investigations on monolithic and laminated glass plates subjected to low-velocity drop weight impacts were studied systematically. Key parameters such as impact velocity, glass plate thickness, impactor mass and PVB interlayer thickness are examined. The impact force, impactor velocity, plate central displacement and contact area are considered of both glass plates with elastic analysis and damaging analysis. In this study, the main outcomes can be outlined as follows:

- In numerical modelling, if the stiffness of impactor is much higher than the target structure, the impactor can be assumed as a rigid body, while the target structure should be treated as a deformable one. If the model is of symmetric nature, a quarter section can be chosen for modelling in the elastic regime. However, if a damage modelling is carried out, a full model is required. In addition, the surface based contact algorithm can be used to model the contact behaviour between the plate and impactor.
- The target plate has been divided into two regions to facilitate different meshing densities between inside and outside of the contact affected zones. Convergence analysis can be carried out to determine the optimum element sizes.

- The numerical model is verified by comparing the results with published data.
- The numerical analysis results include the impact force, displacement and velocity history data. In each parametric study case, the FE elastic results are compared with the analytical results. The peak contact force agrees well for both glass types.
- The impact velocity-time history can be used to identify the number of contacts generated between the impactor and plate from the analysis. It includes the first contact, second contact and rebound of the impactor, respectively. The plate displacement-time history is used to predict the maximum displacement at the plate centre. The peak displacement results from the numerical modelling are compared with those from the wave propagation analytical method and it is found that most data agrees well between both methods.
- By considering similar parameters, the failure response of monolithic glass plate has been investigated by examining the FE output and the force-time history curves. In the case of the low-velocity drop weight impact, star cracks occur in the plate's rare (back) surface and these crack patterns have a good agreement with the published observations (Bouzid et al., 2001). The ultimate failure load of the monolithic glass plate is also predicted in the damage model. The first sudden sharp drop in the contact force history curve indicates an impact failure of glass plate. In addition, the numerical elastic analysis and damage model results are compared and both models make a good agreement.
- A low-velocity impact numerical investigation is performed for the laminated glass plates under four different parametric conditions (i.e. impact velocity, impact mass,

glass ply thickness and PVB interlayer thickness) and three different impact responses, namely, the contact force, plate displacement and impactor velocity, are examined. The force-time and displacement-time histories are compared with the analytic method of wave propagation and results are found in good agreement.

- The contact analysis, which is obtained from the numerical investigation, can be used to predict the maximum contact area of monolithic and laminated glass plates. Furthermore, numerically predicted contact areas are also used to compare with the results of analytical method, and they are in a good agreement for both glass plates.

CHAPTER 5: CONCLUTION AND RECOMMENDATION

5.1 Conclusions and recommendation

In this research, a drop weight impact response of monolithic and laminated glass plates was studied under the lower velocity category by using the analytical and numerical methods. Based on the published literatures, the range of the low-velocity drop weight impacts was identified as 0 – 50 m/s. Furthermore, the published literatures are also reviewed to establish a clear view regarding the dynamic and quasi-static responses of impacts in the normal and oblique directions. The most interesting thing is that the impact damages of monolithic and laminated glasses have been well studied but no publications are found to provide direct impact response analysis (i.e. contact force, displacement, contact area).

Several analytical models have been employed for the impact predictions. The spring- mass model, energy-balance model and infinite thick plate model can all give closed form solutions. The force-time history of Karas study was examined by using a number of analytical methods and finally the results found to be in good agreement with wave propagation analytical method. Therefore, the wave propagation analytical method is recommended in the low-velocity impact predictions of monolithic and laminated plate glasses.

Similarly, the steel sphere impact response on the steel plate (Karas study) was also investigated by using an FE numerical method. A 3D finite element method by employing

ABAQUS commercial software package was adopted. The convergence analysis was initially considered. In the convergence analysis, the contact force, displacement and velocity results are in good agreement with Karas's predictions and the optimum element sizes was found to be 1mm x 1mm x 1mm for the impactor, 0.333 mm x 0.333 mm x 1 mm near the contact zone of steel plate and 4.75 mm x 4.75 mm x 1 mm near the contact zone of steel plate (see Figure 4.13). The verified impact model including the optimum element sizes was subsquently used for the impact analysis of monolithic and laminated plate (LG) glass. Rigid and deformable bodies are recommended to define the material properties of the impactor and plate, respectively.

For both types of plate glasses, a variety of impact parameters were considered by the numerical and analytical investigations, which includes the impact velocity, impact mass, glass plate thickness, PVB interlayer thickness. Three different impact responses of contact force, displacement and velocity were investigated. The peak contact force and displacement in some numerical results exhibit good agreement with the analytical results. From the analysis, it is also found that the effects of impact velocity and plate thickness are much more significant than the impact mass and PVB layer thickness. In some parametric cases, the predictions of first contact and the total contact durations from the wave propagation analytical method are less consistent than the numerical results. However, through comparisons the wave propagation analytical method is recommended in low-velocity plate impact analysis.

As previously described, the optimum element sizes established from the convergence study were used to investigate the low-velocity impact damage response of the monolithic glass plate with the brittle cracking model. The impact damage response of monolithic glass plate was predicted in terms of the force-time history. The sharp peak drops in the force-time history curve and the surface star cracks in plate rear surface were observed. It has been found that the damage initiations in the plate rear surface occurred before the contact force reached the maximum level. The impact failure pattern of monolithic glass plate agrees well with the observations from the low-velocity drop ball impacts stated by Bouzid et al. (2001) (see Appendix A – Figure A.3). FE linear elastic material model and brittle cracking model provides good predictions in the peak contact forces. The failure contact force can be approximately estimated from the FE elastic analysis. The glass plate impact responses vary with the impact velocity, impactor mass and plate thickness. This behaviour is also valid for the laminated glass plates.

5.2 Future work

This research highlights a number of issues which require further investigation.

It is recommended that the following future work should be carried out:

- The study of different geometric shapes (e.g. cylindrical, conical, flat) for impactor should be carried out.

- Further improvement in the wave propagation analytical method can be made to increase the accuracy of analysis, in particular, for the results of contact duration and plate displacement.

- Implementing the damage prediction in ABAQUS by using various materials model to capture various crack patterns (impact surface cracks and particle spalashing) for monolithic glass plates.

- Implementing the damage analysis by including the coupled material models to predict the impact damages for laminated glass plate including the PVB interlayer delamination.

- It is recommended to conduct thorough laboratory investigations to record the real impact response of large size monolithic and laminated plate glasses.

APPENDIX A

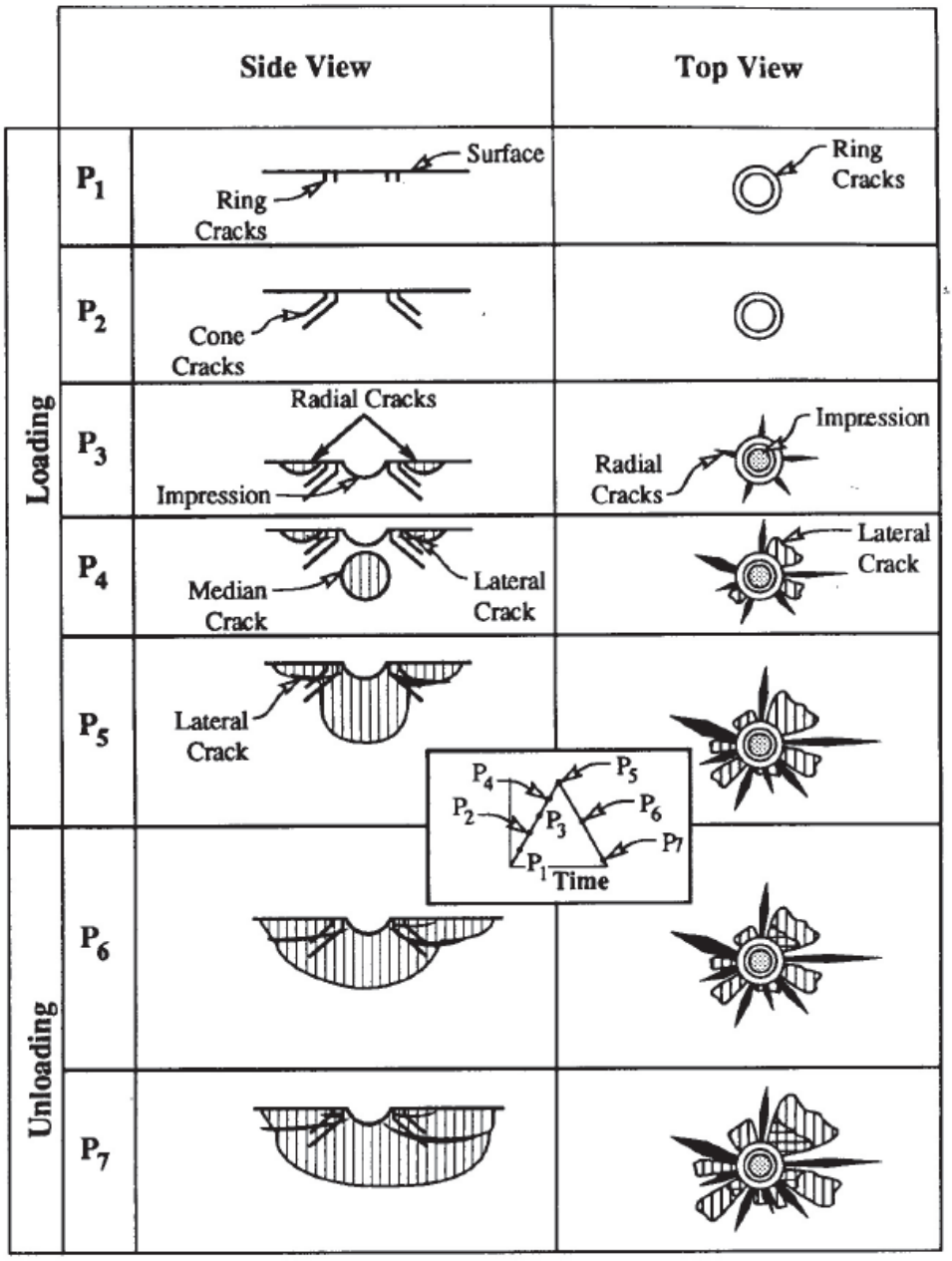

Figure A.1: Particle impact induced damage evaluation of glass plate (Grant and Cantwell., 1999)

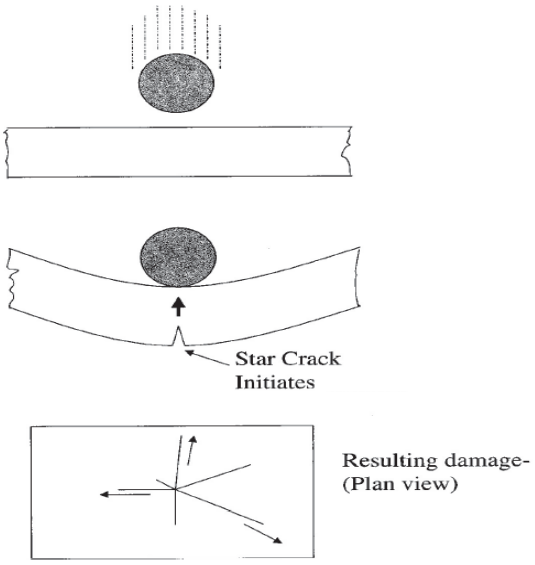

Figure A.2: Impacted monolithic glass plate rare surface damage initiation (Grant and Cantwell., 1999)

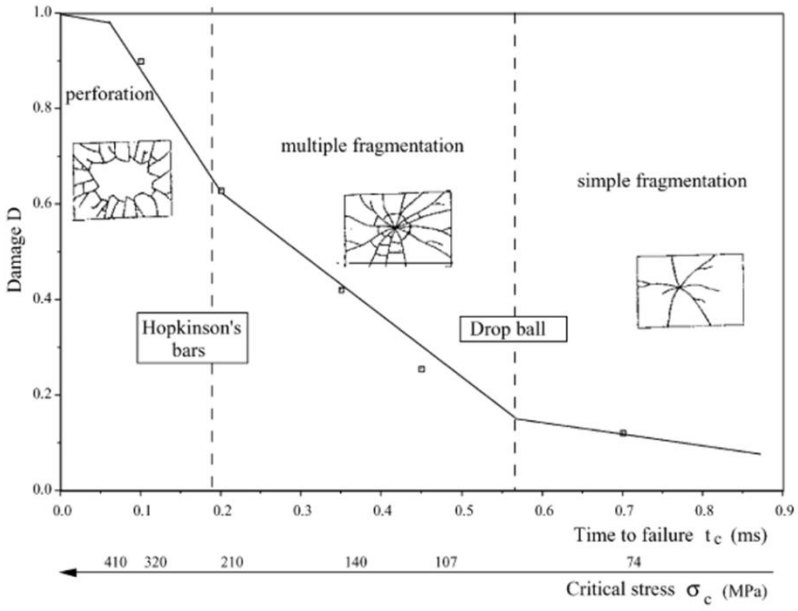

Figure A.3: Failure mechanism of monolithic glass plate under different impact tests (Bouzid et al., 2001)

REFERENCES

ABAQUS (2010) **ABAQUS Analysis User's Manual (V6.10),.** Hibbitt, Karlsson, and Sorensen, Inc, Pawtucket, USA (1996)

(http://mse-license1.mse.drexel.edu:2080/v6.10/books/usb/default.htm).

Abrate, S. (1998) **Impact on composite structures.** Cambridge Univ Pr.

Abrate, S. (2001) **Modeling of impacts on composite structures.** Composite Structures, 51**,** 129-138.

Alman, D., Tylczak, J., Hawk, J. and Hebsur, M. (1999) **Solid particle erosion behavior of an Si_3N_4-MoS_2 composite at room and elevated temperatures.** Materials Science and Engineering: A, 261**,** 245-251.

Aquaro, D. and Fontani, E. (2001) **Erosion of ductile and brittle materials.** Meccanica, 36**,** 651-661.

Aretxabaleta, L., Aurrekoetxea, J., Urrutibeascoa, I. and Sánchez-Soto, M. (2005) **Characterisation of the impact behaviour of polymer thermoplastics.** Polymer Testing, 24**,** 145-151.

Aryaei, A., Hashemnia, K. and Jafarpur, K. (2010) **Experimental and numerical study of ball size effect on restitution coefficient in low velocity impacts.** International Journal of Impact Engineering, 37**,** 1037-1044.

Axinte, E. (2011) **Glasses as engineering materials: A review.** Materials & Design, 32**,** 1717-1732.

Backman, M. E. and Goldsmith, W. (1978) **The mechanics of penetration of projectiles into targets.** International Journal of Engineering Science, 16**,** 1-99.

Ball, A. (1997) **The low velocity impact behaviour of glass-polymer laminated plates.** Journal de Physique(France) IV(France), 7**,** 77.

Ball, A. and McKenzie, H. W. (1994) **On the low velocity impact behaviour of glass plates.** Les Editions de Physique Les Ulis, J. Phys.(France) IV(France), 4**,** 783-788.

Belingardi, G., Koricho, E. G. and Martorana, B. (2002) **Design Optimization and Implementation of Composite and Recyclable Thermoplastic Materials for Automotive Bumper.** International Journal of Impact Engineering, 27**,** 213 - 229.

Belingardi, G. and Vadori, R. (2002) **Low velocity impact tests of laminate glass-fiber-epoxy matrix composite material plates.** International Journal of Impact Engineering, 27**,** 213-229.

Bitter, J. (1963) **A study of erosion phenomena: Part II.** Wear, 6**,** 169-190.

Boccaccini, A. R., Thompstone, J., Desimone, D., Rawlings, R. D., Kasiarova, M. and Srivastava, V. K. (2007) **Characterization of ballistic impact damage in wired glass.** International journal of applied ceramic technology, 4**,** 350-358.

Børvik, T. 2001. **Ballistic penetration and perforation of steel plates**. Norwegian University of Science and Technology.

Børvik, T., Hopperstad, O., Berstad, T. and Langseth, M. (2002) **Perforation of 12mm thick steel plates by 20mm diameter projectiles with flat, hemispherical and conical noses: part II: numerical simulations.** International Journal of Impact Engineering, 27**,** 37-64.

Bouzid, S., Nyoungue, A., Azari, Z., Bouaouadja, N. and Pluvinage, G. (2001) **Fracture criterion for glass under impact loading.** International Journal of Impact Engineering, 25**,** 831-845.

Cantwell, W. J. (2007) **Geometrical effects in the low velocity impact response of GFRP.** Composites science and technology, 67**,** 1900-1908.

Chakraborty, D. (2007) **Delamination of laminated fiber reinforced plastic composites under multiple cylindrical impact.** Materials & Design, 28**,** 1142-1153.

Christoforou, A. P. and Yigit, A. S. (1998) **Characterization of impact in composite plates.** Composite structures, 43**,** 15-24.

Corran, R. S. J., Shadbolt, P. J. and Ruiz, C. (1983) **Impact loading of plates--An experimental investigation.** International Journal of Impact Engineering, 1**,** 3-22.

Cremona Rebecca, L. and Hinkley Jeffrey, A. (2005). **Simulation of impact on a ductile polymer plate**. NASA/TM-2005-213785.

Dhakal, H., Zhang, Z., Bennett, N. and Reis, P. (2012) **Low-velocity impact response of non-woven hemp fibre reinforced unsaturated polyester composites: Influence of impactor geometry and impact velocity.** Composite structures.

Dharani, L. R., Wei, J., Yu, J., Minor, J. E. and Behr, R. (2005) **Laminated Architectural Glass Subjected to Blast, Impact Loading.** American Ceramic Society Bulletin, 84**,** 42-44.

ElTobgy, M., Ng, E. and Elbestawi, M. (2005) **Finite element modeling of erosive wear.** International Journal of Machine Tools and Manufacture, 45**,** 1337-1346.

Feraboli, P. and Kedward, K. T. (2004) **Enhanced evaluation of the low-velocity impact response of composite plates.** AIAA journal, 42**,** 2143-2152.

Feraboli, P. and Kedward, K. T. (2006) **A new composite structure impact performance assessment program.** Composites science and technology, 66**,** 1336-1347.

Flocker, F. W. and Dharani, L. R. (1997a) **Modelling fracture in laminated architectural glass subject to low velocity impact.** Journal of Materials Science, 32**,** 2587-2594.

Flocker, F. W. and Dharani, L. R. (1997b) **Stresses in laminated glass subject to low velocity impact.** Engineering Structures, 19**,** 851-856.

Flocker, F. W. and Dharani, L. R. (1998) **Low Velocity Impact Resistance of Laminated Architectural Glass.** Journal of Architectural Engineering, 4**,** 12-17.

Foo, C., Chai, G. and Seah, L. (2008) **A model to predict low-velocity impact response and damage in sandwich composites.** Composites science and technology, 68**,** 1348-1356.

Goldsmith, W. (1964) **Impact, the theory and physical behavior of colliding solids.**

Goldsmith, W. (2001) **Impact: the theory and physical behaviour of colliding solids.** Dover Pubns.

Goldsmith, W. and Finnegan, S. A. (1986) **Normal and oblique impact of cylindro-conical and cylindrical projectiles on metallic plates.** International Journal of Impact Engineering, 4**,** 83-105.

Grant, P. V. and Cantwell, W. J. (1999) **Impact failure modes in glass structures.** Proceedings of the Institution of Mechanical Engineers, Part D: Journal of Automobile Engineering, 213**,** 519-529.

Grant, P. V., Cantwell, W. J., McKenzie, H. and Corkhill, P. (1998) **The damage threshold of laminated glass structures.** International Journal of Impact Engineering, 21**,** 737-746.

Haldimann, M. 2006. **Fracture strength of structural glass elements: analytical and numerical modelling, testing and design**. EPFL.

Highsmith, A. L. (1997) **A study of the use of contact loading to simulate low velocity impact.** NASA.

IstructE (1999) **Structural use of glass in buildings.** UK, The Institution of Structural Engineers.

James, G. (1913) **Glass handbook.** (http://gjames.com/glass).

Ji, F. S., Dharani, L. R. and Behr, R. A. (1998) **Damage probability in laminated glass subjected to low velocity small missile impacts.** Journal of Materials Science, 33**,** 4775-4782.

Johnson, K. L. (1987) **Contact mechanics.** Cambridge university press.

Khalili, S., Soroush, M., Davar, A. and Rahmani, O. (2011) **Finite element modeling of low-velocity impact on laminated composite plates and cylindrical shells.** Composite structures, 93**,** 1363-1375.

Kirchner, H. P. and Gruver, R. M. (1977) **Localized impact damage in glass.** Materials science and engineering, 28**,** 153-160.

Kirchner, H. P. and Gruver, R. M. (1978) **The effect of localized damage on energy losses during impact.** Materials science and engineering, 33**,** 101-106.

Kishi, N. and Bhatti, A. Q. (2010) **An equivalent fracture energy concept for nonlinear dynamic response analysis of prototype RC girders subjected to falling-weight impact loading.** International Journal of Impact Engineering, 37**,** 103-113.

Knight, C. G., Swain, M. V. and Chaudhri, M. M. (1977) **Impact of small steel spheres on glass surfaces.** Journal of Materials Science, 12**,** 1573-1586.

Lagace, P. A., Williamson, J. E., Tsang, P. H. W., Wolf, E. and Thomas, S. (1993) **A preliminary proposition for a test method to measure (impact) damage resistance.** Journal of reinforced Plastics and Composites, 12**,** 584-601.

Langitan, F. B. and Lawn, B. R. (1968) **Hertzian fracture experiments on abraded glass surfaces as definitive evidence for an energy balance explanation of Auerbach's law.** J Appl Phys, 40**,** 4009–4017.

Ledbetter, S. R., Walker, A. R. and Keiller, A. P. (2006) **Structural use of glass.** Journal of architectural engineering, 12**,** 137.

Leitch, K. K. 2005. **Structure glass technology: systems and applications**. Massachusetts Institute of Technology.

Li, Y., Xuefeng, A. and Xiaosu, Y. (2012) **Comparison with low-velocity impact and quasi-static indentation testing of foam core sandwich composites.**

Liu, B. (2011) **Experimental and numerical study on the impact strength of beams and plates.**

Liu, Y. and Liaw, B. (2009) **Drop-weight impact tests and finite element modeling of cast acrylic plates.** Polymer Testing, 28**,** 599-611.

Maria, L. 2011. **Strength design methods for laminated glass** Lunds Universitet.

Mecholsky, J., RICE, R. and FREIMAN, S. (1974) **Prediction of fracture energy and flaw size in glasses from measurements of mirror size.**

Mittal, R. K. (1987) **A simplified analysis of the effect of transverse shear on the response of elastic plates to impact loading.** International journal of solids and structures, 23**,** 1191-1203.

Nandlall, D. and Chrysler, J. (1998). **A numerical analysis of the ballistic performance of a 6.35-mm transparent polycarbonate plate**. DTIC Document.

Nandlall, D. and Wong, G. (1998). **A Numerical Analysis of the Effect of Mesh Sensitivity on Ballistic Limit Prediction**. DTIC Document.

Nettles, A. T. and Douglas, M. J. (2000) **A comparison of quasi-static indentation to low-velocity impact.** National Aeronautics and Space Administration, Marshall Space Flight Center.

Olsson, R. (2000) **Mass criterion for wave controlled impact response of composite plates.** Composites Part A, 31**,** 879-887.

Pankhardt, K. 2009. **Load bearing glasses**. Budapest Unversity of Technology and Economics.

Pashah, S., Massenzio, M. and Jacquelin, E. (2008) **Prediction of structural response for low velocity impact.** International Journal of Impact Engineering, 35**,** 119.

Poola, R. (2011) **Bird strike impact analysis of vertical stabilizer structure using Abaqus/Explicit.**

Rusinek, A., Rodríguez-Martínez, J. A., Zaera, R., Klepaczko, J. R., Arias, A. and Sauvelet, C. (2009) **Experimental and numerical study on the perforation process of mild steel sheets subjected to perpendicular impact by hemispherical projectiles.** International Journal of Impact Engineering, 36**,** 565-587.

Ryan, E. V. C. (1992) **Catastrophic collisions: Laboratory impact experiments, hydrocode simulations, and the scaling problem.**

Schittich, C., Staib, G., Balkow, D., Schuler, M. and Sobek, W. (2007) **Glass construction manual.** Birkhäuser.

Schmidt, M. E. and Cheng, L. (2009) **Impact Response of Externally Strengthened Unreinforced Masonry Walls Using CFRP.** Journal of Composites for Construction, 13**,** 252.

Schonberg, W., Keer, L. and Woo, T. (1987) **Low velocity impact of transversely isotropic beams and plates.** International Journal of Solids and Structures, 23**,** 871-896.

Setoodeh, A. R., Malekzadeh, P. and Nikbin, K. (2009) **Low velocity impact analysis of laminated composite plates using a 3D elasticity based layerwise FEM.** Materials & Design, 30**,** 3795-3801.

Shivakumar, K. N., Elber, W. and Illg, W. (1985) **Prediction of impact force and duration due to low-velocity impact on circular composite laminates.** Journal of Applied Mechanics, 52**,** 674.

Shutov, A. I., Frank, A. N., Novikov, I. A., Ostapko, A. S., Bonchuk, A. S. and Burdov, A. N. (2004) **Testing Laminated Glass for Impact Resistance.** Glass and Ceramics, 61**,** 67-69.

Smith, R. A. 1997. **History of the use of B203 in commercial glass.**

Stiles (2010) **Stiles $^{(R)}$ steel door + window system: basic glass guide.** (http://www.stilesdoor.com).

Stronge, W. J. (2004) **Impact mechanics.** Cambridge Univ Pr.

Swanson, S. R. (1992) **Limits of quasi-static solutions in impact of composite structures.** Composites Engineering, 2**,** 261-267.

Tillett, J. P. A. (1954) **A Study of the Impact of Spheres on Plates.** Proceedings of the Physical Society. Section B, 67**,** 677.

Timmel, M., Kolling, S., Osterrieder, P. and Du Bois, P. A. (2007) **A finite element model for impact simulation with laminated glass.** International Journal of Impact Engineering, 34**,** 1465-1478.

Wang, Y. F. and Yang, Z. G. (2008) **Finite element model of erosive wear on ductile and brittle materials.** Wear, 265**,** 871-878.

Weller, B., WÃnsch, J. and HÃ¤rth, K. (2005). Experimental study on different interlayer materials for laminated glass. 120-123.

Wiederhorn, S. and Lawn, B. (1977) **Strength degradation of glass resulting from impact with spheres.** Journal of the American Ceramic Society, 60**,** 451-458.

Wu, C. D., Yan, X. Q. and Shen, L. M. (2010). A numerical study on dynamic failure of nanomaterial enhanced laminated glass under impact. IOP Publishing, 012176.

Wu, H. Y. T. and Chang, F. K. (1989) **Transient dynamic analysis of laminated composite plates subjected to transverse impact.** Computers & structures, 31**,** 453-466.

Xu, J., Li, Y., Ge, D., Liu, B. and Zhu, M. (2011) **Experimental investigation on constitutive behavior of PVB under impact loading.** International Journal of Impact Engineering, 38**,** 106-114.

Xu, J., Li, Y., Lu, G. and Zhou, W. (2009) **Reconstruction model of vehicle impact speed in pedestrian-vehicle accident.** International Journal of Impact Engineering, 36**,** 783-788.

Yang, J. (1971) **Impact on plates and shells.** International Journal of Solids and Structures, 7**,** 445-458.

Zang, M. Y., Lei, Z. and Wang, S. F. (2007) **Investigation of impact fracture behavior of automobile laminated glass by 3D discrete element method.** Springer.

Zhao, S., Dharani, L. R., Chai, L. and Barbat, S. D. (2006) **Analysis of damage in laminated automotive glazing subjected to simulated head impact.** Engineering Failure Analysis, 13**,** 582-597.

Zhao, S., Dharani, L. R., Liang, X., Chai, L. and Barbat, S. D. (2005) **Crack initiation in laminated automotive glazing subjected to simulated head impact.** International Journal of Crashworthiness, 10**,** 229-236.

Zhu, S. and Chai, G. (2010) **Ductile and brittle material failures in low-velocity impact.** Proceedings of the Institution of Mechanical Engineers, Part L: Journal of Materials Design and Applications, 224**,** 162-172.

Zukas, J. (1982) **Impact dynamics.** John Wiley & Sons, Inc, 605 Third Ave, New York, N. Y. 10158, U. S. A, 1982. 452.

Zukas, J. A. (1990) **High velocity impact dynamics.** Wiley-Interscience.